DESIGN OF LEADING EDGE VORTEX FLAPS FOR SLENDER AND NONSLENDER DELTA-TYPE WINGS AT LOW SPEEDS

Undergraduate Honors Thesis

Presented in Partial Fulfillment of the Requirements for the Degree of Bachelor of Science with Honors Research Distinction at The Ohio State University

By

Benjamin M. Wagner

The Ohio State University

2015

Professor Clifford A. Whitfield, Advisor

Professor Richard Freuler

Matthew McCrink

Department of Mechanical and Aerospace Engineering

April 2015

ABSTRACT

Small unmanned aerial vehicles (UAVs) have become increasingly important in the role of tactical reconnaissance. Frontline troops rely on the ability to easily deploy UAVs from any position in order to collect time sensitive intelligence. One of the primary criteria for small UAVs is that of portability. In order to address this need, it has been proposed to design a UAV with a foldable delta wing made of a flexible material. However, delta wings typically suffer from decreased aerodynamic efficiency which is the ratio of the lift created to the drag produced. Poor performance in this regard is especially pronounced at low speeds. Since range is directly proportional to the maximum achievable aerodynamic efficiency, a delta wing equipped UAV would need to expend more propulsive energy to accomplish a given mission in comparison to conventional designs. A potential solution exists in the form of Leading Edge Vortex Flaps (LEVF). Essentially a flap-like control surface attached to the wings leading edge, such devices have been shown to improve aerodynamic efficiency by as much as 20 percent on conventional delta wing aircraft. The objective of this research was to determine an effective flap design with the goal of achieving the same aerodynamic improvements for flexible delta wings at low speeds. A secondary objective relating to the potential use of LEVF devices as a means of vehicle control was also investigated. Using Computational Fluid Dynamic (CFD), two and three dimensional analysis was performed on 30° and 60° delta wings in combination with

various LEVF geometries. Effort was given to refining the geometry of a fully three-dimensional flap model as well as to determining the primary flow mechanisms that govern the creation of lift, drag, and ultimately aerodynamic efficiency. The results indicated that, at the low velocities tested, LEVF devices could improve the Aerodynamic Efficiency of a 30° delta wing by 4 percent and a 60° delta wing by as much as 10 percent. While a preliminary investigation into the potential for using LEVF devices as a means of vehicle control produced some encouraging results, additional work would be needed in order to make any definitive conclusions.

DEDICATION

Dedicated to my wife, Christina and our little Ivy who we are very excited to meet.

ACKNOWLEDGEMENTS

I am first and foremost grateful to God who is, for me, the ultimate source and creator of knowledge as well as the giver of strength to pursue it. Next, I must thank my dear wife, who has been an unshakeable constant throughout the nonlinearities of life and without whom I would never have dared to take a different path.

I would like to express special thanks to my advisor, Dr. Clifford Whitfield who has guided me through the research process and has given many hours to helping me turn what began as a jumble of numbers and half formed thoughts into a thesis representing a year spent in discovery and learning.

I must also thank Greg Padgett for his invaluable role in helping to secure the computational tools that made my research possible and for his continued support and advice that saved me much time as I navigated the steep learning curve of Computational Fluid Dynamics.

Finally, Dr. Richard Freuler and Matthew McCrink were kind enough to make up the balance of my research defense committee, providing the benefit of their knowledge and experience.

TABLE OF CONTENTS

LIST OF FIGURES

LIST OF TABLES

NOMENCLATURE

Parameters

AR	Aspect Ratio	[m]
b	Wing Span	[m]
c	Chord Length	[m]
$\overline{c}$	Mean Aerodynamic Chord	
C_D	Drag Coefficient	
C_L	Lift Coefficient	
C_M	Moment Coefficient	
$C_{M\,ac}$	Moment Coefficient about the Aerodynamic Center	
$\delta C_{M,ac}/\delta F$	Moment Derivative with Respect to Flap Deflection	
K_P	Potential Lift	
K_V	Vortex Lift	
L/D	Aerodynamic Efficiency	
q	Dynamic Pressure	[N/m^2]
V	Velocity	[m/s]
Re	Reynolds Number	
S	Wing Area	[m^2]
α	Angle of Attack	[deg]
δF	Vortex Flap Deflection Angle	[deg]
Λ	Leading Edge Sweep Angle	[deg]
ρ	Air Density	[kg/m^3]

Abbreviations

ac	Aerodynamic Center
CAE	Computer Automated Engineering
CFD	Computational Fluid Dynamics
LE	Leading Edge
LEVF	Leading Edge Vortex Flap
UAV	Unmanned Aerial Vehicle

CHAPTER 1: INTRODUCTION

1.1 Background

On August 13, 2001, an unmanned aerial vehicle (UAV) called Helios achieved a world altitude record for sustained horizontal flight of 96,863 feet. Not long afterwards, Helios experienced catastrophic structural failure when it encountered low altitude turbulence that induced pitch instability. Designed by Aerovironment, Helios was built around the requirements for flight at high altitude necessitating an extremely light structure. Unfortunately, this compromised its ability to withstand the stress of high freestream turbulence caused by weather at lower altitudes[9].

As UAVs continually take on new roles, their design faces the challenge of satisfying mission imposed constraints while maintaining well balanced flight characteristics across multiple flight regimes. Such challenges are even more evident in the area of small UAVs, a class of UAV that is currently experiencing wide growth in mission capability and potential application. In addition to traditional military applications, small sized UAVs have now proved successful in roles as varied as agriculture and firefighting. The primary benefit offered by a small UAV is that it can be easily packed, transported, and deployed in a time sensitive manner without extensive ground support. Portability has been achieved by either making the UAV extremely

small, such as quad-copters, or by conventional winged vehicles that can be disassembled and packed. In general, the payload capacity of these types is limited. The challenge lies in achieving an easily transportable design capable of carrying a useful payload while successfully performing its mission in varying flight conditions[7].

In Military service, small sized UAV's have become an essential part of daily operations. Often referred to as "tactical" UAV's, typical missions include reconnaissance, surveillance, target acquisition, damage assessment, and battle management. They are often carried in a backpack and then launched either by hand or else with the assistance of a bungee. Tactical UAV's generally operate below 18,000 feet altitude and have a maximum range of less than 100 miles. The military classification of a tactical UAV is more generally defined as "Tier I". Specific examples include the General Atomics GNAT 750 (Air Force), AeroVironment RQ-14 Dragon Eye (Marine Corp), and AeroVironment RQ-11 Raven (Army). While most hand launched UAV's generally operate below 18,000 feet, the Tier I classification does include some air vehicle that can reach altitudes up to 30,000 feet. The General Atomics IGANET-ER is operated by the U.S. Army and has a service ceiling of 30,000 feet. It also has the capability of launching the AGM-114 Hellfire and FIM-92 Stinger guided missiles from underwing hardpoints [7].

A unique design concept exists that would fulfill the need for an easily packable UAV as well as offer an alternative solution to several design challenges that hinder the expansion of UAV roles at high altitudes. It has been proposed to design a foldable wing of delta-type planform made of highly flexible material such as Polyimide film[14]. The primary advantage of a highly flexible delta-type wing is that it naturally lends itself to a

variety of packing options while maintaining light weight and durability. Such a wing is uniquely suitable to a portable UAV design because the delta shape allows for a system of folding spars hinged at a single fuselage location. This concept is termed a “parawing” in that it combines the lifting properties of a traditional wing with the flexibility of a parachute. It was first seriously investigated for use in space capsule recovery by Francis Rogallo, an engineer with NASA, in the early 1950’s. In the context of UAV operations, the parawing concept could be applied to several of the portability and deployment challenges encountered in missions such as high altitude flight and low-level tactical reconnaissance, rendering some unique solutions.

Specifically, a UAV employing a flexible wing could potentially be air-dropped by another aircraft or balloon, and possibly boosted to operating altitude on a rocket for extreme high altitude flight. In the case of HALE vehicles such as Helios, these deployment methods could provide the capability to avoid much of the low altitude atmospheric turbulence that can compromises light structures. When applied to small tactical UAVs, flexible delta wings could eliminate the need to disassemble the vehicle in order to pack and transport it.

1.2 Motivation and Significance

Several key obstacles stand in the way of implementing a flexible delta wing design. The most significant obstacle is that, at low speeds, delta wings generally have poor aerodynamic performance characteristics compared to higher aspect ratio wings. The maximum lift-to-drag ratio, also known as aerodynamic efficiency, is much lower

than that of conventional wings. This is of critical importance in performance terms since the range of a propeller driven aircraft (typical of UAVs) is directly proportional to its maximum lift-to-drag ratio[2]. While a flexible wing is of great benefit to efficient packing and deployment, it renders the wing trailing edge unsuitable for conventional control surfaces. In order to achieve truly functional UAV design that implements the flexible delta wing concept, the inherent deficiencies relating to aerodynamic performance and means of control must be addressed.

A solution exits in the form of leading edge vortex flaps (LEVF). LEVF devices have been shown to improve delta wing aerodynamics by reducing drag and increasing the maximum lift-to-drag ratio[1]. Such flaps are particularly effective when applied to slender delta wings with large leading edge sweep angles. In general, slender delta wing aerodynamics are characterized by a vortex flow pattern that forms when the oncoming flow separates over the leading edge. The net effect of this vortex is to create a region of suction on the wings upper surface that increases drag as well as lift. LEVF devices have the ability to position the leading edge vortex such that the force vector due to suction is tilted forward in the direction of flight, adding a thrust component and effectively reducing drag. Previous research and testing indicates that an LEVF system consisting of single or possibly multiple elements could be used to increase the lift-to-drag ratio by as much as twenty percent[1]. There is also potential to utilized LEVF devices to provide longitudinal and lateral control in the absence of conventional control surfaces. This configuration would facilitate the flexible wing concept, keeping control actuators and support structure localized along the leading edge while allowing the wing to neatly fold back along the fuselage.

Although some research has been conducted on the aerodynamic properties of flexible delta wings, there currently lacks supportive computational and experimental data investigating the potential for improved performance through application of LEVF devices[14]. Additionally, it is unknown whether the success of LEVF devices in improving slender delta wing performance could be extended to non-slender delta wings. The lack of knowledge regarding the performance of LEVF devices as applied to any type of delta wing at low speeds presents a final unknown. Without concrete data, effective application of LEVF devices to flexible delta wings is difficult.

1.3 Research Objectives

Consequently, the current research sought to gain a better understanding of the effects of leading edge vortex flaps on both slender and non-slender delta-type wings at low velocities. The primary objectives were as follows:

a) Design a leading edge vortex flap that attains meaningful improvement in aerodynamic efficiency for slender and non-slender delta wings at low speeds.
b) Determine the potential for using LEVF devices as a primary method of flight vehicle control.

While wing flexibility was not taken into account, this research generated data documenting the effects of LEVF devices on delta wings operating at the low speeds expected to be typical for flexible delta wings. The primary research goal was to propose

an LEVF design that could potentially address the aerodynamic and control challenges facing the foldable delta wing concept.

Previous research on a slender, highly flexible sixty degree delta wing showed that a maximum lift coefficient on the order of 1.3 and a maximum lift-to-drag ratio on the order of fourteen are attainable[14]. It is projected that gains of up to twenty percent in maximum lift-to-drag ratio can be achieved by incorporating LEVF devices[1]. As state above, range is directly proportional maximum lift-to-drag ratio. Consequently, range could potentially be improved by the same factor. If LEVF devices can provide the projected improvements in aerodynamic performance and control, the flexible delta wing concept could find multiple applications such as increasing the altitude capability of HALE class UAVs and further improving the ease of packaging and deployment for small UAVs performing localized reconnaissance for the military.

1.4 Thesis Overview

This thesis presents the results of research that was conducted with the goal of designing a leading edge vortex flap for a delta-type wing at low speeds. Computational Fluid Dynamics (CFD) was the primary means of investigation. The first phase of the project was focused on analyzing the relative performance of selected 2D flap geometries. The most effective combination of design variables was down selected and incorporated into a 3D flap model for further analysis. The second project phase involved 3D analysis of the selected flap design in combination with two different delta wing models; one with 30 degrees of leading edge sweep and one with 60 degrees. Each wing

–flap combination was assessed based on maximum lift, aerodynamic efficiency, and moment behavior. Upon completion of the CFD analysis, post processing was performed in order to better understand the flow behavior primarily responsible for the observed flap performance. A final flap design was selected and predictions were made regarding both real world performance as well as potential flap applications.

CHAPTER 2: METHODOLOGY

The research was conducted in two stages: flap design and performance analysis. Design of the flap was carried out primarily with the aid of CFD and focused on varying the flap geometry to achieve the best aerodynamic efficiency. The test model was designed to replicate both in dimension and Reynolds number the flexible delta wing model used in previous research conducted by Mathew Warchol (Ref. 13). Initial worked involved understanding how several geometric design variables effected the lift and drag of a 2D cross section. These variables were flap length, curvature, and gap. For each cross section, aerodynamic data was collected at angles of attack ranging from 0 to 16 degrees. Using this data, a single flap cross section was chosen based on relative advantage in both aerodynamic efficiency and stall behavior. The chosen flap cross section was then incorporated into a 3D model for analysis that focused on determining an appropriate flap deflection for best aerodynamic overall efficiency. The flap was designed as a single surface spanning the length of the wing leading edge. Once the most effective deflection angle was found, it was selected as the cruise condition and flap deflection was redefined as zero at the chosen angle.

Performance analysis of the flap assessed the lift, drag, aerodynamic efficiency, and moment characteristics of the final flap design. The flap/wing combination was compared to a reference wing as well as existing experimental and computational data in

order to validate the current results and to determine the relative incremental increase in performance due to the flap. The effects of the flow on flap performance was explored by comparing the 2D cross sectional performance to the 3D results and utilizing flow visualization to better understand the underlying fluid mechanics. In order to examine the potential for using the flap system as a primary mean of control, a study of longitudinal moment behavior was conducted by varying the flap deflection angle and examining the changes in moment with angle of attack. Upon completion of the performance analysis, conclusions were made regarding the overall effectiveness of the flap design in achieving the research goals along with suggestions for future work.

2.1 Delta Wing Lift

Delta wings possess unusual aerodynamic properties in comparison to the various planforms that have taken to the air since the Wright brothers first achieved powered flight in 1903[2]. Usually classified as either slender or non-slender based on leading edge sweep angle, delta wings have been particularly useful in high speed applications. High speed aircraft have made particular use of slender delta wings with leading edge sweeps of 60 degrees or greater since, at supersonic Mach numbers, delta wings have proved quite successful at minimizing wave drag[6].

At subsonic speeds, slender delta wings experience an aerodynamic phenomenon that results in the development of a “leading edge vortex” which provides additional lift. For angles of attack greater than 5 degrees, vortex lift results from the boundary layer

separating at the leading edge (especially if it is sharp) and rolling up into a primary and secondary vortex on the upper wing surface as depicted in Figure 1[12].

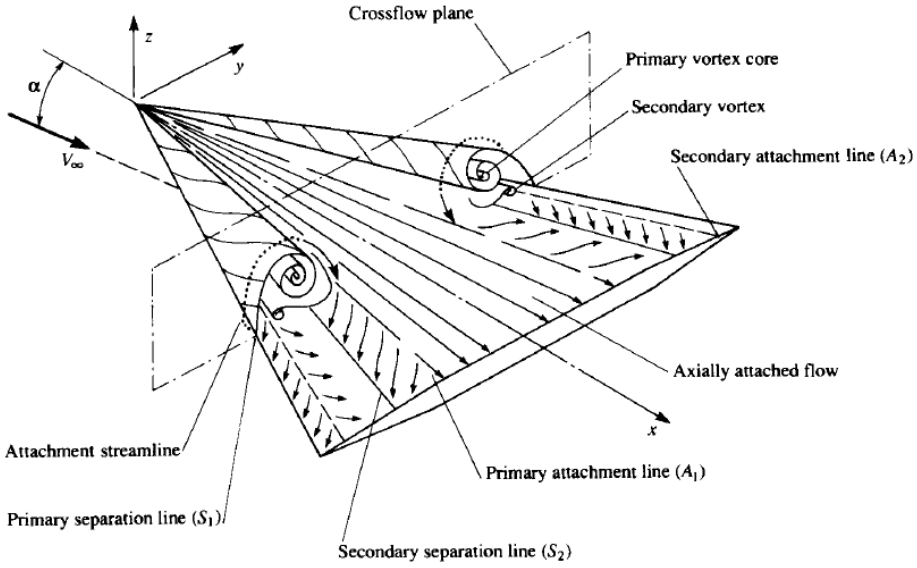

Figure 1: Subsonic Flow Field over a Slender Delta Wing

The vortex is characterized by high rotational velocities at its core and low static pressure which is translated into additional "vortex" lift. Slender delta wings have been found to benefit from this extra lift well past angles of attack where conventional wings experience flow separation leading to stall. Beyond some critical angle of attack, however, the vortex will "burst" or breaks down accompanied by an increase of static pressure and a loss of lift[8]. Using potential flow theory based on linearization of the Navier-Stokes equations as well as a hypothesis first put forward by E.C. Polhamus in 1971, the total lift of a delta wing can be described in terms of potential lift and vortex lift[10]. Figure 2 shows a plot of potential and vortex lift versus angle of attack. At high

angles of attack, the vortex lift accounts for approximately half of the total lift of a delta wing.

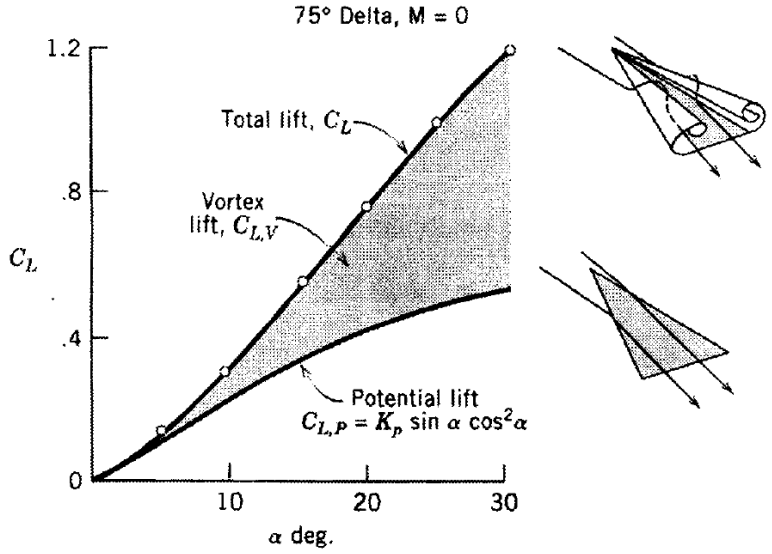

Figure 2: Total Lift of a Delta Wing

According to Polhamus, vortex lift can be attributed to the fact that the flow stagnation line at the wing leading edge has rotated the leading edge suction 90 degrees to the upper wing surface, creating additional lift. In other words, the increment in lift (L_V) is equal to the thrust component of the leading edge suction force (S) by the following relation:

$$L_V = S\cos\alpha = T\frac{\cos\alpha}{\cos\Lambda} \qquad \text{(eq. 1)}$$

Where T is the thrust force oriented in the freestream direction and Λ is the wing sweep angle. The magnitude of the suction force for a two dimensional cross section can be written as:

$$S = \rho V_\infty \Gamma \sin\alpha \qquad \text{(eq. 2)}$$

Using an effective circulation (Γ) and delta wing span (b_e), the thrust force is written as:

$$T = \rho \Gamma b_e (V_\infty \sin\alpha - w_i) \qquad \text{(eq. 3)}$$

Where w_i is an induced velocity. The lift increment and thrust component are then written as coefficients using the dynamic pressure (q_∞) and referenced to the wing area (A_w);

$$C_T = \frac{T}{q_\infty A_w} = \left(1 - \frac{w_i}{V_\infty \sin\alpha}\right) \frac{\rho \Gamma b_e V_\infty \sin\alpha}{\frac{1}{2}\rho V_\infty^2 A_w} \cdot \frac{\sin\alpha}{\sin\alpha} = \left(1 - \frac{w_i}{V_\infty \sin\alpha}\right) K_P \sin^2\alpha \qquad \text{(eq. 4)}$$

$$\text{where:} \qquad K_P = 2 b_e \Gamma / A_w V_\infty \sin\alpha \qquad \text{(eq. 5)}$$

The potential flow lift coefficient can be written as:

$$C_{L,P} = C_{N,P} \cos\alpha = K_P \sin\alpha \cos^2\alpha \qquad \text{(eq. 6)}$$

Combining equations (1) and (5), the vortex lift coefficient can be written as:

$$C_{L,V} = C_{N,V} \cos\alpha = \left(1 - \frac{w_i}{V_\infty \sin\alpha}\right) K_P \sin^2\alpha \frac{\cos\alpha}{\cos\Lambda} = K_V \sin^2\alpha \cos\alpha \qquad \text{(eq. 7)}$$

Combining equations (6) and (7), the coefficient for total lift of a delta wing can be expressed as:

$$C_L = C_{L,P} + C_{L,V} = K_P \sin\alpha \cos^2\alpha + K_V \cos\alpha \sin^2\alpha \qquad \text{(eq. 8)}$$

The constants appearing in equation (8) have been tabulated and plotted as a function of delta wing aspect ratio defined as b_e^2/A_w. This plot is provided in Figure 3 courtesy of NACA[8]

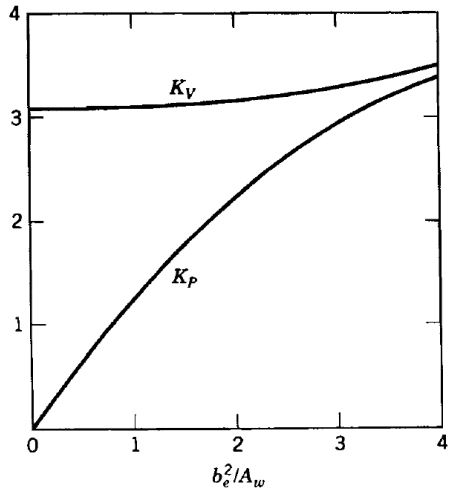

Figure 3: Vortex and Potential Lift Coefficients

While vortex lift is undoubtedly a positive characteristic of slender delta wings, it comes at the cost of increasing induced drag[12]. Induced drag is the result of the vortex lift vector tilting slightly to the rear and contributing a component of drag. A shifting of the lift vector generally results from downwash over the wing changing the effective angle of attack but is also exacerbated by fact that delta wings have a shallower lift curve slope and must therefore cruise at a higher angle of attack.

A solution to this problem was found by drooping the leading edge in such a manner that the vortex is moved further forward, and the lift force resulting from the suction is tilted forward contributing a component of thrust in the direction of flight. While some delta wing aircraft designs such as the Convair F-106 have incorporated

permanent droop into the wing leading edge (cambered leading edge), it is most often achieved by means of a hinged leading edge, termed a leading edge vortex flap or LEVF. The benefit of such flaps has been validated in both testing and practical application[1]. LEVF devices have frequently been used to improve the aerodynamic efficiency of delta wing aircraft at moderate subsonic speeds, particularly when the wing sweep is in excess of 60 degrees. Using flap deflections between 10 and 15 degrees, the aerodynamic efficiency of an otherwise flat delta wing can be improved by as much as 10 to 20 percent[12].

Stall for a slender delta wing is related to the breakdown, or bursting, of the leading edge vortex. For angles of attack between zero and approximately 6 degrees, the flow over a delta wing is fairly smooth without excessive separation. As the angle of attack increases beyond 6 degrees, the flow tends to separate cleanly at the leading edge and roll up into a primary a vortex. At low angles of attack, the vortex positioned over a delta wings upper surface continues downstream from the wing, gradually losing energy until it breaks down at some distance behind the wing. As the angle of attack increases, the location of vortex breakdown moves closer to the wing trailing edge. Stall begins to occur when the vortex moves onto the upper wing surface. For slender delta wings, this generally occurs at an angle of attack on the order of 30 degrees or higher[1]. Unlike wings of higher aspect ratio, stall manifests its self as a gradual loss of lift caused by the vortex losing energy and the static pressure rising. Non-slender delta wings stall in a manner more typical of conventional wings. Due to the instability of the leading edge vortex, breakdown occurs at a much lower angle of attack.

2.2 Computational Fluid Dynamics Background

For the present research, CFD served as the primary means of investigation and analysis. CFD is a method of numerically approximating the physical behavior of fluids based on three fundamental conservation laws: conservation of mass, momentum, and energy. The conservation laws, commonly referred to as the Navier-Stokes equations are commonly cast in integral form and approximated with finite volume expressions. The resulting algebraic equations can be iteratively solved over a spatially discretized domain[3].

2.3 Fluid Model

The fluid model is of great importance in CFD. It defines how the various phenomena of fluid dynamics are approximated in order to converge to a solution and achieve numerical results. The current research was primarily interested in viscous, low-speed, low Reynolds number flow where the assumption of incompressibility was valid and the Mach number was essentially zero[1].

Within the fluid model, the representation of turbulence is extremely important. A flow is turbulent when it is characterized by three-dimensional unsteady random motion. Full numerical simulation of turbulence is generally not practical, and so many turbulence models have been developed to produce smooth variations in flow properties by filtering out turbulent structures using averaging procedures such as Reynolds-

Averaging[4]. Of these models, the k-ε turbulence model has been widely used in engineering applications due to its robustness and good accuracy across a wide range of flow types[5].

Because of its proven results, the k-ε model was chosen for the current research. The k-ε model is also a fairly economical model in terms of the required computing power to reach a solution. This is due to the fact that it simplifies the problem by using a Reynolds Averaging procedure on the Navier-Stokes equations. The role of the turbulence model is to solve for the additional unknowns introduced by the averaging procedure. The k-ε model handles the extra variables (termed Reynolds Stresses and Fluxes) by making use of two additional transport equations as well as an Eddy-Viscosity.

The basic k-ε model comes in several variants, one of which – the Realizable k-ε-Model is particularly recommended for its ability to better predict boundary layer separation. Additionally this model can be run with Enhanced Wall Treatment that allows for smaller y+ values (finer grid resolution) near the wall[4]. While some experimentation with other models was conducted, the Realizable k-ε model with Enhanced Wall Treatment was used for all results presented in this report. Table 1 provides a summary of the fluid model settings used for this research.

Table 1: CFD Fluid Model

Conditions	Sea Level, Incompressible
Freestream Velocity	10.78 m/s
Reynolds Number	300,000
Turbulence Model	k-ε , Realizable, Enhanced Wall Treatment
Solver	2^{nd} order, Upwind Scheme
Courant Number	$5 \leq CFL \leq 200$ (Utilized Solution Steering)
Convergence Criteria	Residuals for Continuity, x & y Velocity, k, and epsilon $\leq 1 \times 10^{-6}$

2.4 Physical Model

Both 2D and 3D computer generated models were constructed to represent the geometry of interest and used as the basis for CFD modeling. All geometry construction and meshing was done with ANSA, an advanced computer automated engineering (CAE) pre-processing tool produced by Beta CAE Systems. The 2D models were used primarily to investigate the relative effects of manipulating specific geometric variables. The 3D models were constructed in greater detail and used to predict aerodynamic performance and model velocity flow fields.

In order to isolate the best combination of LEVF geometric properties in terms of aerodynamic performance, three primary variables were chosen to be tested on a series of 2D cross sections. These variables, listed in Table 2, were flap chord length, flap curvature (defined as a radius), and slot size. Each variable was non-dimensionalized in terms of the same reference length drawn from the primary delta wing models Mean

Aerodynamic Chord (MAC) which was 0.4064 meters. All flap designs had the same thickness: 0.5 percent of the MAC.

Table 2: Two-Dimensional Design Variables

Flap Chord Length	4 %, 8 %, 12 %
Flap Radius of Curvature	Straight (∞), 22.1 %, 9.8 %, 8.6 %, 7.1 %, 5.2 %
Slot Size	1.2 %, 2.3 %, 3.5 %
Airfoil Angle of Attack	0° to 16°

*** Values are listed as a percent of the wing MAC (0.4064 m)

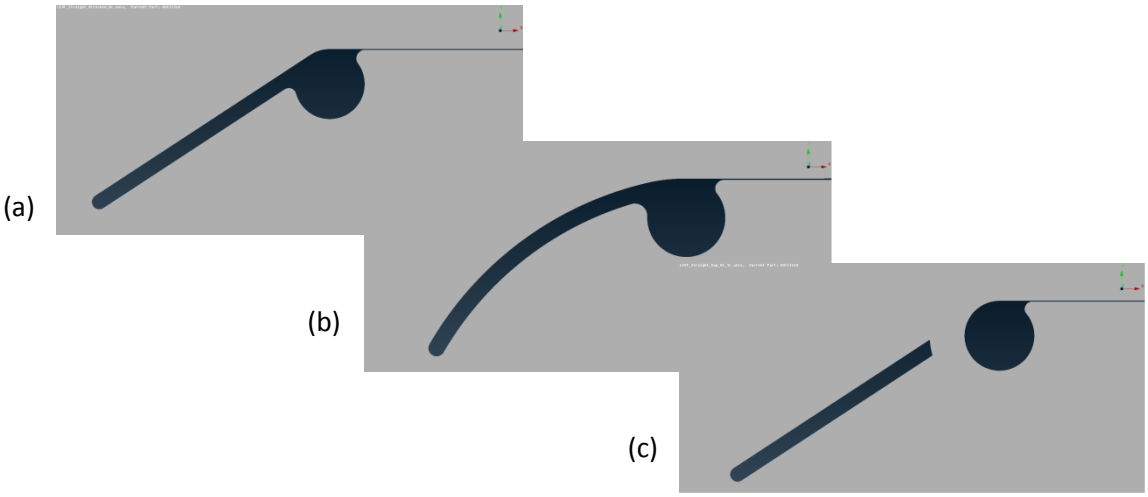

Figure 4 (a-c): Two-Dimensional Flap Cross Sections

The flap chord length, measured from the center of the leading edge spar to the flap leading edge, was tested on a straight flap in lengths equal to 4, 8, and 12 percent of the wing MAC. This flap design is depicted in Figure 4 (a). Flap curvature was modeled using a constant radius of curvature that created an arc connecting the wing upper surface, directly over the spar centerline, to the flap leading edge. For all tests involving

curvature, the flap chord length was held constant at 8 percent of the MAC. (Figure 4b) The slotted geometry was based on the straight flap design with a gap added between the flap trailing edge and the wing spar. The flap chord length was also held constant at 8 percent of the MAC.

The 3D CFD analysis focused on studying the effect of adding LEVF devices to delta wing models with both 30 and 60 degrees of wing sweep. For each wing sweep case, four different wing models were constructed. Due to symmetry of the wing and expected flow field about the central axis, only half of the wing was modeled. The basic design shape and dimensions for each wing (with the exception of the baseline wing) was based on the CFD model used in the work of Whitfield and Warchol (Ref. 14) as presented in Chapter 1. Each flap model was designed with 30 degrees of positive (downward) deflection.

The four models included (1), a baseline flat-plate wing, (2) a reference wing without a flap, (3) a wing with an attached flap, and (4) a wing with a slotted flap. Since the same model designs were used for both cases of wing sweep, only the 60 degree sweep models are shown below.

1) **Flat-Plate Wing:** The flat plate, shown in Figure 5, model consisted of a uniformly flat wing with rounded edges. It was approximately 3 percent thick. (referenced to the wing MAC).

Figure 5: Sixty Degree Flat-Plate Wing

2) **Reference Wing:** The reference model was constructed to resemble the flexible winged UAV design used in the work of Whitfield and Warchol. It consisted of a tube spar running the length of the leading edge and a thin, film-like wing surface extending rearward to a free trailing edge. The surface, meant to approximate a flexible material such as ploymide film[14], had a thickness of approximately 0.019 percent of the wing MAC. (Figure 6)

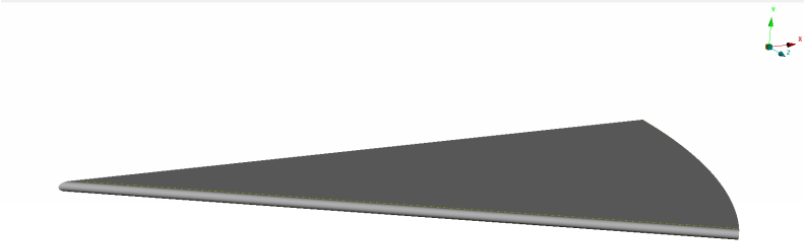

Figure 6: Sixty Degree Reference Wing

3) **Wing with an Attached Flap:** The attached flap was simply an extrusion of the 2D flap cross section that was fused to the reference wing models leading edge (described above). No effort was made to model hinge mechanisms.

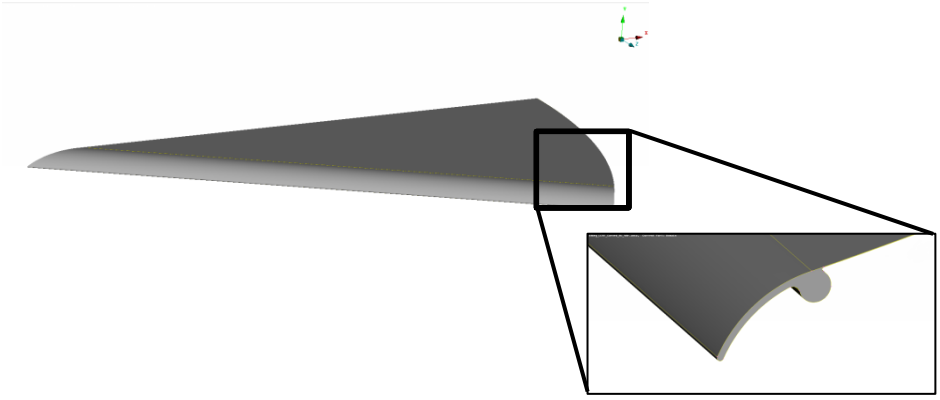

Figure 7: Sixty Degree Wing with Curved Flap

4) **Wing with a Slotted Flap:** The slotted flap was also a simple extrusion of the corresponding 2D cross section, although it was not connected in any way to the reference wing geometry. Unlike the 2D analysis which analyzed only a straight slotted flap, curvature was added for the 3D analysis.

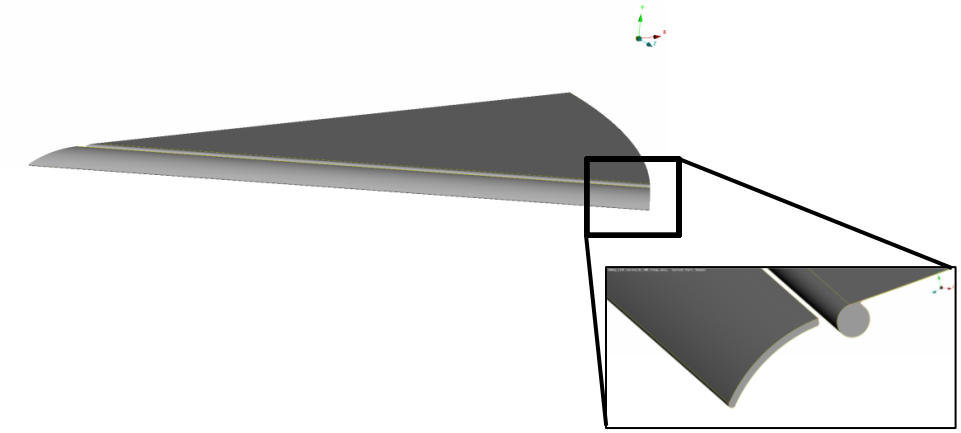

Figure 8: Sixty Degree Wing with Slotted Flap

2.5 Mesh Generation

Mesh design is an important aspect of CFD in terms of solution accuracy and flow field resolution. When designing a mesh, special attention must be given to the overall

shape of the domain, the type of boundary conditions used, the grid resolution near the wall (the model surface), and mesh quality metrics. One of the primary challenges of building a mesh is balancing the desire for flow accuracy with the need for a reasonable computation time. This problem is inherently linked to the amount of computing power available[5].

Since the present research was focused on the external aerodynamics of a wing in an un-bounded flow, a C-type mesh (Figure 9) was considered most efficient[4]. With this type of mesh, the inlet boundary conditions could be varied without making any adjustments to the mesh or model. Both the 2D and 3D meshes were un-structured and made use of quad type elements. The mesh-specific details are given in Table 3.

Table 3: CFD Mesh Parameters

Domain	Un-structured C-Mesh, with Quad Elements
y+	1 - 30
2D Cell Count	75,0000- 100,000
3D Cell Count	$2 \times 10^6 - 2.4 \times 10^6$
Num. Iterations (2D)	600 - 1000
Num. Iterations (3D)	400 – 700

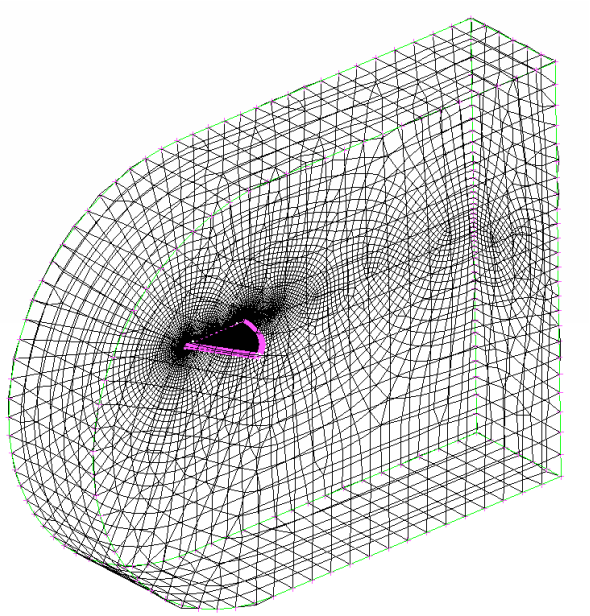

Figure 9: Three Dimensional C-Mesh

A frequently used method of measuring grid resolution near the wall is the y^+ metric. It is the non-dimensional distance of the first cell height at the wall[4].

$$y^+ = \frac{u_* y}{\nu} \qquad \text{(eq. 9)}$$

The geometric distance (y) is made dimensionless with the frictional velocity (u_*) and the kinematic viscosity (ν). Typically, the k-ε turbulence model with standard wall functions requires that y^+values be greater than 30, limiting the resolution and potentially the accuracy of the boundary layer solution. By making use of the Enhanced Wall Treatment, the present research was performed using y^+values on the order of 1 at the wall with 3 layers of prism cells in the boundary region. Figure 10 shows the general design of the mesh close to the wing surface[4].

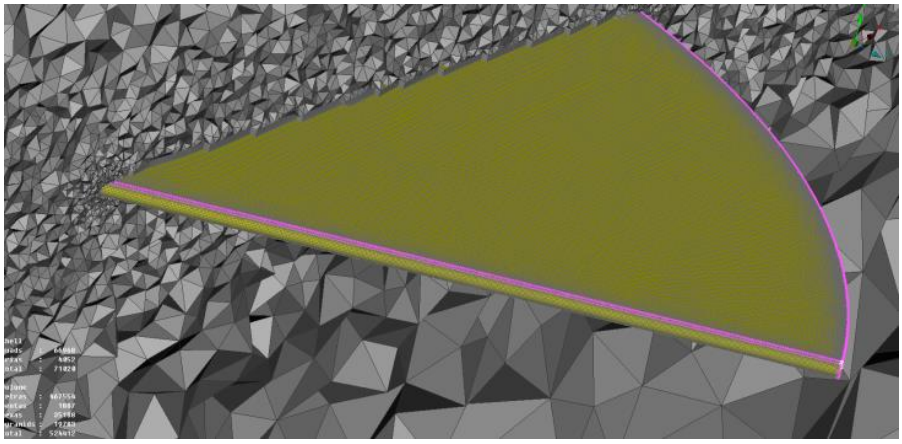

Figure 10: Finite Volume Mesh

2.6 Design Process

The procedure followed in producing the final LEVF design was divided into three main parts: 2D analysis, 3D analysis, and post processing. Upon finishing each major project segment, the obtained results were analyzed and down selection of the flap geometry was performed. Once the 2D analysis was completed, the cross sectional design was frozen and then applied to the 3D geometry. In addition to examining the general performance of the complete flap design, the 3D analysis also tested the relative performance of the flap at various deflection angles. The post processing phase sought to understand the underlying flow mechanics driving the flap performance and to make predictions regarding its real-world performance.

CHAPTER 3: NUMERICAL RESULTS

3.1 Two-Dimensional Analysis

The purpose of the 2D analysis was to explore the relative effects of the chosen design variables on the performance three basic flap designs: straight, curved, and slotted. The design variables are listed in Table 2 of Chapter 2. As described in the previous chapter, each 2D flap profile was connected to a wing cross section designed to match that of the 3D reference wing model at its MAC location.

In the interest of validating the computational model, the reference cross section was first analyzed without a flap and the resulting plot of lift versus angle of attack compared to a lift curve representative of thin airfoil theory. The reference cross section was essentially a flat plate with a rounded leading edge as was expected to produce flow behavior similar to a very thin airfoil. This plot is given in Figure 11. The lift curve slope of the representative "flat plate" airfoil was set at 0.11 per degree.

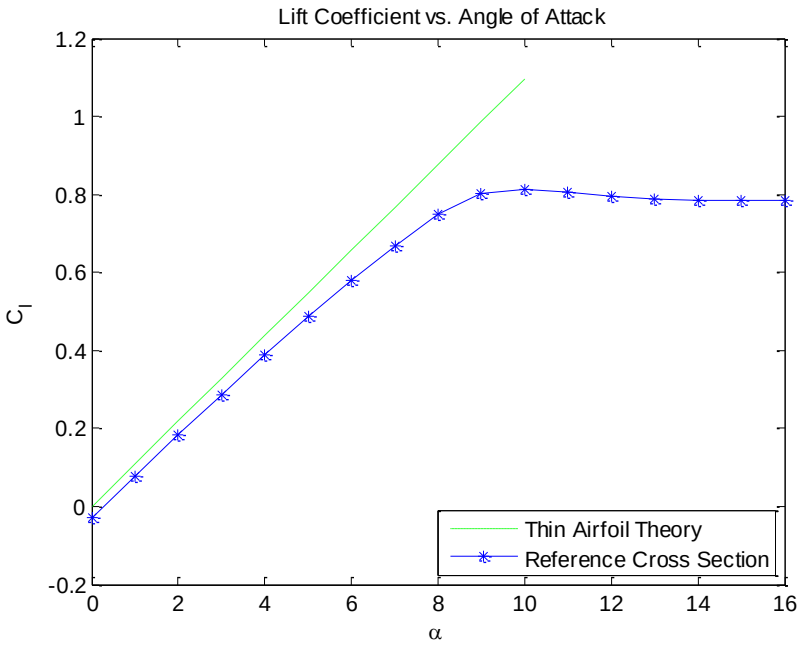

Figure 11: Thin Airfoil Theory Comparison to 2D Cross Section

While the lift curve slope of the 2D reference cross section was somewhat shallower than the flat plate baseline curve, the discrepancy was likely a result of the CFD solution predicting a smaller pressure differential at the leading edge. At small angles of attack (where thin airfoil theory is valid), the lift slopes were almost identical[1].

Exploration of flap cross sectional geometry began by first examining the effect of flap chord length on the aerodynamics of a simple, straight flap set at 30 degrees of deflection. Three flap lengths were chosen based on a percentage of the reference wing chord length. The lengths were 4, 8, and 12 percent, each with the same thickness of 0.5 percent of the reference chord. Figure 12 (a-c) shows the straight flap cross sections.

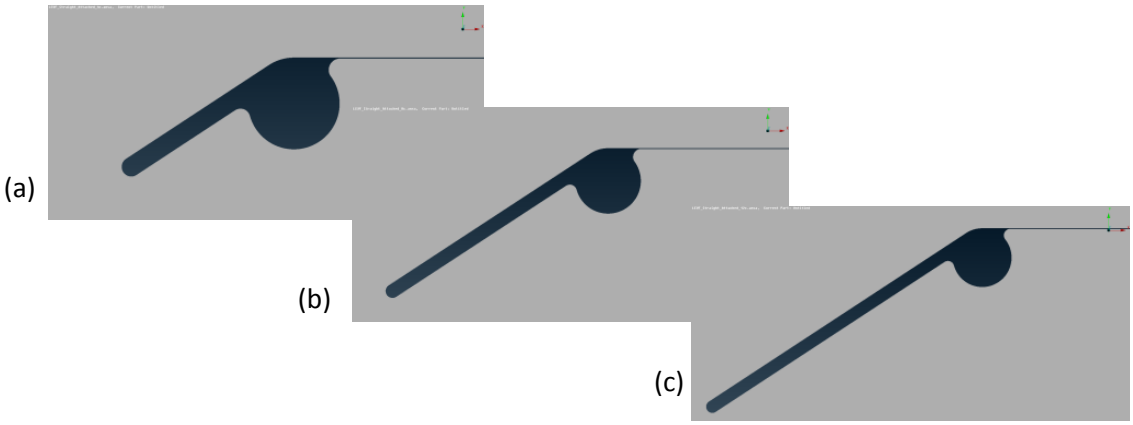

Figure 12: Two-Dimensional Cross Sections of Varying Lengths

The result of varying the length of the straight leading edge flap was primarily seen in the zero lift angle of attack, the maximum lift coefficient, and the stall behavior. As would be expected, Figure 13 clearly shows that addition of a flap to the reference configuration produced an immediate increase in the maximum lift coefficient. This trend was a result of the new, "effective" chord line and increased camber of the complete cross section. The 4 percent chord length resulted in a $C_{l,max}$ that was 12.5 percent greater than that achieved by the reference configuration. The 8 percent chord length increased $C_{l,max}$ by an additional 5.8 percent while further lengthening of the flap resulted in a decrease in $C_{l,max}$. It is interesting to note that the maximum lift coefficient corresponding to each flap length occurred at the same angle of attack. This was due to the fact that increasing the flap length changed the effective chord length but left the camber relatively constant.

Variations in the flap length did, however, correspond to changes in the angle of attack effectively "seen" by the cross section. This was manifested by the zero lift angle of attack gradually becoming more positive as the flap length was increased. Given that

the angle of attack corresponding to $C_{l,max}$ remained constant for each flap length, the lift curves became increasingly non-linear with lengthening of the flap. Unlike the reference configuration which produced an essentially constant lift coefficient upon reaching $C_{l,max}$, each flap case resulted in stall behavior typical of airfoils with camber. In all cases, the stall was fairly gentle, although the 8 and 12 percent cases witnessed a slight increase in lift coefficient after the initial stall.

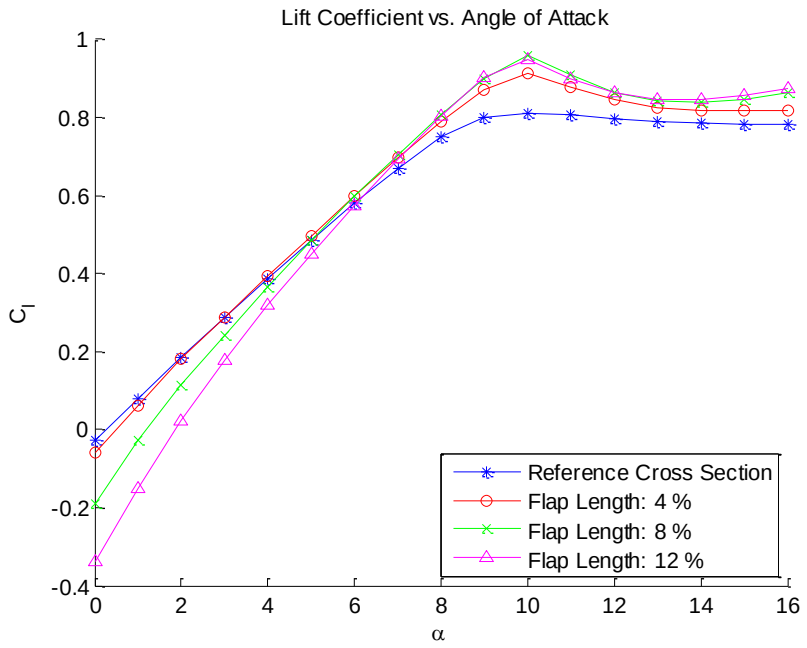

Figure 13: Two Dimensional Cross Sections - Length Comparison - Lift

Figure 14 shows the drag polar for the straight flap geometries. The flap with a length corresponding to 4 percent of the reference chord was found to have the best minimum drag coefficient but at a relatively low lift coefficient. The 8 and 12 percent chord lengths had somewhat larger minimum drag coefficients at successively higher lift

coefficients indicating potential for better lift to drag ratios, or aerodynamic efficiency. In general, the 8 percent chord length demonstrated the best drag characteristics over the widest range lift coefficients.

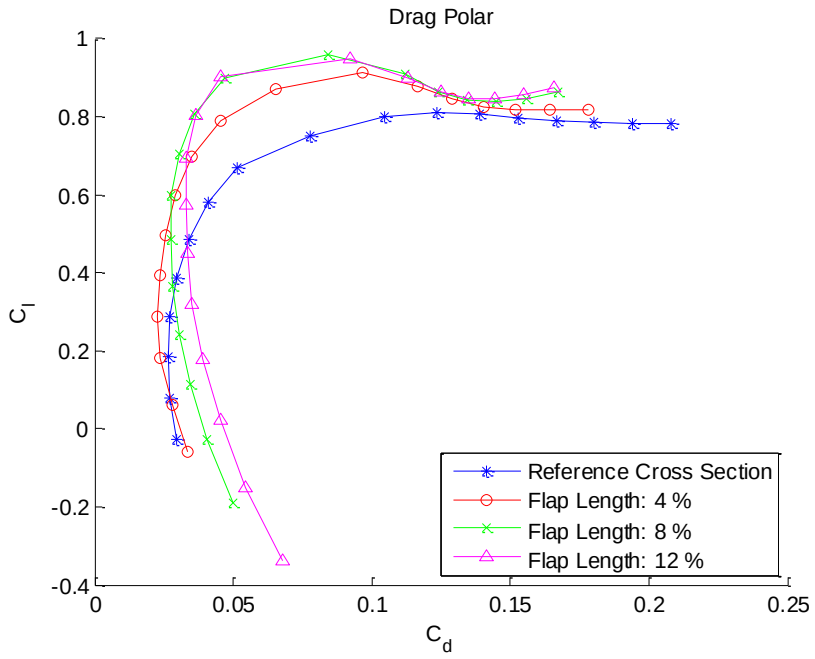

Figure 14: Two Dimensional Cross Sections - Length Comparison - Drag

Plotting aerodynamic efficiency versus lift coefficient as shown in Figure 15 indicated that a flap length of 8 percent chord was best for obtaining maximum aerodynamic efficiency. However, the flap with a 4 percent chord length outperformed the other flap lengths at lower lift coefficients and achieved an improvement in maximum aerodynamic efficiency of 46.1 percent as compared to the reference configuration. While the 8 percent flap did not perform quite as well at lower lift coefficients due to its slightly higher drag, it further improved the maximum aerodynamic efficiency by 17

percent and maintained this advantage at higher lift coefficients. The longest flap configuration (12 percent reference chord) reached a slightly lower maximum value and then fell away quite rapidly.

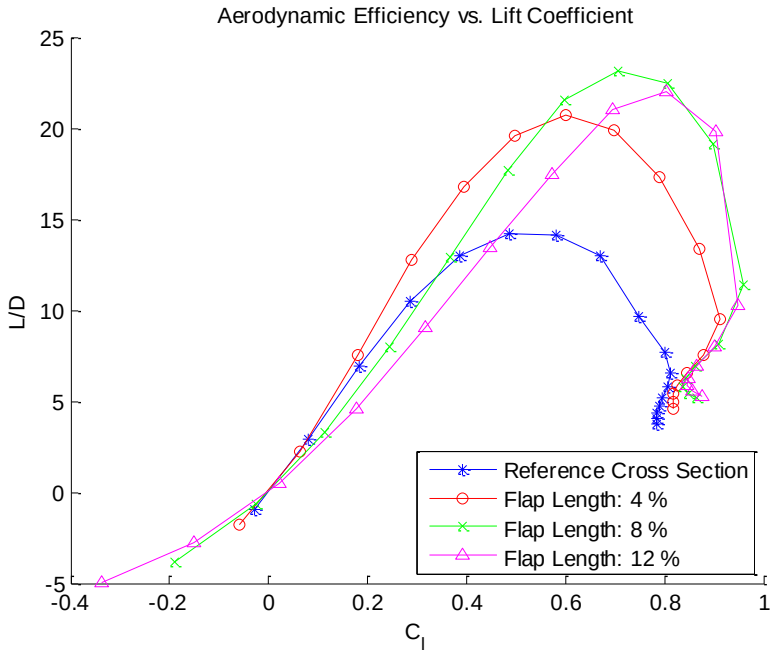

Figure 15: Two Dimensional Cross Sections - Length Comparison - L/D

The moment characteristics of each flap case were assessed in reference to the quarter chord location of the reference cross section. Figure 16 shows that varying the flap length had a pronounced effect on moment behavior. At low angles of attack, moment behavior became increasingly nonlinear and the occurrence of stall at high angles of attack produced increasingly more abrupt shifts in the moment coefficient. All flap lengths tested witnessed a shift from negative moment to positive moment at angles of attack between 5 and 6.5 degrees. The 4 percent chord flap length remained

approximately linear with angles of attack up to 8 degrees while the 8 and 12 percent lengths were roughly linear between the incidence angles 3 and 9 degrees.

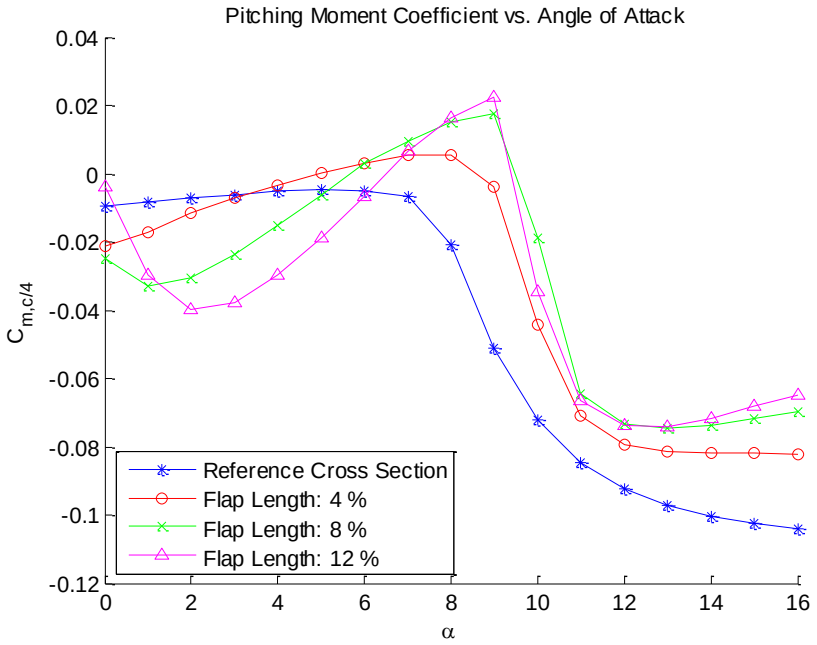

Figure 16: Two Dimensional Cross Sections - Length Comparison - Moment

Upon determining that a flap length of 8 percent of the reference chord provided the best performance in terms of aerodynamic efficiency and lifting behavior, flap length was fixed at this value and testing proceeded to examine the effect of adding curvature to the flap geometry. Curvature was measured in terms of a constant radius with 5 different lengths tested. As shown in Table 2, the lengths were 22.1, 9.8, 8.6, 7.1, and 5.2 all measured as a percentage of the reference chord length.

Adding curvature to the flap produced a significant increase in maximum lift coefficient while preserving a constant slope in the linear region (Figure 17). As the

maximum lift coefficient increased, so did the angle of attack at which stall occurred. The 9.8 percent radius flap produced the greatest increase in maximum lift coefficient; an increase of 55.6 % over the reference configuration. The overall slope of the linear region for the curved geometries was distinctly greater than that of the reference geometry. An increase in slope was reasonable since addition of the flap to the reference cross section effectively increased the overall camber. This made the effective angle of attack slightly negative, resulting in the zero lift angle of attack increasing.

In general, varying the amount of flap curvature produced some conflicting results. The greatest amount of curvature (22.1 percent radius) achieved a lower maximum lift coefficient than the least amount of curvature (5.4 percent radius) which was only slightly curved in comparison the completely flat flap case. However, Radii in between the maximum and minimum did not exhibit any clear trend. The 9.8 and 7.1 percent radii produced almost identical maximum lift coefficients and both achieved the greatest angle of attack before the occurrence of stall. The in between radius of 8.6 percent experienced stall at an earlier angle of attack and did not achieve as high of a maximum lift coefficient.

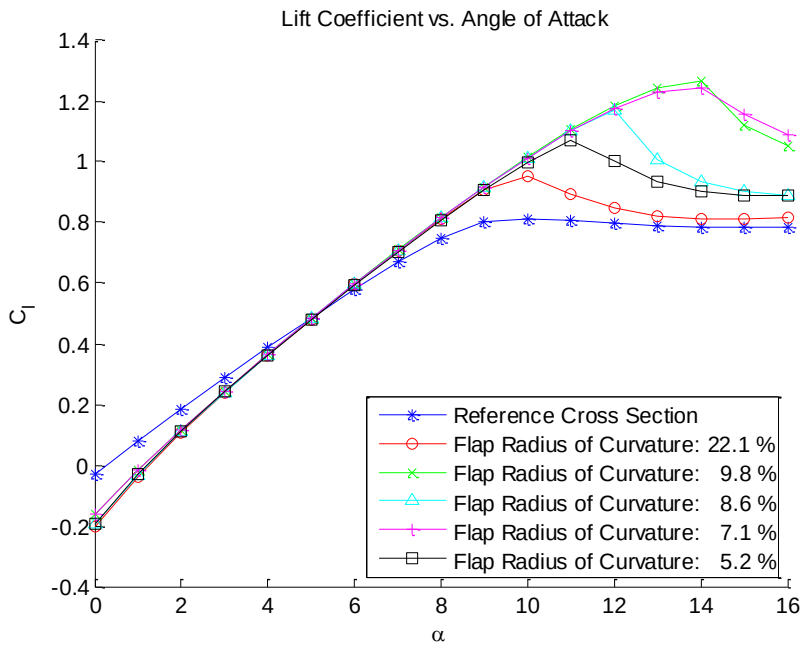

Figure 17: Two Dimensional Cross Sections - Curvature Comparison - Lift

Each curved flap contour produced an almost identical drag polar (shown in Figure 18) with the respective minimum drag coefficients occurring at a similar lift coefficient. For lift coefficients ranging between 0.3 and 0.8, drag appeared to decrease with increasing radius of curvature with the exception of the 8.6 percent case. The flap with an 8.6 percent radius of curvature exhibited the lowest amount of drag over all lift coefficients up to stall.

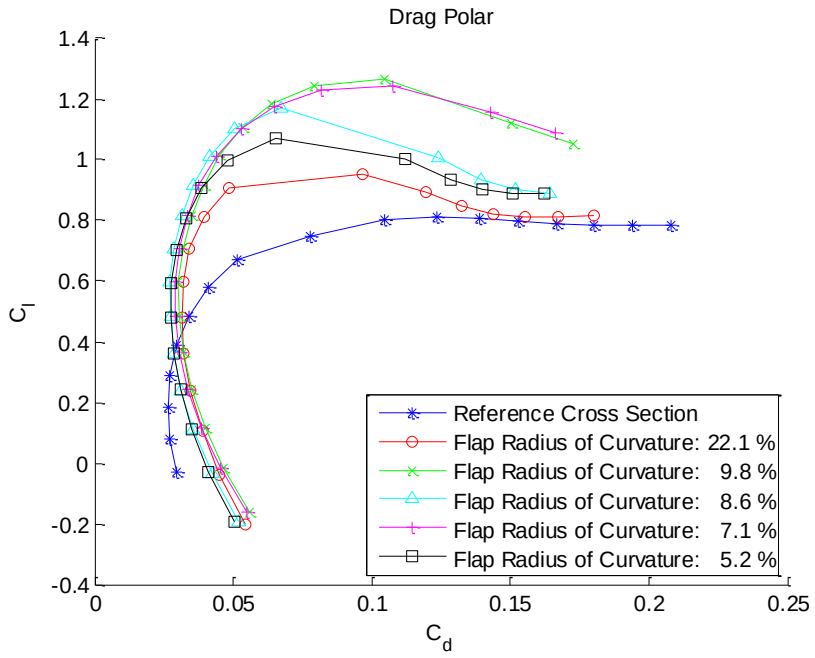

Figure 18: Two Dimensional Cross Sections - Curvature Comparison - Drag

Given that the 8.6 percent case exhibited consistently lower drag than any other radius in the linear region, it is unsurprising that it achieved the greatest maximum aerodynamic efficiency as shown in Figure 19. However, its advantage in aerodynamic efficiency was only marginally better than the 7.1 percent and 9.8 percent cases which extended acceptable values all the way to their respective maximum lift coefficients. All cases produced great improvement over the reference configuration.

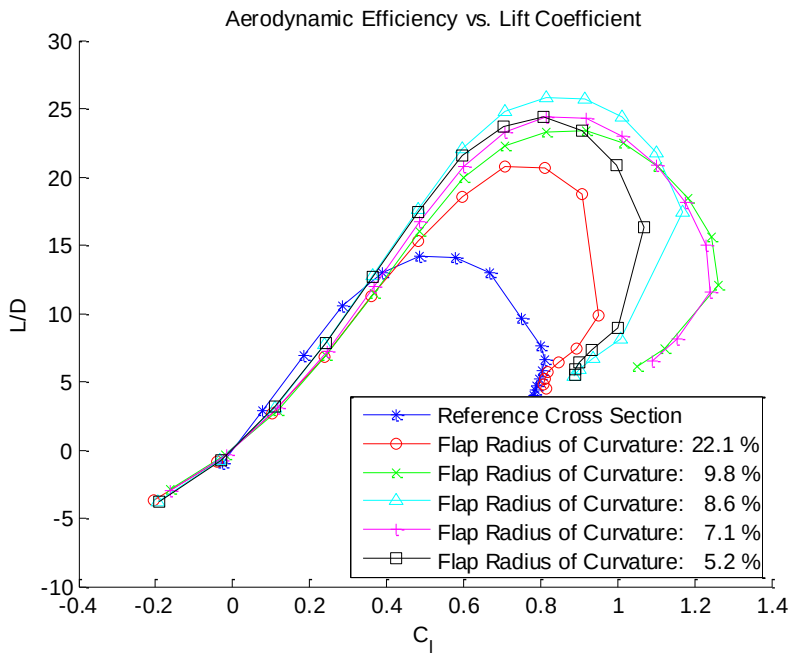

Figure 19: Two Dimensional Cross Sections - Curvature Comparison - L/D

Much like the straight flaps, Figure 20 shows that the curved flap geometries exhibited nonlinear moment behavior at low angles of attack followed by a region of essentially linear behavior. For each case, the linear region began at approximately 2 degrees angle of attack and extended up to the respective stall lift coefficients. For any given angle of attack within the linear region, an increase in curvature corresponded to an increase in moment coefficient. Each moment became positive between 5 and 5.5 degrees angle of attack.

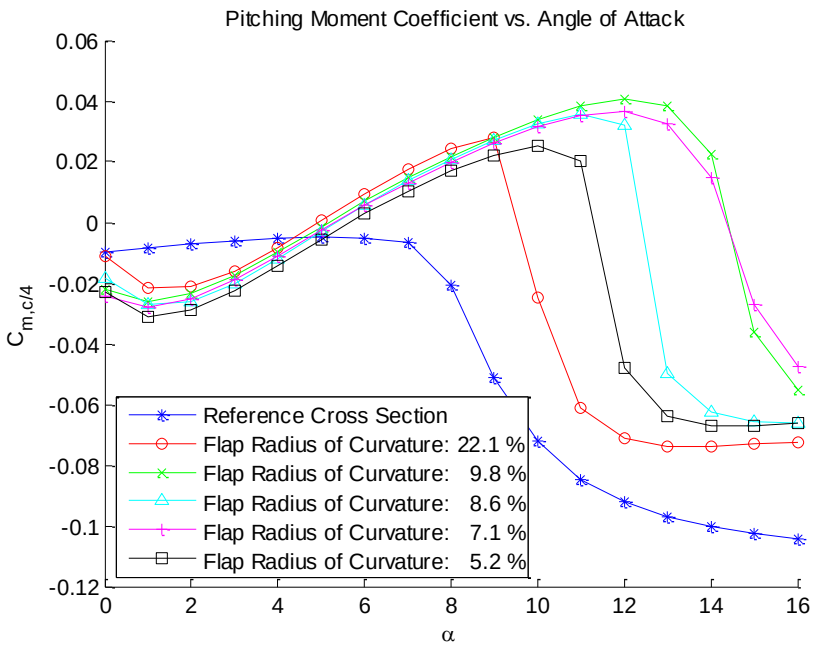

Figure 20: Two Dimensional Cross Sections - Curvature Comparison - Moment

Addition of a slot (or gap) to the flap geometry was generally expected to further improve maximum lift at high angles of attack due to the secondary flow adding extra energy to the primary flow over the upper surface and delaying separation. In actuality, the expected improvements did not materialize, as evident in Figure 21.

All variations of the slotted geometry exhibited gentle stall behavior as would be expected. However, the maximum lift generated by each case fell short of the value attained by the reference configuration. Of the three slot sizes, the 2.3 percent case was most resistant to stall and attained a maximum lift coefficient very close to that of the reference configuration. All three cases had nearly identical zero lift angles of attack and slopes of the linear region.

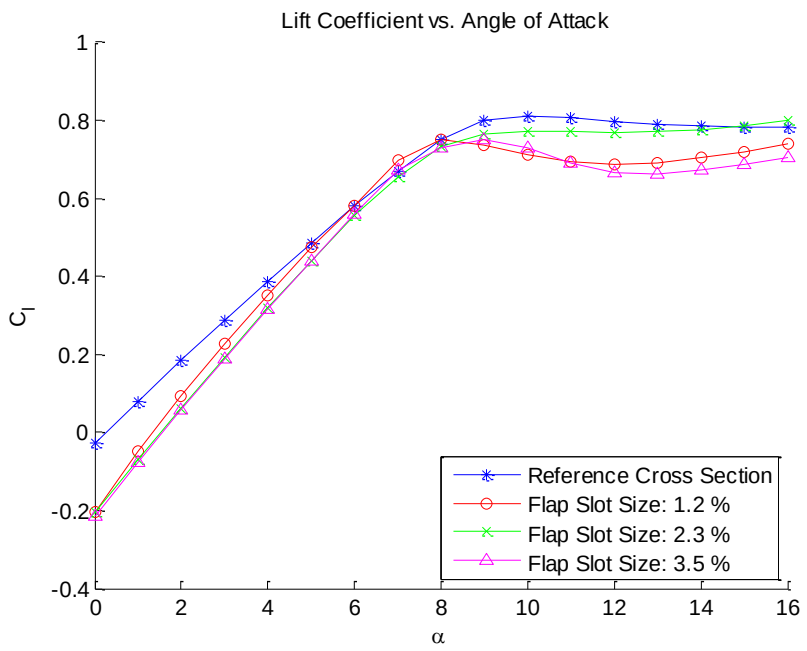

Figure 21: Two Dimensional Cross Sections – Slot Comparison - Lift

Figure 22 displays the drag polar for the slotted flap geometries. Once again, the reference configuration clearly outperformed all three cases, exhibiting significantly lower drag over all lift coefficients. Of the three cases, the smallest slot size exhibited nominally lower drag than the other larger sizes.

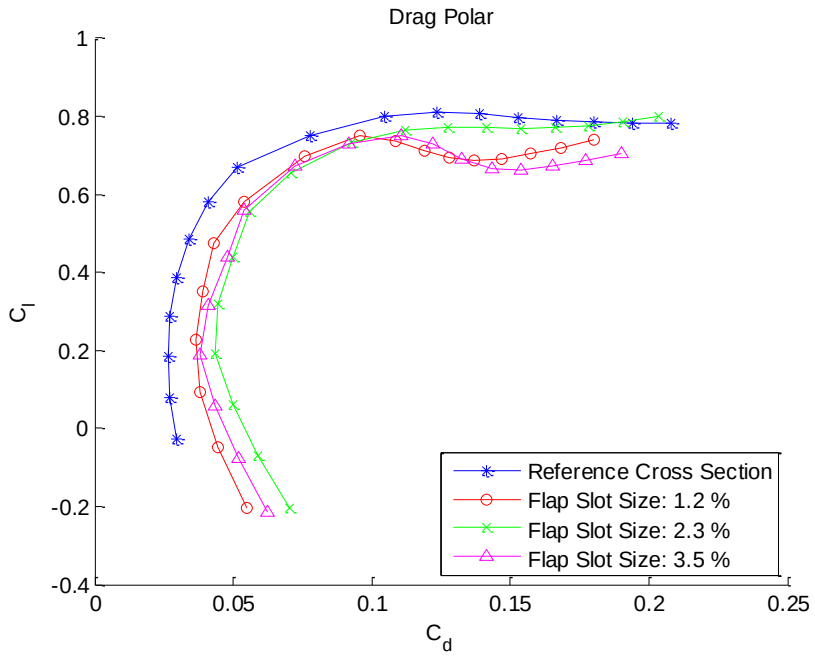

Figure 22: Two Dimensional Cross Sections – Slot Comparison - Drag

In terms of aerodynamic efficiency, Figure 23 shows that the smallest slot size also produced a 7 percent advantage in maximum aerodynamic efficiency over the other slot geometries, but was still 22 percent lower than that achieved by the reference configuration

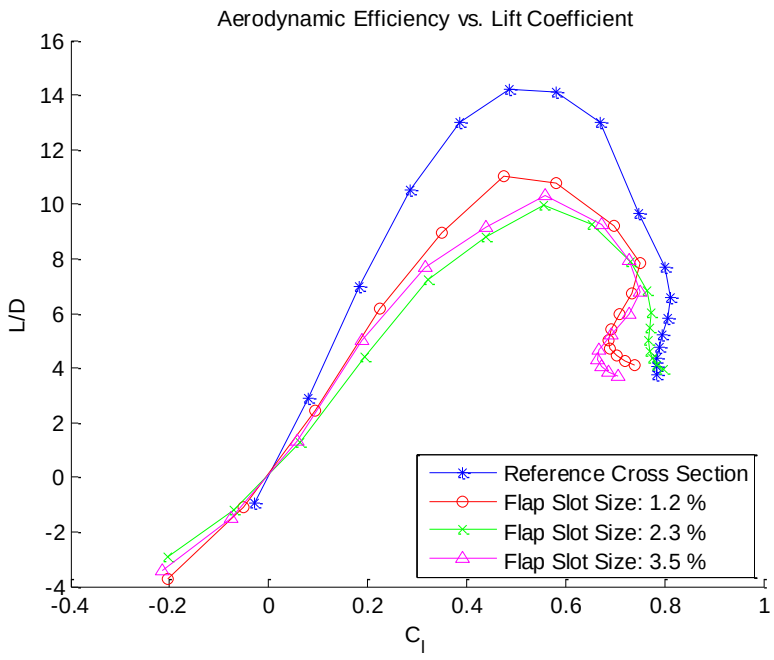

Figure 23: Two Dimensional Cross Sections – Slot Comparison - L/D

In comparison to the reference case, the slotted flap geometries exhibited a very small linear moment range extending from 3 to 6 degrees angle of attack (Figure 24). Unlike the curved and straight flap configurations, the slotted flap geometries did not experience a transition to a positive moment. At approximately 6 degrees angle of attack the moment curves of all three cases became abruptly more negative. This change appeared well in advance of the stall angle of attack which was 8 degrees for all three cases.

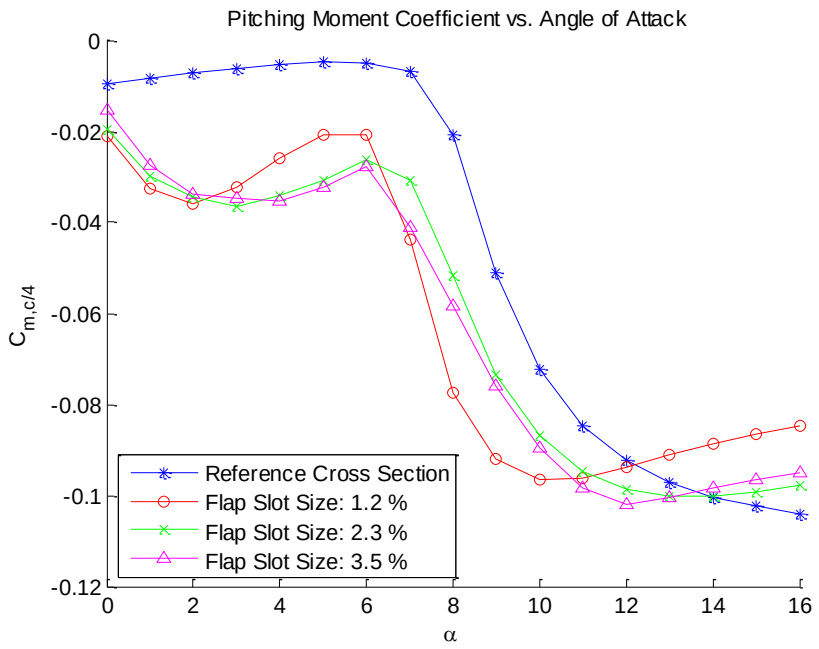

Figure 24: Two Dimensional Cross Sections – Slot Comparison - Moment

Based on the preceding 2D analysis of flap cross sections with varying amounts of length, curvature, and slot size, the most effective cross section was determined to have a chord length of 8 percent MAC in combination with curvature based on a radius of 9.8 percent MAC. While the attached flap geometry clearly outperformed the slotted flap case, both were selected for further analysis in 3D. Due to the well documented performance of slotted flaps in real-world application it was suspected that its poor performance in the 2D analysis may have been due to the absence of 3D flow effects[2].

3.2 Three-Dimensional Analysis

Using the results of the preceding 2 dimensional analysis, down selection of a final flap cross section was based on three criteria; maximum aerodynamic efficiency, stall behavior, and moment characteristics about the quarter chord. The final cross section consisted of a curved flap with a radius of curvature equal to 7.1 percent of the reference chord and a length equal to 8 percent of the reference chord.

It was noted that the 2D results relating to the slotted flap were somewhat surprising since such configurations have generally been used quite successfully to improve maximum lift in many applications[2]. It was also speculated that the poor results may have been inherent to the limitations of a 2D analysis. With this in mind, a secondary flap design that incorporated a slot into an otherwise similar flap profile with the same curvature and length was analyzed in parallel to the primary design. Both flap designs were compared to the reference configuration using the same criteria as before: aerodynamic efficiency, maximum lift coefficient, stall behavior, and moment about the reference quarter-chord.

3.2.1 Thirty Degree Leading Edge Sweep Case

Analysis of the non-slender delta wing with a leading-edge sweep angle of 30 degrees was expected to produce results somewhat similar in stall behavior to

conventional wings of higher aspect ratio while also showing characteristics typical of truly slender delta wings[12].

In order to establish some confidence in the CFD analysis, the lift results for the 30 degree flat-plate and reference wings were first compared to a representative lift curve with a slope of 0.05 per degree typical of a 60 degree wing[1]. Figure 25 displays this comparison. To a reasonable extent, the lift curve slope of both cases was slightly greater than that of the representative lift curve. As is characteristic for delta wings with relatively sharp leading edges, the flat plate wing exhibited no true tall behavior. The reference configuration reached a much greater maximum lift coefficient as a result of its rounded leading edge. It also, consequently, experienced a minor stall with the lift coefficient settling down to a constant value that was slightly lower than C_{Lmax}. The simple addition of a rounded leading edge to the 30 degree wing improved maximum lift by 30 percent.

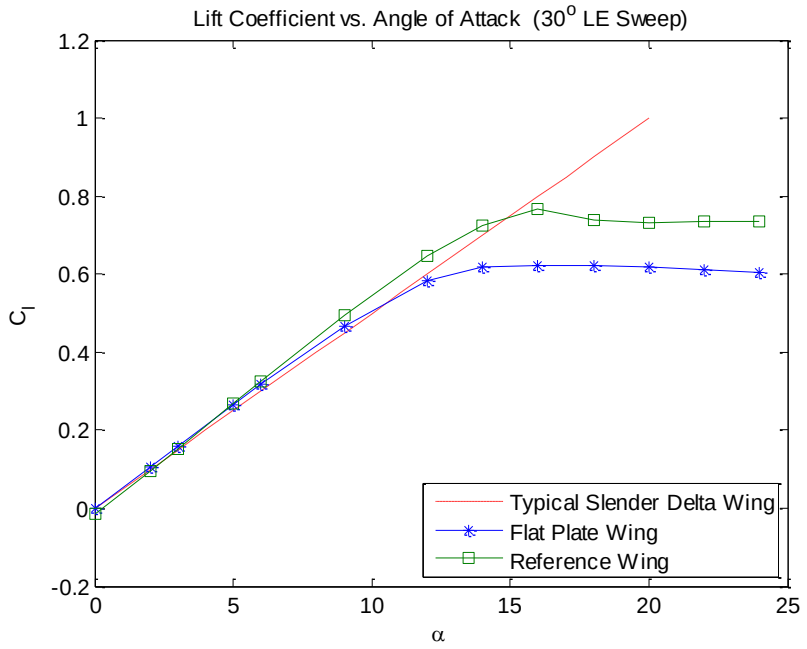

Figure 25: Thirty Degree Wing Comparison to Typical Slender Delta Wing

Adding an attached flap to the 30 degree reference wing produced an increase in maximum lift coefficient of 26 percent. (Figure 26) Including a slot in the geometry further extended this improvement over the reference wing to 35.3 percent. The stall behavior of both configurations was fairly gradual and occurred at an 18 degree angle of attack with the subsequent lift measurements dropping by an average of 9.9 percent over the remaining measured domain.

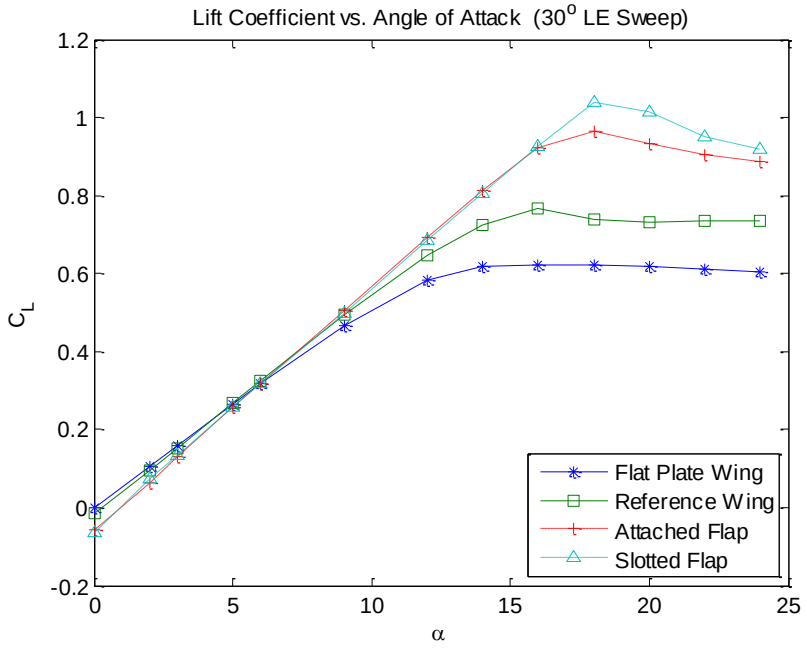

Figure 26: Thirty Degree Wing Comparison – Lift

At lift coefficients below 0.3, Figure 27 shows that the baseline and reference geometry had a clear advantage in terms of drag. The addition of a flap did not appear to provide any significant benefit at lift coefficients below 0.3 which corresponded to an incidence angle of approximately 6 degrees. This behavior was likely a result of vortex

formation being delayed until the angle of attack had increased beyond 5 to 6 degrees. At lift coefficients above 0.3, formation of the leading edge vortex is evidenced by the flatter drag profiles of the flapped geometry. Both flap cases exhibited lower drag than the baseline and reference wings. The fact that the leading edge vortex did not become evident till higher incidence angles were reached was likely a result of the non-slender nature of the 30 degree wing. With the exception of lift coefficients close to 1, the attached flap exhibited lower drag than the flap with a slot

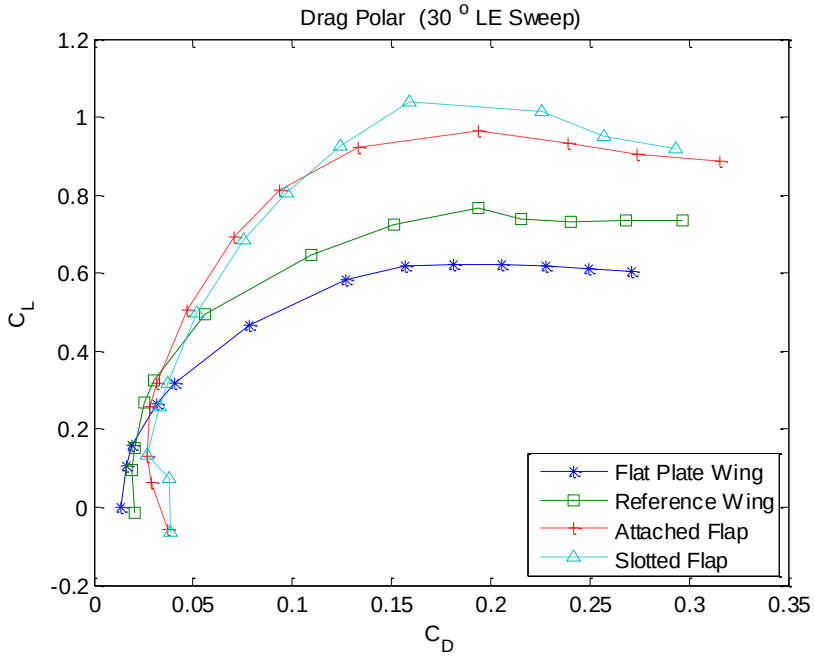

Figure 27: Thirty Degree Wing Comparison - Drag

In terms of maximum aerodynamic efficiency, the flapped geometries did not necessarily improve upon the reference wing. Figure 28 shows that the reference wing by itself produced an improvement of 26.5 percent in maximum aerodynamic efficiency

over the flat plate wing. The maximum aerodynamic efficiency of the wing with an attached flap was 12.6 percent better than the slotted geometry but only produced an improvement of approximately 1 percent over the reference wing. In general, the addition of a leading edge flap to the reference wing did greatly improve aerodynamic efficiency at higher lift coefficients as a result of the increased maximum lift coefficient. At a lift coefficient of 0.8, the aerodynamic efficiencies of both the attached flap and slotted flap were only decreased by 20 percent from their respective maximum values.

Based on the metric of aerodynamic efficiency, the attached flap clearly performed better than the slotted flap. This result was not necessarily surprising since a true vortex flap is meant to shift the vortex suction peak forward onto the flap thereby reducing drag whereas a slotted flap delays separation over the wing itself, increasing lift without reducing drag. Consequently, aerodynamic efficiency would not necessarily be improved by the presence of a slot in the flap geometry. These results serve as a clear illustration of the effectiveness of leading edge vortex flaps; net drag is reduced by creating a component of thrust[12].

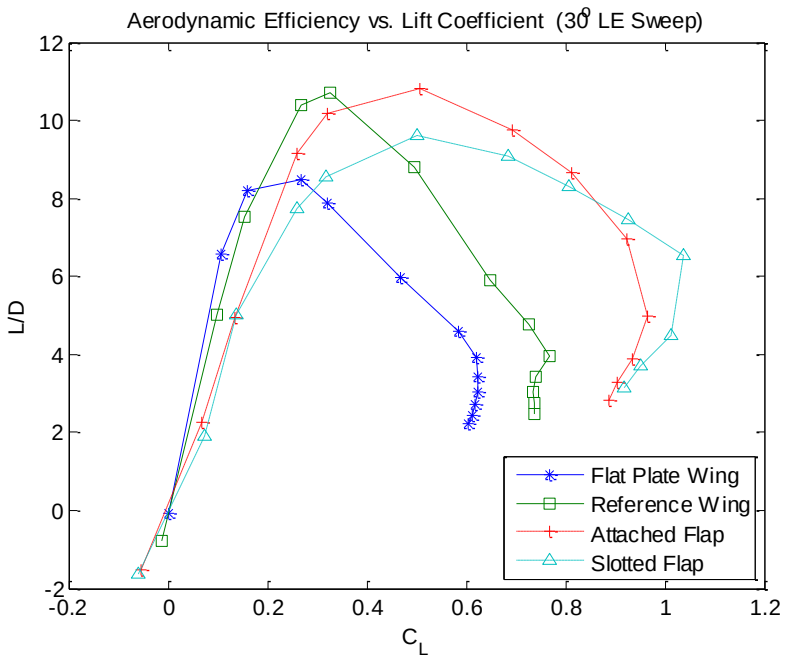

Figure 28: Thirty Degree Wing Comparison - L/D

Analysis of moment behavior (Figure 29) showed that addition of a leading edge flap to the reference geometry produced a significant increase in the linear region of the moment curve. The moments of both flap geometries increased linearly up to the respective stall angles of attack, at which point they experienced an abrupt decrease.

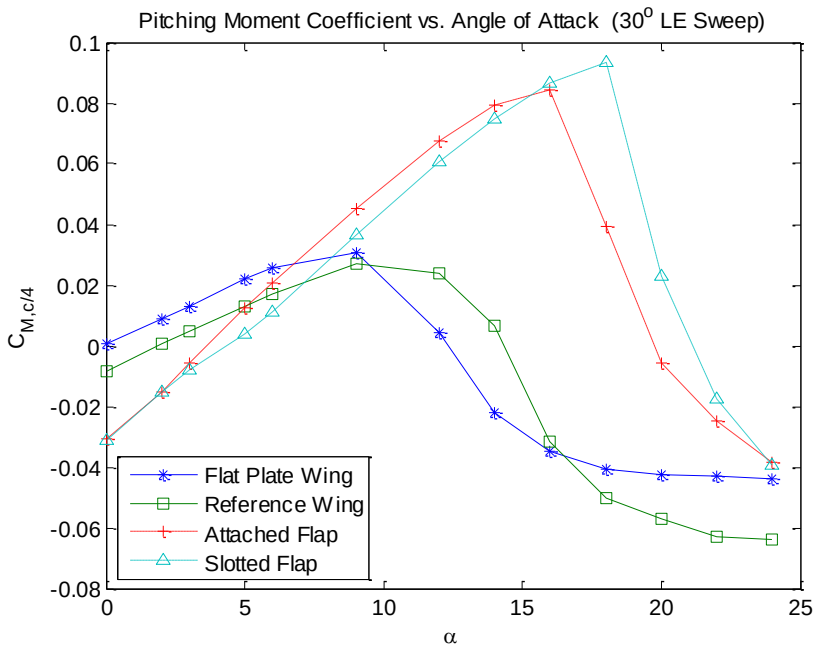

Figure 29: Thirty Degree Wing Comparison - Moment

3.2.2 Sixty Degree Leading Edge Sweep Case

The wing with 60 degrees of leading edge sweep was projected to benefit most from the addition of leading edge vortex flaps. Wind tunnel testing and real-world experience have consistently documented the tendency of flow to separate over slender delta wings with sharp leading edges, forming stable vortices across a wide range of incidence angles[12].

Once again, the general shape of the lift curves for the flat plate and reference delta wings agreed closely with the representative lift curve of a typical 60 degree delta wing (Figure 30). The lift curve slopes of the two baseline wings were approximately 0.05 per degree and mirrored each other quite closely. Unlike the 30 degree wing case,

the more rounded leading edge of the reference wing did not appreciably increase the maximum lift coefficient. The reference wing did, however, achieve a delay in the onset of stall. The flat plate wing experienced a sharp decrease in lift at a 28 degree angle of attack whereas the reference 60 degree wing reached a lift plateau that extended up to an incidence angle of 32 degrees before dropping off.

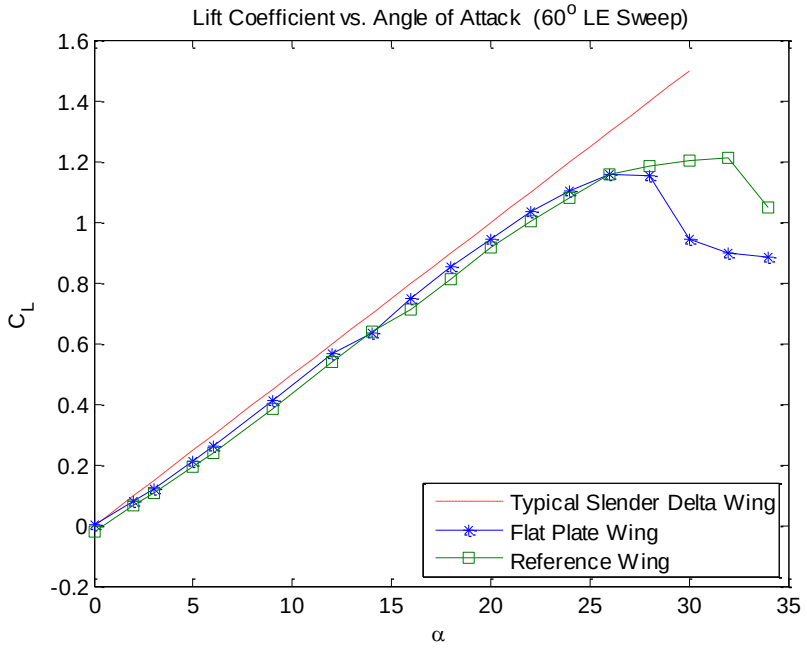

Figure 30: Sixty Degree Wing Comparison to Typical Slender Delta Wing

The most noticeable difference between the 60 degree and 30 degree wings was that the linear region of the lift curve for the 60 degree wings extended to an angle of attack of approximately 30 degrees before stall behavior was encountered. Figure 31 shows that the lift curve slopes of the two flapped geometries were approximately 0.05 per degree up to an incidence angle of 12 degrees. At higher angles of attack, the same

lift curve slopes increased slightly allowing the flapped geometries to reach significantly higher maximum lift coefficients than the reference wing. The flat plate and reference wings reached similar maximum lift coefficients although the flat plate wing experienced stall and a drop in lift much earlier than the reference wing.

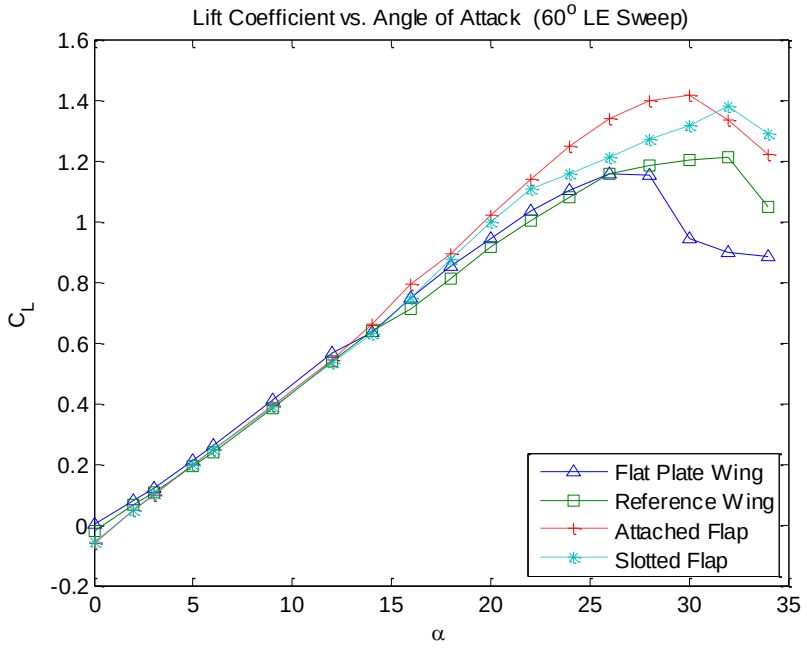

Figure 31: Sixty Degree Wing Comparison – Lift

Based on the drag polar for the 60 degree wings provided in Figure 32, the leading edge vortex appeared to have taken effect at a lift coefficient of 0.25 corresponding to an incidence angle of 6 degrees. Above the lift coefficient of 0.25, the flapped geometries produced lower drag than the reference wing by a factor that was almost constant over much of the measured range.

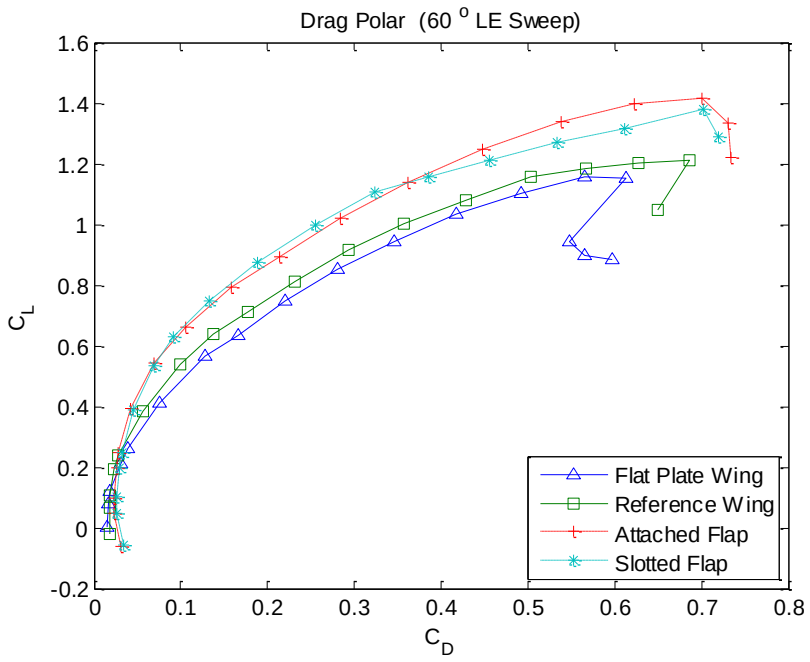

Figure 32: Sixty Degree Wing Comparison – Drag

In terms of aerodynamic efficiency, the addition of flaps to the 60 degree wing produced a more noticeable increase in the maximum value than was observed for the 30 degree wing. In Figure 33, the attached flap can be seen to have achieved an improvement of 10.5 percent over the reference wing and 33.3 percent over the flat plate wing. It is interesting to note that the 60 degree wing with a flap reached its maximum aerodynamic efficiency at a lower lift coefficient than the 30 degree wing but at the same incidence angle of 9 degrees. Although the slotted flap saw an improvement of only 1.1 percent over the reference wing in terms of maximum aerodynamic efficiency, it averaged 39.9 percent better at higher lift coefficients. The attached flap averaged 37 percent better over the same range.

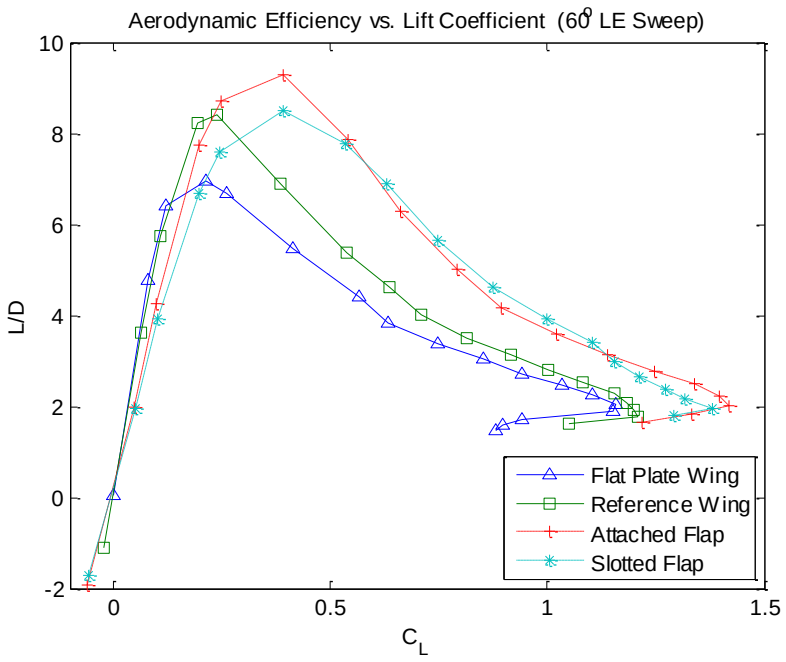

Figure 33: Sixty Degree Wing Comparison – L/D

Analysis of moment behavior for the 60 degree wings produced some equally encouraging results (Figure 34). Addition of a leading edge flap to the 60 degree wing had the significant effect of producing a relatively constant moment about the quarter chord up to an incidence angle of approximately 18 degrees. The difference between the attached flap and the geometry with a gap was minimal up to 18 degrees angle of attack, after which both moment curves became quadratic in nature. Stall did not appear to have a significant effect on the moment curves of either the flapped wings or the reference and flat plate wings.

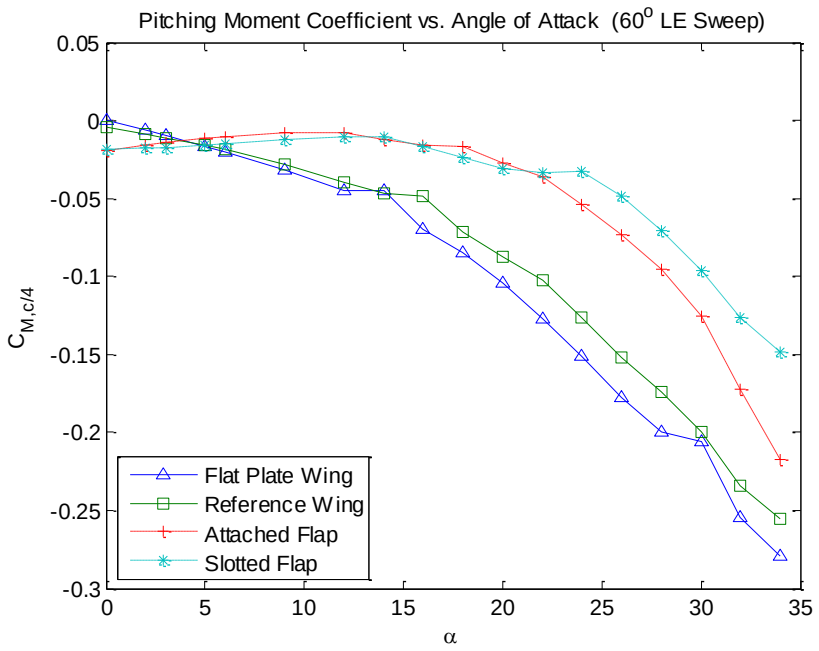

Figure 34: Sixty Degree Wing Comparison – Moment

As was suspected, 3D analysis showed a marked improvement in the performance of the slotted flap. When applied to the 30 degree wing, the slot was particularly successful at increasing the maximum lift coefficient and delaying stall behavior. However, the attached flap produced the best aerodynamic efficiency for both wing sweeps. For this reason, the attached flap geometry was determined to be the best choice for continued analysis relating to flap deflection.

3.3 Flap Deflection Study

The two central objectives of this research were to design a leading edge vortex flap that improves overall aerodynamic efficiency and to determine whether or not flap design could function as a primary means of vehicle control. Although significantly

more extensive research would be required in order to make any definitive claims on the subject, the results of the current research did provide evidence from which some predictive conclusions were drawn. It should be noted, however, that the scope of the current research was limited to examination of moment behavior in the longitudinal direction only.

Control potential of the leading edge flap design was assessed by examining its ability to fulfill one of the key requirements of aircraft longitudinal static stability; that a constant moment about the aerodynamic center exists and that it be positive at the zero lift angle of attack[11]. In the previous results, the attached flap with a curved cross section was shown to possess a moment about the quarter chord location that was constant with angle of attack. However, its sense was in the negative direction. With a change in flap deflection, it was reasonable to assume that the moment might be made positive.

Additionally, the preceding analysis examined each flap design at a single deflection angle: 30 degrees. This deflection angle may or may not yield the best possible behavior in terms of aerodynamic efficiency, maximum lift coefficient, and any other qualities of interest. Many aspects of an aircraft's performance, such as range for a propeller driven vehicle, depend on its maximum aerodynamic efficiency[2]. Therefore, was important to determine the exact vehicle configuration and attitude that corresponded to flight at the maximum possible aerodynamic efficiency.

Consequently, a study was conducted that examined the effect of control surface deflection on lift, drag, aerodynamic efficiency, and moment. Using the attached flap design with a length of 8 percent of the reference chord and a 7.1 percent radius of curvature, the flap deflection study was conducted with two primary objectives:

a) Determination of the best flap deflection angle for maximum aerodynamic efficiency
b) Determination of the flaps ability to achieve a positive moment at the zero lift angle of attack

3.3.1 Thirty Degree Leading Edge Sweep Case

The effect of flap deflection on the 30 degree delta wing was similar to the effect of a leading edge flap on a more conventional wing. Typically, as flap deflection increases, the general shape of the lift curve is preserved and simply translated co-linearly upwards from the linear region, increasing the maximum lift coefficient and delaying stall to higher angles of attack. This behavior can be clearly seen in Figure 35. Changing the deflection from 0 to 40 degrees increased the maximum lift coefficient by approximately 37 percent. Stall behavior was fairly minimal and remained essentially unchanged up to 20 degrees of deflection. For deflection angles of 30 and 40 degrees, stall produced a small reduction in lift coefficient.

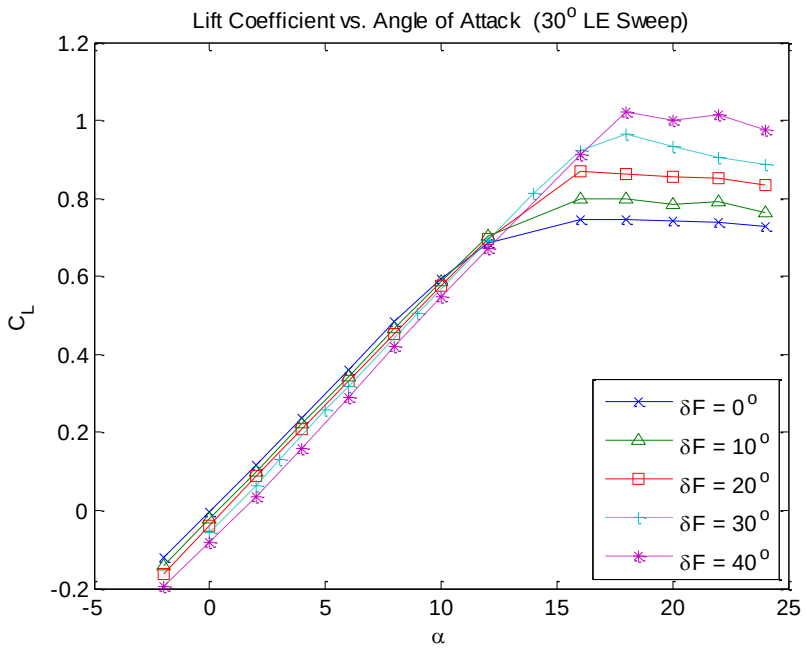

Figure 35: Thirty Degree Wing Flap Deflection - Lift

At low lift coefficients, Figure 36 shows that 10 to 20 degrees of flap deflection produced the least drag. Since the flap cross section was curved, zero degrees of deflection actually caused the flap to protrude above the upper wing surface. This possibly introduced an adverse pressure gradient over the rear portion of the flap as well as potential for flow separation, resulting in slightly higher drag when compared to cases with a small amount of positive flap deflection. As the lift coefficient was increased beyond 0.4, the point at which each deflection case lost the vortex effect was clearly evidenced by the sharp increase in drag.

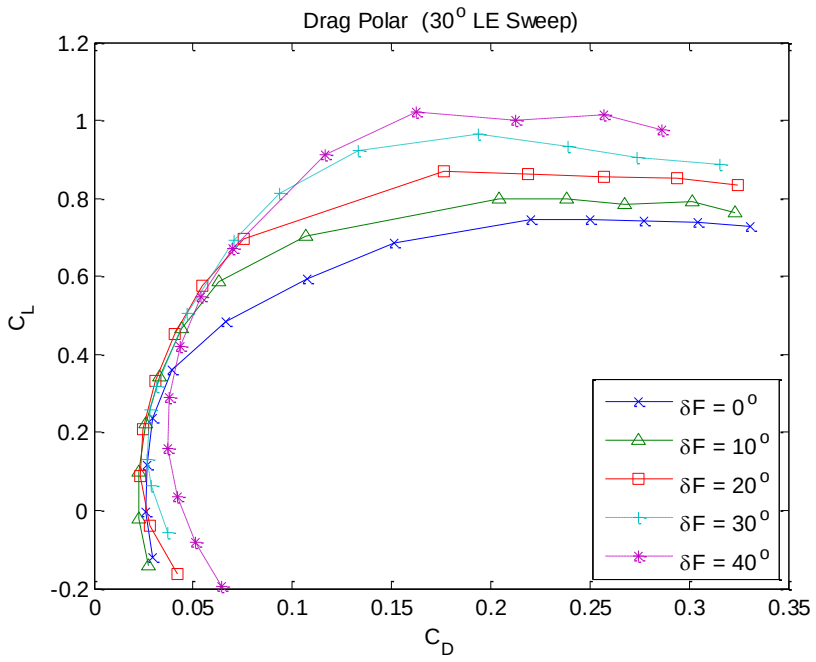

Figure 36: Thirty Degree Wing Flap Deflection - Drag

In terms of aerodynamic efficiency, the best flap deflection angle was shown to be 20 degrees (Figure 37). At this deflection angle, the maximum aerodynamic efficiency was approximately 3 percent better than the nearest maximum produced by 30 degrees of deflection and was 21.8 percent better than that attained at 0 degrees of flap deflection. Although the 40 degrees deflection case achieved a somewhat lower maximum aerodynamic efficiency, it is worth noting that it remained within 25 percent of its maximum value up to lift coefficients very close to stall.

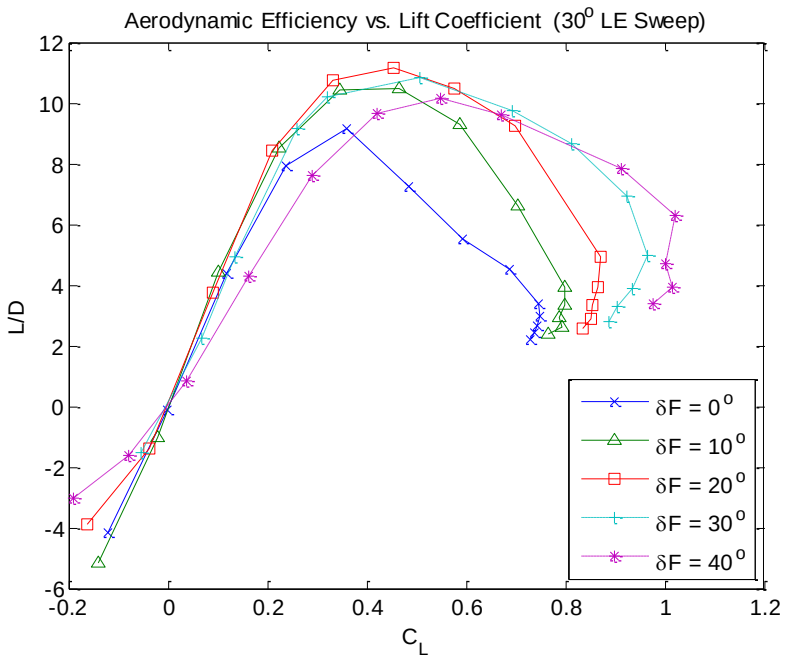

Figure 37: Thirty Degree Wing Flap Deflection - L/D

In the previous analysis of the 30 degree wing case, all moments were taken about the reference wings quarter chord location. For the flap deflection study, the moments were taken about the true aerodynamic center which was somewhat forward of the quarter chord. The true aerodynamic center is defined as the point about which moments are constant with angle of attack[11]. As can be seen in Figure 38, there is a linear region for each deflection case where the moments remained constant with angle of attack. The extent of this linear region was increased to higher incidence angles with increasing flap deflection. The fact that the change in moment was approximately linear with flap deflection was significant in terms of longitudinal control.

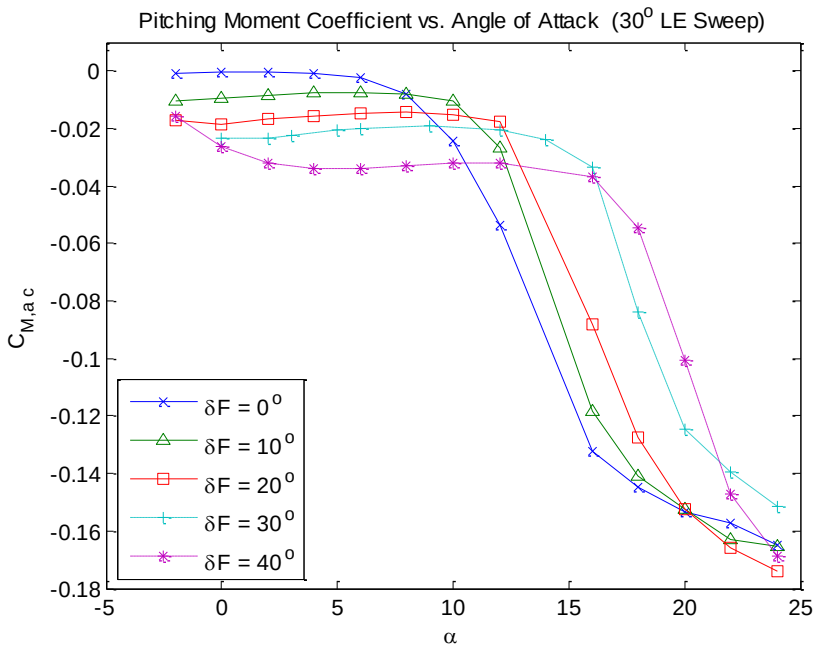

Figure 38: Thirty Degree Wing Flap Deflection - Moment

3.3.2 Sixty Degree Leading Edge Sweep Case

When applied to the 60 degree wing, varying the flap deflection angle did not produce significant increases in maximum lift coefficient as with the 30 degree wing. Figure 39 shows that, with the exception of the 20 degree case, maximum lift coefficient remained essentially constant for all flap deflection angles. For 20 degrees of flap deflection, the maximum lift coefficient increased by approximately 5 percent with respect to the other deflection angles. The general result of flap deflection was to shift the lift curve horizontally to increasingly higher angles of attack.

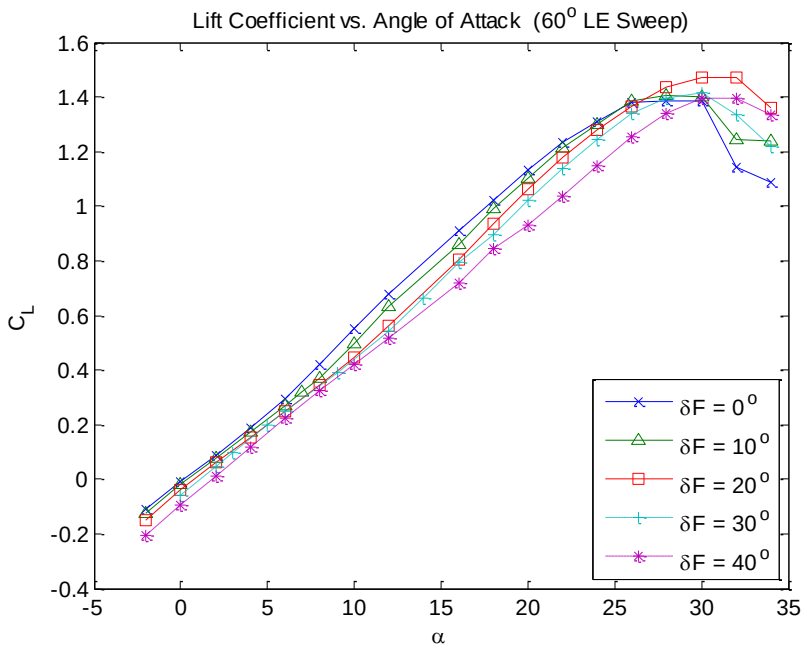

Figure 39: Sixty Degree Wing Flap Deflection - Lift

In Figure 40, the drag polar for the flap deflection study depicts a very uniform set of curves. At low lift coefficients, deflection angles between 10 and 30 degrees produced a minimum amount of drag. As the lift coefficient was increased beyond 0.2, the leading edge vortex took effect causing a flattening of the drag profiles corresponding to higher flap deflection angles. At lift coefficients in excess of 0.6, drag became inversely proportional to flap deflection. For a given lift coefficient, increasing the flap deflection caused a proportional decrease in drag.

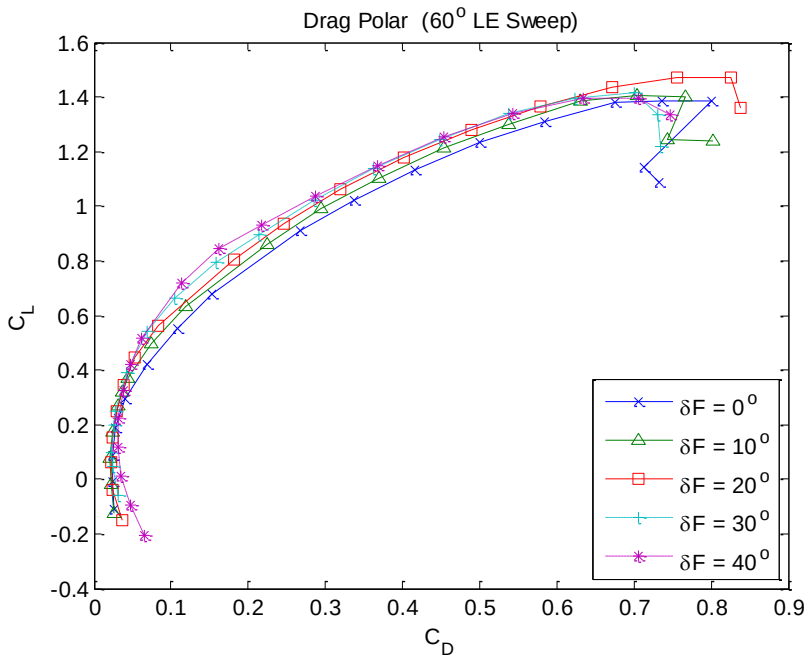

Figure 40: Sixty Degree Wing Flap Deflection - Drag

The results for aerodynamic efficiency (Figure 41) showed that flap deflection produced an effect on the 60 degree wing that was very similar to the 30 degree wing. Increased deflection initially improved maximum aerodynamic efficiency, but then lost its advantage passed a certain deflection angle. The only difference from the previous wing case was that 30 degrees of flap deflection produced the optimum aerodynamic efficiency by a small margin. Additionally, aerodynamic efficiency at all flap deflection angles fell away more rapidly after reaching a maximum than was observed for the 30 degree wing.

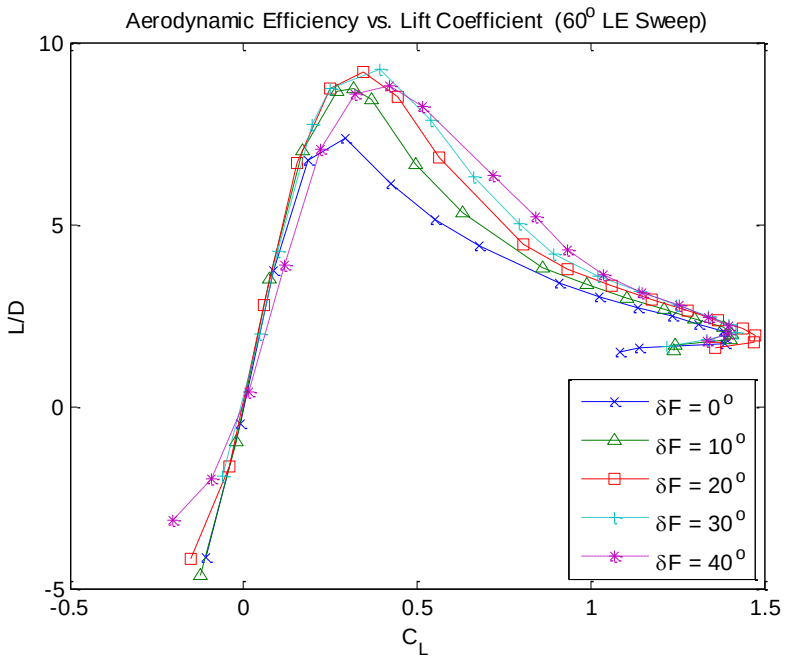

Figure 41: Sixty Degree Wing Flap Deflection - L/D

Moment behavior was very consistent across all flap deflection angles for the 60 degree wing as can be seen in Figure 42. At angles of attack between 0 and 12 degrees, the moments for all cases were essentially constant. Within this range, an increase in flap deflection produced a proportional increase in the moment magnitude. At 0 degrees of flap deflection, the moment coefficient was very close to zero. Increasing the flap deflection to its maximum value produced a moment coefficient of -0.26. For angles of attack between 10 and 15 degrees, the slopes of the moment curves changed only slightly. Above 15 degrees, the moment curves became quadratic in nature. Below this incidence angle, the moment variation with respect to flap deflection was essential linear.

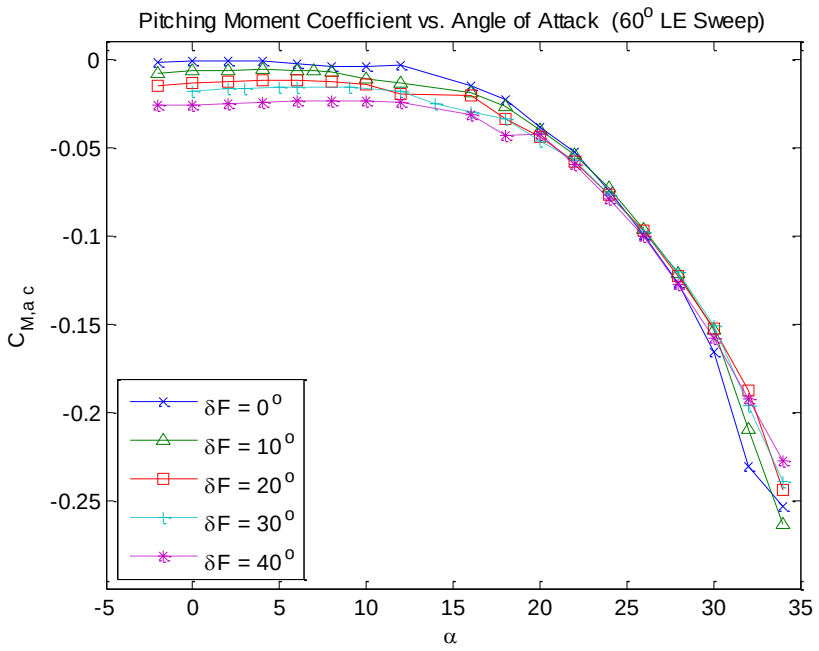

Figure 42: Sixty Degree Wing Flap Deflection - Moment

The deflection study of the chosen flap design produced some important results relating to flap performance characteristics that were then used to draw several important conclusions. The resultant data clearly showed that there was a best flap deflection angle corresponding to maximum values of lift coefficient and aerodynamic efficiency for each wing sweep. While not necessarily the best in all performance categories, 30 degrees of flap deflection was found to provide the best all-around performance for the 30 degree wing case. A flap deflection of 20 degrees provided a slightly higher maximum aerodynamic efficiency but also saw significantly lower efficiency values at higher lift coefficients due to the lower maximum. For the 60 degree wing, 20 degrees of deflection was determined to be the best setting. It produced a maximum lift coefficient

significantly higher than any other deflection angle and was very close to being the most effective in terms of aerodynamic efficiency.

In order to achieve positive longitudinal stability in the absence of tail surfaces, the moment about the aerodynamic center would have to be made positive[11]. The results of this study have shown that the moment varies linearly with flap deflection and is relatively constant over a reasonable range of incidence angles. Although only positive flap deflection angles were tested, it can be concluded that a negative deflection angle could produce the positive moment about the aerodynamic center required by static stability.

CHAPTER 4: POST PROCESSING

4.1 Results Validation

Upon completion of the 3D analysis, post processing began by comparing the obtained results to linearized potential flow theory, experimental data, and other researchers CFD results. The primary goal was to increase confidence in the acquired data.

4.1.1 Analytical Verification

The hypothesis of Polhamus (Ref. 10) describing the total lift of a delta wing in terms of potential and vortex lift has been well established through many experiments conducted both in wind tunnels and in actual flight tests[12]. Although (eq. 8) derived in chapter 2 is based on linearization of potential flow theory, and is a simple representation of the underlying flow physics it has been shown to be quite accurate in predicting delta wing lift for low to moderate angles of attack[8]. Therefore, it served as an effective preliminary point of validation by which to judge the results of this research. As was stated in chapter 2, (eq. 8) is most applicable to thin wings of low aspect ratio. For this

reason CFD analysis was initially performed on a simple, flat-plate wing in order to generate a baseline of data for comparison purposes.

The CFD was performed using mesh and solver settings identical to those used on the reference and flapped models. Using (eq. 8) and the baseline model parameters given in Table 4, analytical lift curves were generated for both wing sweeps and then compared to the computational results.

Table 4: Delta Wing Potential and Vortex Lift Parameters

	b (m)	*S (m^2)*	*AR*	K_P	K_V
30° Sweep	1.0559	0.3888	2.87	2.82	3.25
60° Sweep	0.6096	0.1968	1.89	2.15	3.125

The coefficients Kp and Kv were estimated for both the 30 degree and 60 degree wings from Figure 3 using the respective wing aspect ratios. Figure 43 shows the plot of analytical lift as well as the lift curves for the baseline and reference wings. The analytical lift curve (representing the sum of potential lift and vortex lift) agreed quite closely with the baseline wing up to an angle of attack of approximately 5 degrees. At angles of attack greater than 5 degrees, the numerical results for the baseline wing gradually diverged from the theoretical lift curve. The discrepancy at higher angles of attack was a result of stall, or vortex breakdown, occurring in the numerical simulation. As has been mentioned, 30 degrees of wing sweep is considered non-slender and causes the loss of lift to begin at lower incidence angles than it otherwise would for wings with greater sweep[1].

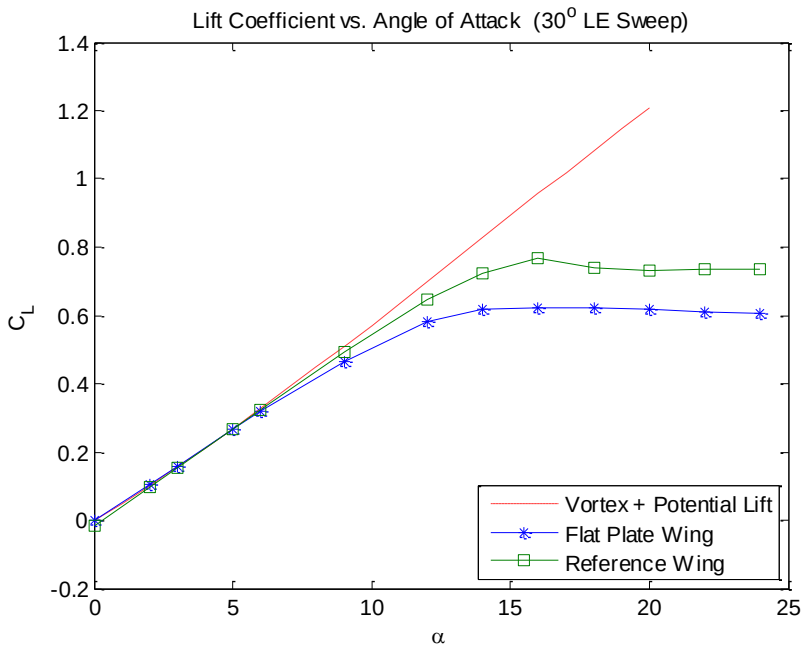

Figure 43: Analytical Lift Comparison – 30° Wing

The reference wing exhibited a lift curve slope that was initially steeper than what was shown by the theoretical and baseline wing lift curves. The difference was likely due to the reference wing having a fairly round leading edge[12]. Like the baseline wing, the reference wing also experienced a reduction in lift starting at an incidence angle of 5 degrees. It, however, reached a higher maximum lift coefficient and remained closer to the theoretical prediction in the preceding region.

The analytical and numerical lift curves corresponding to the wing with 60 degrees of sweep are shown in Figure 44. The baseline wing clearly matched the theoretical predictions to much higher angles of attack than were achieved by the previous case. The lift curve slope of the numerical results exhibited very little deviation from that of the analytical curve over almost the entire linear region. The reference wing

reported almost identical characteristics with the exception of stall which occurred at a higher angle of attack. The fact that the 60 degree wing case matched analytical lift predictions more closely than in the 30 degree wing case was indicative of the fact that slender delta wings produce a much more stable vortex[1].

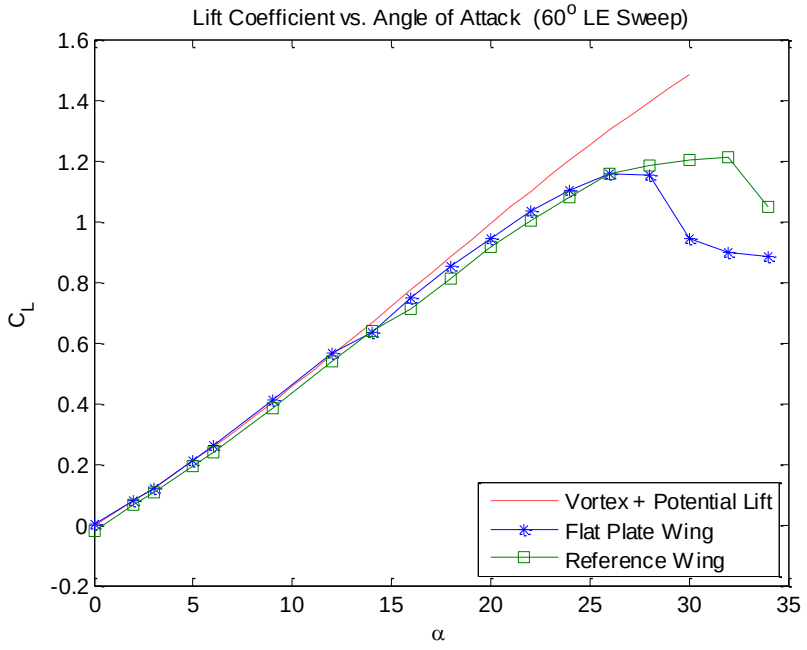

Figure 44: Analytical Lift Comparison – 60° Wing

The relative vortex stability of the 60 degree wing as compared to that of the 30 degree wing was clearly illustrated by figures 45 and 46. At 16 degrees angle of attack, the 30 degree wing showed a single, large outer vortex sheet surrounding the inner vortex core that was beginning to experience breakdown over the wing trailing edge. (Figure 45) The progression of vortex breakdown toward the wing leading edge accounts for the gradual loss of lift shown by the lift curve in Figure 43.

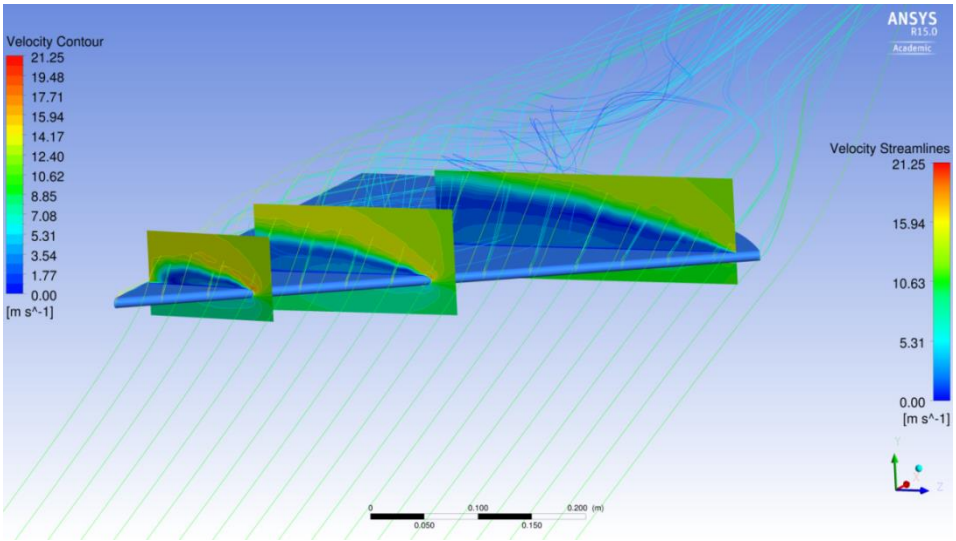

Figure 45: Thirty Degree Wing at α = 16° – Unstable Vortex

At the same angle of attack, vortex breakdown was clearly not evident in the flow visualization for the 60 degree reference wing. (Figure 46) The flow was characterized by a much more compact vortex system consisting of an outer vortex surrounding an inner, counter-rotating vortex. Vortex stability is evidenced by the lack of recirculation as the flow exits the wing trailing edge.

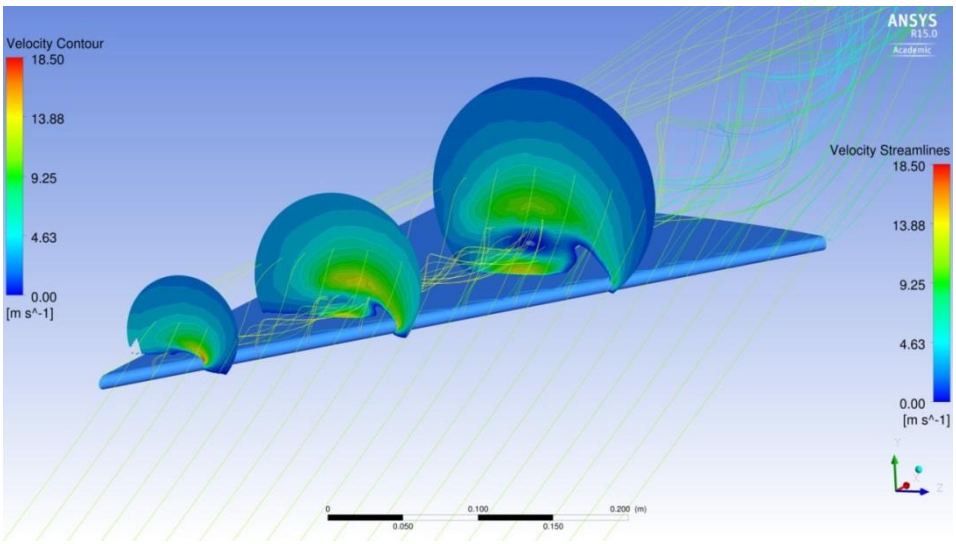

Figure 46: Sixty Degree Wing at α = 16° – Stable Vortex

As shown in the previous two figures, the numerical simulation clearly captured the difference in flow characteristics that define the fundamental difference between slender and non-slender delta wings. Based on this brief comparison, it can be concluded that the numerical results obtained through CFD analysis are a reasonably valid prediction of what might be achieved through experiment. However, since the ultimate goal of this research was to produce an actual flap design, it was important to further compare the numerical and theoretical predictions to actual experimental results before drawing further conclusions.

4.1.2 Experimental Verification

Since the 1950's, much effort has been put into understanding the aerodynamic properties of delta wings, especially in the area of high speed flight. Delta shaped wings remain a popular choice for fighter aircraft due to the resultant low wave drag, but their use comes at a price; poor aerodynamic efficiency. Consequently, there exists a large body of research that has been conducted on leading edge vortex flaps due to the well documented benefit to delta wing lift[1].

In 1990, B.K. Hu and professor J.L. Stollery of Cranfield England performed a series of wind tunnel test on a 60 degree delta wing with leading edge vortex flaps[12]. Their goal was to study the effect of leading edge radius on delta wing performance. These tests, conducted at a Reynolds number of 600,000 based on root chord, have provided a useful body of experimental data that has been built on by many researchers since then. Their findings clearly showed that a sharp edged vortex flap significantly

reduce drag on a slender delta wing when at incidence angles greater than 6 degrees. Although lift was reduced by the presence of an LEVF device, they found that overall aerodynamic efficiency was significantly improved for delta wings with sharp leading edges.

Figures 47 and 48 present the sharp edged delta wing data collected by Stollery and Hu as well as the CFD results for the flat plate and attached flap 60 degree wings. Stollery and Hu reported all lift coefficients referenced to a wing area that included the leading edge flaps at zero degrees deflection. For the purpose of comparison, the CFD results pertaining to the wing with leading edge flaps were adjusted to use a reference area defined in a similar manner.

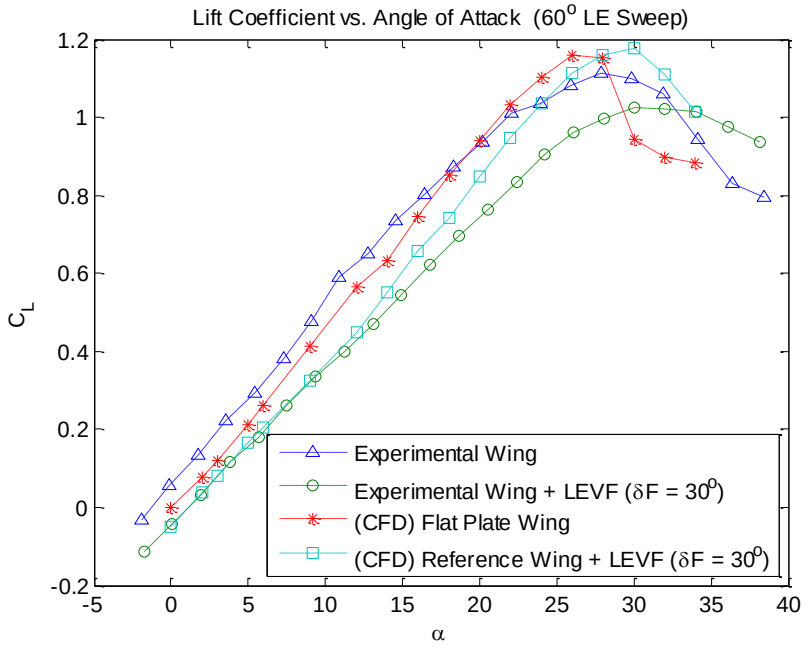

Figure 47: Experimental Results vs CFD Results – Lift

At incidence angles between 0 and 10 degrees, the lift generated by the experimental and CFD wings with LEVF devices was almost identical. Although the baseline wing used in this research was somewhat different in design than the wing with the LEVF attached, the CFD results clearly followed a trend similar to that of the experimental results. As can be seen in Figure 4.5, both sets of results showed that an un-flapped wing produces more lift than a wing with deflected leading edge flaps. However, the CFD results reported greater lift at higher angles of attack which could likely be attributed to additional curvature in the respective leading edges. In the current research, the leading edge flap was curved whereas the flap used by Stollery and Hu was flat on both sides. In terms of lift, the relative superiority of a rounded leading edge was highlighted by their experiments on a wing with a large leading edge radius. Such a wing was found to produce markedly greater lift than the sharp edged delta wing, both with and without the leading edge flap.

When comparison was made in terms of aerodynamic efficiency (Figure 48), the CFD results indicated higher aerodynamic efficiency over low to moderate lift coefficients.

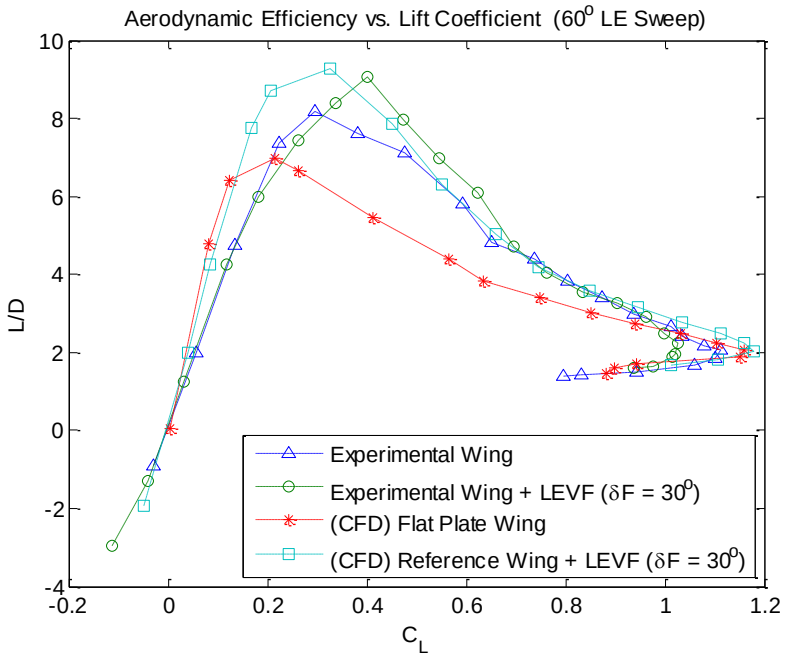

Figure 48: Experimental Results vs CFD Results – L/D

As in the experimental results, the CFD results showed that the wing with an LEVF device possessed better aerodynamic efficiency than the un-flapped wing despite producing less lift.

A paper presented at the 2001 Research and Technology Organization (RTO) Applied Vehicle Panel (AVT) Symposium held in Loen, Norway detailed a study that focused on in-flight flow visualization of vortex flows on a delta wing aircraft fitted with leading edge vortex flaps[6]. The goal of the research was to validate design techniques and expected performance benefits by measuring pressure profiles along the vortex flaps. The test-bed aircraft, a delta wing F-106B with 60 degrees of sweep, was fitted with a two position leading edge flap and tested at incidence angles from 9 to 18 degrees and Mach numbers from 0.3 to 0.9. Using an off-surface vapor screen system for flow

visualization, movement of the vortices across the wing was captured in a series of 2D images and later superimposed on a computer generated model of the aircraft as shown in Figures 49. In so doing, the study was able to document the true behavior of delta wing vortices in flight.

(a) 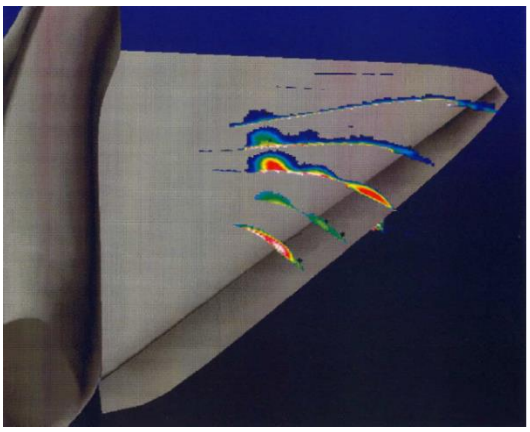 (b) 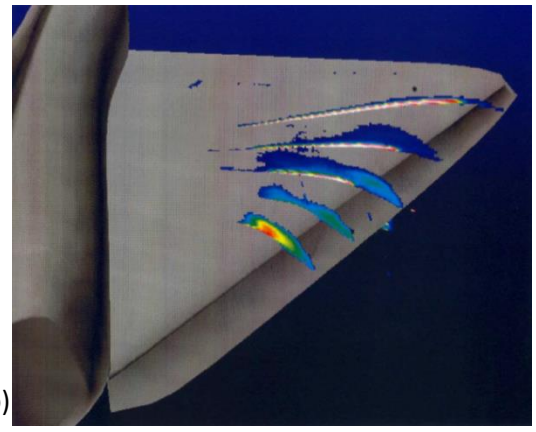

Figure 49: (a & b): Flight Test Results – α = 11° (left)
α = 15° (right)

In general, visualizations such as those shown above validated the vortex behavior that had been expected based on CFD and wind tunnel test. Leading edge vortices originated and built up along the inboard flap and then migrated off the flap to run streamwise across the wing. This process repeated multiple times during each interval of observation.

Similar behavior was observed in the current research. Figure 50 presents a visualization of the flow over the 60 degree delta wing with the attached LEVF at 30 degrees of deflection. The wing was at an angle of attack of 16 degrees. The image shows a vortex forming over the inboard flap upper surface and then moving off the flap at approximately the same location shown by the images from the F106B flight test Study.

The vortex then trails off at an angle to the leading edge, although not fully in the streamwise direction.

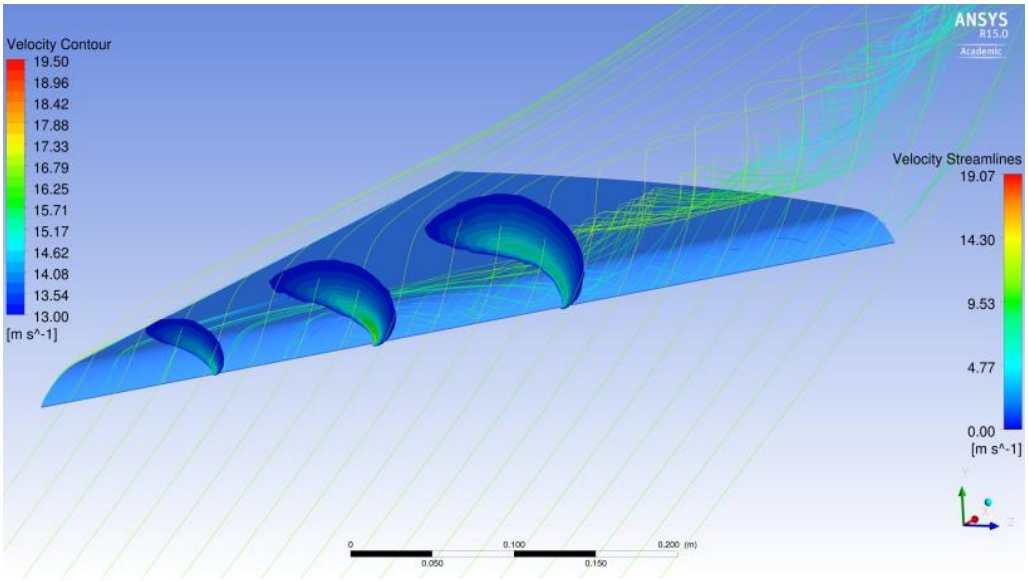

Figure 50: CFD Results – α = 16°

The in-flight flow visualization also showed that, as angle of attack increased, the number of vortices gradually decreased till one or two primary vortices remained. This trend is illustrated by the angle of attack progression shown in Figure 49, (a) to (b). The aircraft in Figure 49 at 11 degrees angle of attack has at least 3 vortices along its wing while the following figure (15 degrees angle of attack) shows only two larger vortices on the wing.

The F106B study also encountered some unexpected behavior; small discontinuities in the wing and flap surface caused a pattern of multiple vortices to grow

followed by repeated shedding. This behavior was not predicted by either wind tunnel tests or CFD analysis. It was then hypothesized that, under true operating conditions, an aircraft fitted with LEVF devices would typically experience vortex flow characterized by complex patterns of vortex growth and shedding resulting from surface imperfections. However, despite the somewhat drastic differences in real-life flow field, the overall effectiveness of LEVF devices was found to be very close to wind tunnel and CFD predictions.

4.1.3 Numerical Verification

In the previous section, the results of this research were examined in light of data compiled through theory and experiment. Prediction of the baseline wings aerodynamic performance was shown to be reasonable when compared to the typical lift and drag characteristics of real delta wings. This was due in large part to the robustness of the computational model. The techniques and models used in CFD have improved greatly and achieved a significant amount of success since their use became widespread. As was mentioned previously, the flight test results from the F106 study had been found to closely match the CFD predictions. While CFD is capable of producing results of high quality and trustworthiness, there is also a susceptibility to minor variations of input parameters, boundary, conditions, mesh resolution, and especially human error causing the solution to vary significantly. For this reason, it is often helpful to use existing CFD results based on a similar analysis as a point of comparison.

In order to further establish the validity of the CFD results for the baseline wing models, comparison was made to research conducted at The Ohio State University from 2010 to 2011by Dr. Clifford Whitfield and Matthew Warchol[14]. As mentioned in chapter 1, their research was focused on the concept of flexible delta wings with application to UAVs. In preparation for extensive wind tunnel testing of a flexible winged model, they performed a substantial amount of CFD analysis on a model with ridged wings similar in design to the flat plate delta wing used in the present research. The body of data compiled by Whitfield and Warchol served as a useful standard for further validation of the present research.

The relevant model parameters used in the flexible delta wing research are given in Table 5.With the exception of the 60 degree wing Reynolds number, the parameter values are identical to those of the current research.

Table 5: Whitfield & Warchol Comparison CFD Parameters

	Re	*q (lbs/ft^2)*	*b (ft)*	*S (ft^2)*	*AR*
30° Wing	300,000	1.47	3.63	4.17	3.15
60° Wing	970,000	15.72	2.17	2.08	2.25

The CFD results from the flexible delta wing study are presented in parallel with the current research results as shown in Figures 51 through 54.

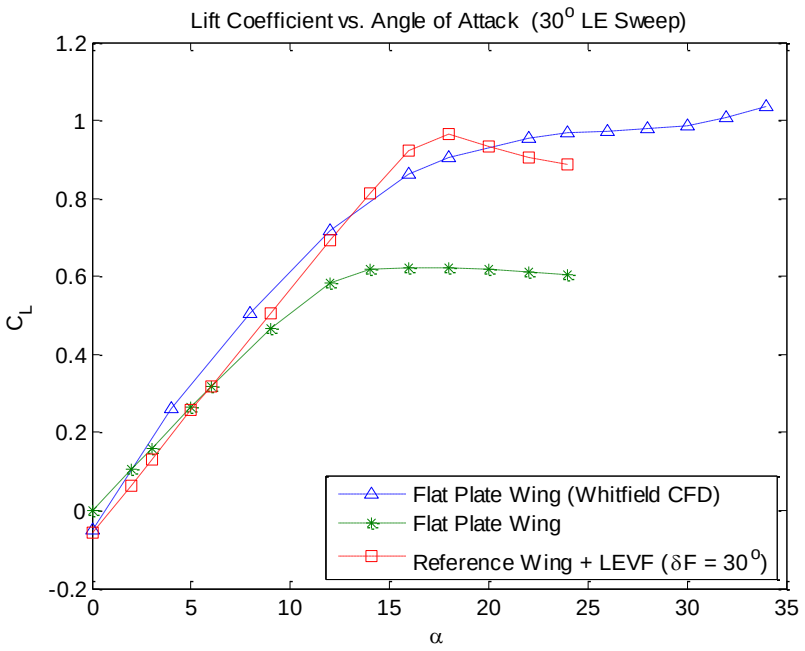

Figure 51: CFD Comparison for 30° Wing – Lift

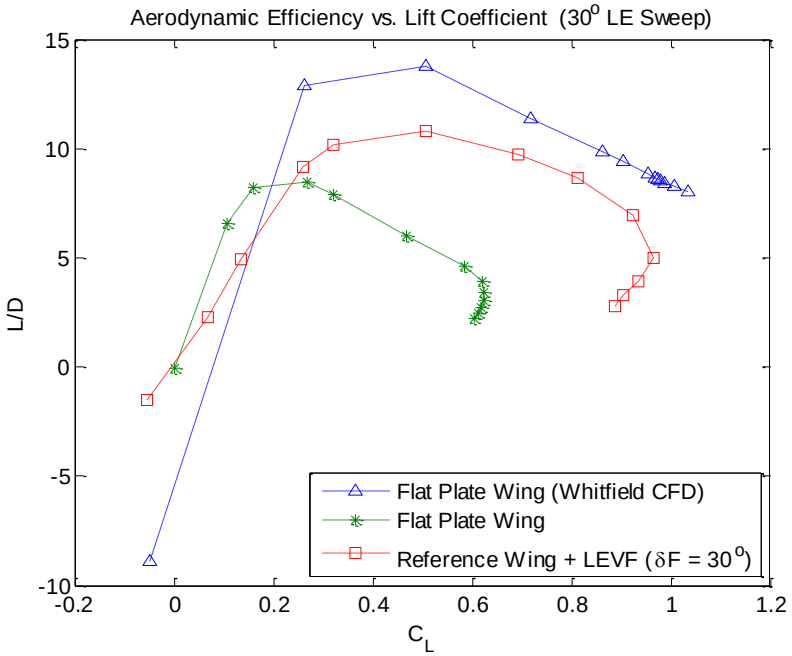

Figure 52: CFD Comparison for 30° Wing – L/D

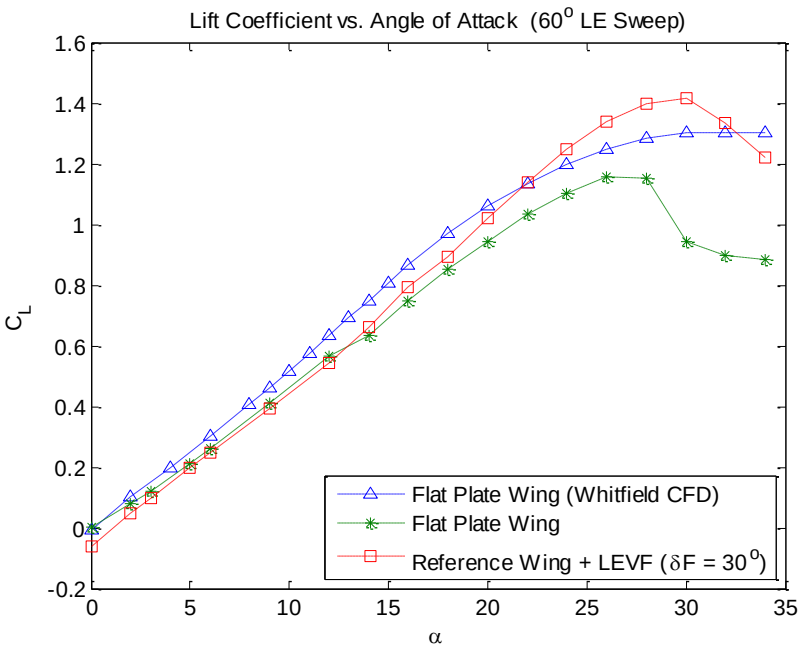

Figure 53: CFD Comparison for 60° Wing – Lift

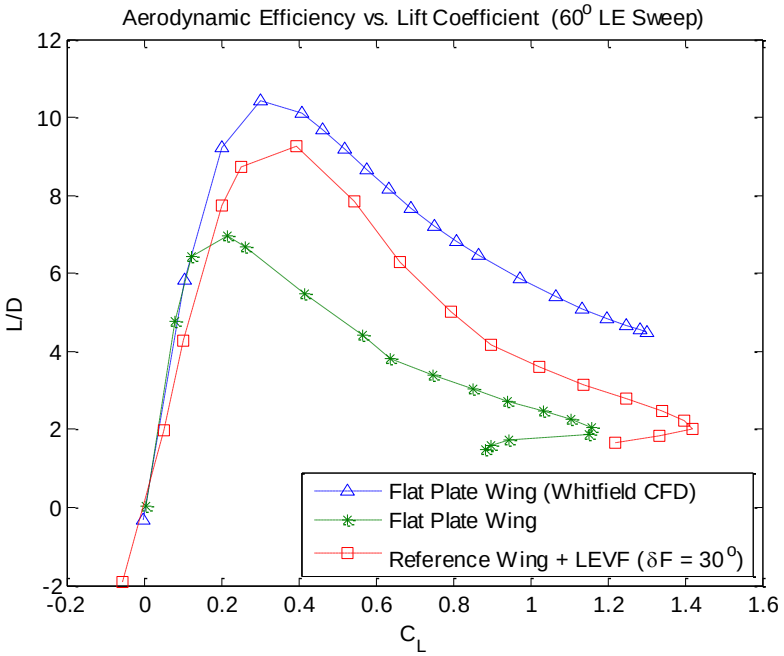

Figure 54: CFD Comparison for 60° Wing – L/D

In comparison to the current research, the CFD results of Whitfield and Warchol show similar maximum lift values but much greater aerodynamic efficiency in both wing sweep cases. Given the similarity of the CFD setup, the significant difference between the two results was perplexing. The high values of aerodynamic efficiency indicate that significantly lower drag was being reported. One possible explanation could involve settings used in the turbulence model. The fact that the results of the current research predict higher drag could be attributed to use of Enhanced Wall Treatment. Enhanced wall treatment provides the most consistent prediction of wall shear stress and is relatively insensitive to y+ values[4]. It avoids the error caused by wall functions assuming an extended logarithmic layer. Use of wall functions is especially to be avoided for low Reynolds numbers: 10^4 - 10^6 In the 60 degree wing case, differences could also be related to the higher Reynolds number used in the comparative results. Figures 55 and 56 show velocity streamlines and pressure contours for both sets of results.

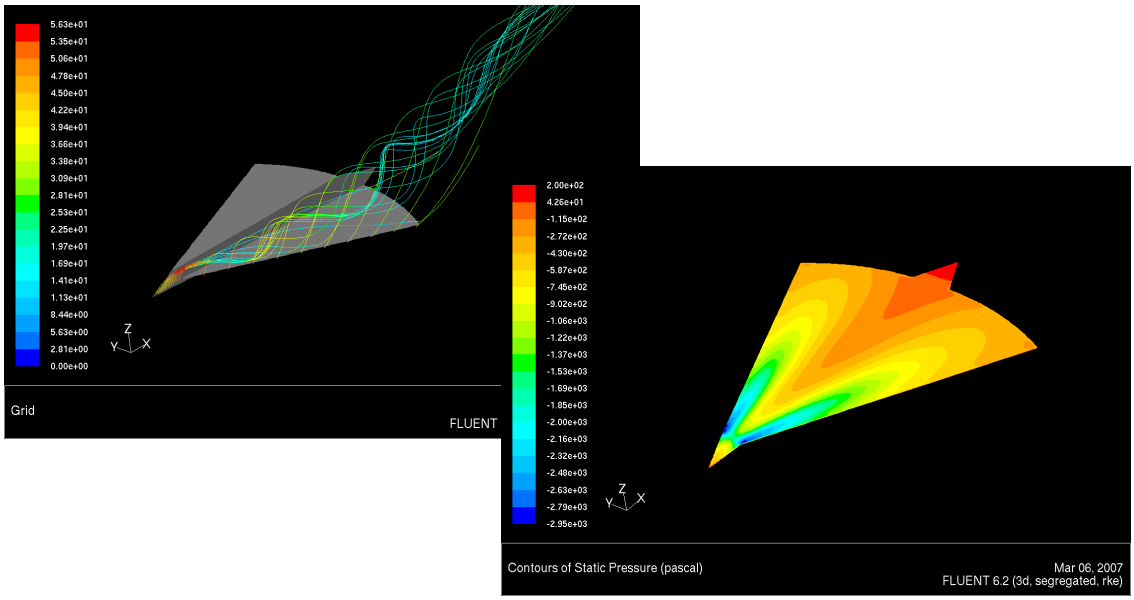

Figure 55: Whitfield CFD for 60° Wing – Velocity and Pressure

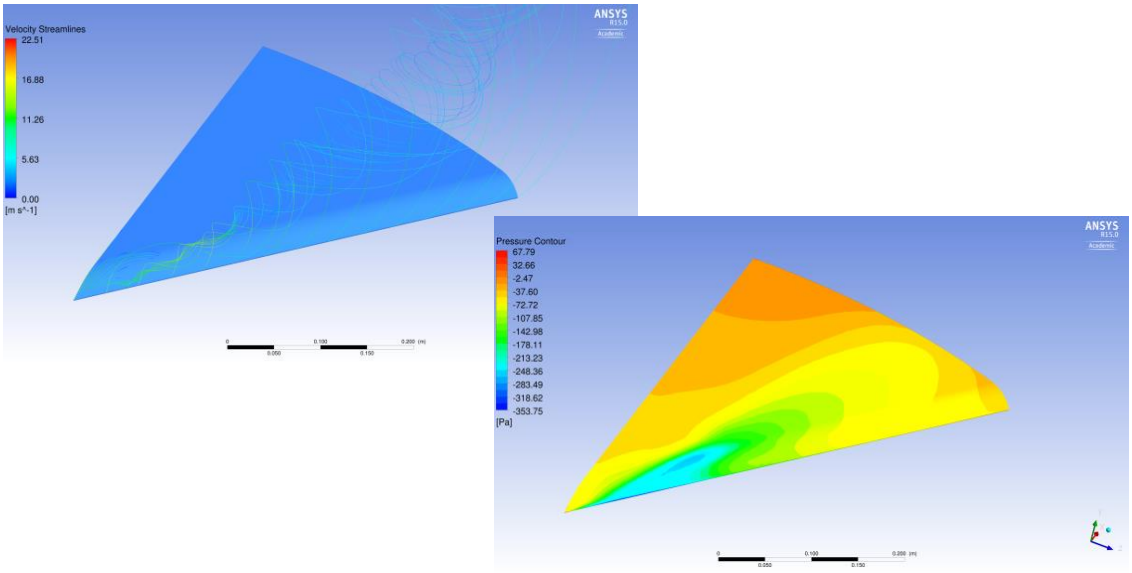

Figure 56: Current Results for Sixty Degree – Velocity and Pressure

The figures clearly show that the 60° Wing from the Whitfield and Warchol study is experiencing higher velocities and lower pressures on its upper surface near the wing apex.

In assessing the merit of the current CFD results relative to pre-existing data, it is important to also examine potential sources of error. In general, error can be divided into two broad categories:

1. Error that is inherent to the numerical approximation of something physical
2. Error that is specific to single case or instance.

The first general category of error is an unavoidable part of CFD. Enough computing power to model a flow down to the smallest sub-atomic particle is simply not available and so numerical approximations must be used. Therefore, it is important to make sure that an approximation is chosen that best suits the given scenario. In the realm of fluid dynamics, the turbulence model is of primary importance[5].

As described in Chapter 2, the results of this study were obtained using the k-epsilon turbulence model which has been widely used by industry for aerodynamic applications. Preference for this model has been a result of its efficiency, proven robustness, and accuracy in a wide range of applications. It has, however, been known to frequently overestimate the extent of regions with attached flow and under predict separation[5]. This is due to its insensitivity to adverse pressure gradients and boundary layer separation. The k-epsilon turbulence model with standard wall functions requires that y+ values be no lower than 30 anywhere in the flow, seriously limiting boundary layer resolution[4]. A solution to this problem in the form of enhanced wall treatment was implemented by ANSYS Fluent in the most recent software releases. It allows for much smaller y+ values without necessitating excessive layers in the boundary layer, resulting in better accuracy without excessive computational time. In order to fully benefit from enhanced wall treatment, however, Fluent recommends that y+ values at the wall be close to 1.

In order to achieve the highest possible accuracy while minimizing computation time, the k-epsilon model was run with enhanced wall treatment for all CFD cases. Three layers of prism cells were used in the boundary layer and y+ values were on the order of 1.5 in regions of high gradients. The maximum y+ values near the wall were on the order of 30. In an effort to achieve additional accuracy, a third order accurate scheme was used for the flow equations and a second order accurate scheme for the equations involving turbulent kinetic energy and dissipation rate.

In CFD, the second general category of error can involve inappropriate boundary conditions and/or initial conditions, inadequate mesh design, and poor mesh quality. In

the context of the current research, the boundary conditions were relatively simple: the flow entered the domain through a velocity inlet, and exited through a pressure outlet set to zero gauge pressure. The initial conditions for the turbulence model were left at their default values which occasionally delayed convergence but did not affect solution accuracy.

Mesh design can have a significant effect on solution accuracy. The domain must be designed in such a way that is appropriate for the desired type of boundary condition. The standard C-mesh used in the present research (see Chapter 2) was designed to ensure uniform flow at the boundaries by allowing for a minimum of 3 chord lengths in any direction from the wing. It was assumed that no flux would cross the wings plane of symmetry as well as the opposing far-field boundary and so symmetry-type boundary conditions were assigned.

Perhaps the most significant source of error is mesh quality and resolution. In viscous fluid simulations, wall shear stress is the predominant driver of fluid behavior and so it is essential to have adequate resolution in the boundary layer[4]. The fluent Users Guide (Ref. 5) recommends a minimum of 10 layers near the wall for SRS simulations (Scale-Resolving Simulations). As an alternative, numerical schemes based on Reynolds Averaged Navier-Stokes (RANS) equations can be used, relaxing the cell requirement for near wall treatment but requiring careful matching of selected turbulence model and required y+ values. By using enhanced wall treatment with the k-epsilon model, the mesh design utilized fine grid resolution in regions of expected high gradients while still coarsening the mesh in wall regions where properties were likely to remain roughly constant.

In terms of mesh quality, the most significant metrics were found to be skew, aspect ratio, and orthogonality. The primary effect of these parameters was closely related to solution convergence and number of iterations to reach convergence. Using the values given in Table 6 as a threshold, 3D Fluent simulations reached convergence in an average of 400 iterations for small to medium angles of attack, and 700 iterations for high angles of attack.

Table 6: Mesh Quality Parameter Thresholds

Aspect Ratio	> 40
Orthogonality	> 0.4
Skew	< 0.7

Finally, convergence in of itself can be a source of error. Generally, the most accessible means of assessing convergence is by observing the solution residuals in combination with the force coefficient history. Frequently, the residual will decrease to a certain level, at which point a steady oscillation develops. Despite this lack of convergence in the residuals, the force coefficients generally arrive at a fixed, steady-state value signaling that the solution is fully converged. In the majority of the 3D cases run as part of this research, the force coefficients were found to have reached convergence by the time the residuals had decreased to values on the order of 4×10^{-4}. Figures 57 through 58 show the solution history for the 60 degree wing with the attached

flap at an incidence angle of 16 degrees. The damped oscillating behavior of the force coefficients was typical of the majority of cases run for both wing sweeps.

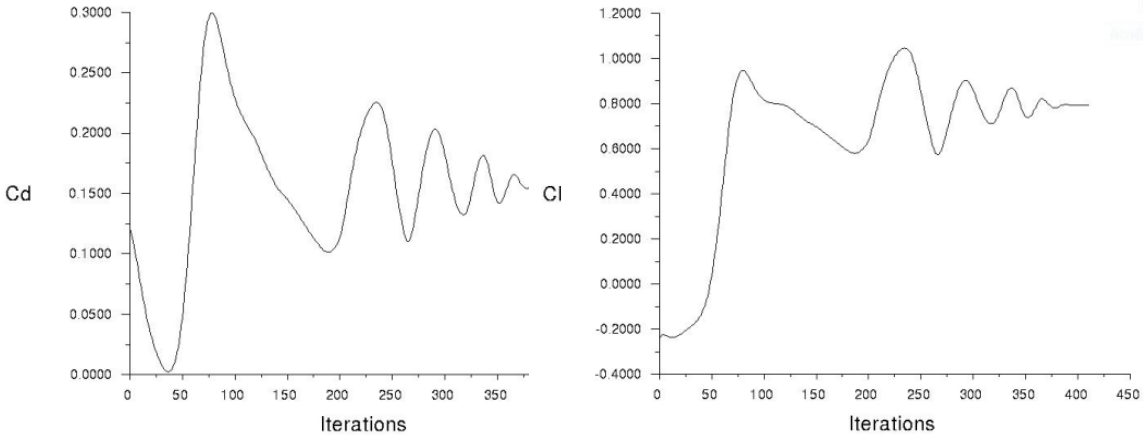

Figure 57: Force Coefficient Convergence History – 60° Wing at α = 16°

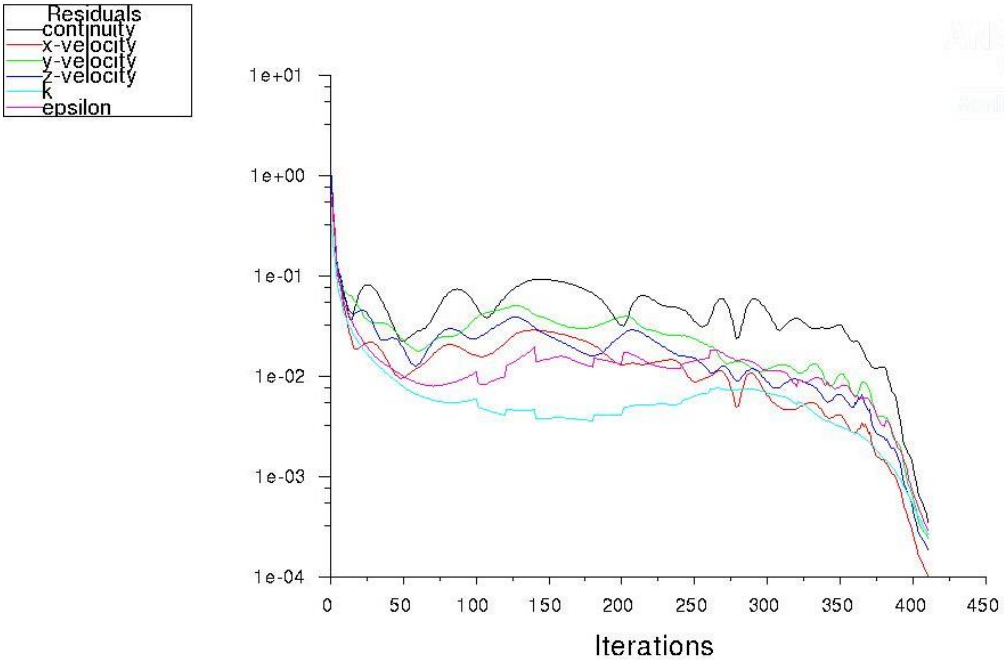

Figure 58: Residual Convergence History – 60° Wing at α = 16°

Before proceeding with the proposed LEVF design, it was important to evaluate the merit of the computational methods and results pertaining to the current research against the existing body of knowledge related to the subject. The conclusions drawn are listed below.

1. The current research results matched the predictions of simple linearized theory quite closely up to moderate angles of attack. At higher angles of attack, vortex breakdown reduced the lift of both wing sweeps somewhat earlier than theory would predict.
2. The 60 degree wing with an LEVF produced less lift at low to medium angles of attack than was indicated in both the experimental results as well as the flexible delta wing CFD study. It did, however, reach a higher maximum lift coefficient.
3. The aerodynamic efficiency of the 60 degree wing with an LEVF corresponded well to the experimental results and even exhibited a small improvement. In comparison to the flexible delta wing CFD study, however, both the 30 degree wing and 60 degree wing showed significantly lower aerodynamic efficiency. It is possible that the drag of the flexible delta wing study was under estimated.
4. Based on the comparison made to theory, experiment, and CFD, the results of the current research were deemed sufficiently valid to serve as a prediction of possible relative improvement to the aerodynamic performance of a low Reynolds number delta wing fitted with the proposed LEVF design.

4.2 Three-Dimensional Flow Effects

The design methodology used in this research was dependent on the transferability of 2D aerodynamic behavior observed on flap cross sectional geometry to that of a fully 3D wing. CFD analysis of the 2D cross sections essentially assumed an infinitely long flap and wing, which implied uniform flow in the streamwise direction and no cross flow. In fully 3D flows, this is rarely the case, especially when vortices are present. While significant differences in specific aerodynamic performance parameters were expected, it was anticipated that the overall trends resulting from varying the selected design variables would be preserved.

In the case of the reference wing, the lift slope of the 2D cross section was greater than the lift slopes of both the 30 degree and 60 degree reference wings. In terms of maximum lift coefficient, the 2D case was only slightly greater than that of the 30 degree wing but much less than the 60 degree wing. As would be expected, the 2D analysis significantly under-predicted drag at higher lift coefficients. However, the 3D wings exhibited lower overall minimum drag coefficients. The aerodynamic efficiency of all three cases matched closely up to a lift coefficient of 0.2, after which the 2D analysis predicted a much higher maximum value due to the previously mentioned under prediction of drag. The 2D analysis under reported the range of incidence angles for which the moment curve was linear. This was a result of the fact that it predicted stall at a much earlier angle of attack.

Two-D analysis of the attached flap overestimated maximum lift coefficient by 29 percent and predicted more severe stall characteristics. The drag prediction of the 2D analysis bore little resemblance to the actual drag polars of the 3D wings. However, at low lift coefficients, the 3D cases showed better drag characteristics. Similar to the reference wing, aerodynamic efficiency at medium to high lift coefficients was greatly over estimated by the 2D analysis. The general moment profile of the 2D analysis was fairly similar to that of the 30 degree wing except that it under predicted the linear moment region.

The results from analysis of the slotted flap geometry in 2D were rather surprising. The performance was significantly worse than any of the other geometries tested. Based on the successful application of slotted flaps to many current aircraft, it was expected that the secondary flow coming through the slot would add energy to the primary flow, delaying separation and increasing the maximum lift coefficient. The 2D analysis was conducted using a straight flap with a slot but, due to its poor performance, curvature in combination with the slot was not examined. Despite the poor 2D performance, a slot was re-introduced during the 3D testing and applied to the curved flap geometry. In comparison to the 2D analysis of a slotted, straight flap, the 3D analysis of a slotted flap with curvature showed great improvement in term of maximum lift coefficient. The 30 degree wing showed an improvement of 38 percent and the 60 degree wing an improvement of 84 percent. Each 3D wing case more than doubled the previous cases stall angle of attack. These results were closer to the expected behavior.

While 2D analysis of the flap and wing cross sections produced some overestimated results in terms of lift slope and maximum aerodynamic efficiency, it was

successful at predicting relative variations in performance. The advantage in performance observed by adding the curved flap geometry to the 2D reference wing was only slightly lessened when the same combination was reproduced in 3D. The 2D analysis was most successful at predicting the general shape of the 30 degree wings aerodynamic performance curves rather than those of the 60 degree wing. The assumption of an 'infinite wing" was poorly equipped to account for the phenomenon of vortex lift characteristic of low aspect ratios. Finally, the 2D analysis greatly underestimated the benefit of including a slot in the flap geometry.

4.3 Reference Wing Comparison

The flow characteristics of 30 and 60 degree delta wings are quite different as has been illustrated by the preceding analysis and discussion. For example, the wing with 60 degrees of leading edge sweep was able to reach much higher lift coefficients before experiencing stall than the wing with 30 degrees of sweep. This behavior is typical of true delta wings and is roughly predicted by vortex lift theory[8]. The behavior of the wing with 30 degrees of sweep was much closer to that of more conventional wings, i.e. higher aspect ratio wings. Consequently, when applied to each wing, the leading edge vortex flap produced differing results.

4.3.1 Vortex Behavior

In Chapter 2, stall for a delta wing was said to have occurred when the vortex breakdown location had moved over the wing trailing edge. Without the vortex in place over the wing, a significant portion of the total lift is lost. For 60 degree delta wings with sharp leading edges, the forward progression of the vortex breakdown location is gradual and does not typically move onto the wing till incidence angles of 30 or more are reached[12].

Figure 59 shows the 60 degree reference wing at an incidence angle 32 degrees. The streamlines indicate that the flow is separating cleanly off the leading edge and rolling up into a stable vortex. At this angle of attack, the wing was producing its maximum lift.

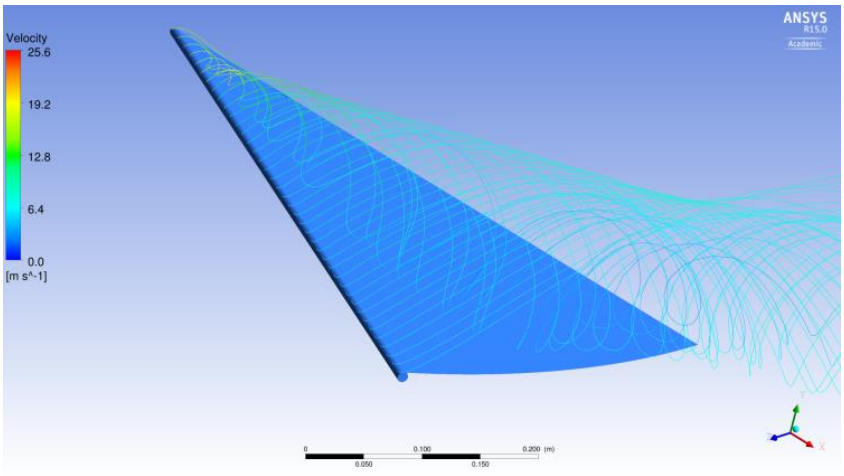

Figure 59: Sixty Degree Wing at α= 32° – Vortex Formation

In Figure 60, the 30 degree wing was at an incidence angle of only 24 degrees and was experiencing complete vortex breakdown. While the flow had also separated completely off the leading edge, only random re-circulatory motion had been established.

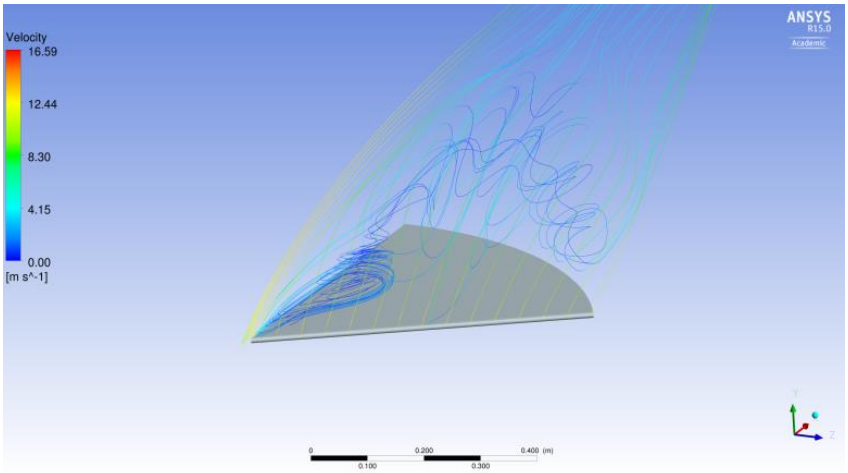

Figure 60: Thirty Degree Wing at α= 24° – Vortex Breakdown

As can be seen from the stream lines of the re-circulating flow (dark blue), the velocity was much lower that the streamlines of the vortex flow (light blue) in Figure 60.

4.3.2 Aerodynamic Forces

CFD post processing clearly showed that a lower velocity characterized the re-circulatory flow field of the 30 degree wing when experiencing vortex breakdown. This had direct implications in terms of the lower maximum lift it achieved in comparison to the 60 degree wing. The reduced velocity implied a higher local static pressure over the wing. Thus, the lift of the 30 degree wing was reduced due to a smaller differential between the pressures of the upper and lower wing surface. As can be seen from the data

presented in Table 7, the maximum lift coefficient corresponding to the 60 degree wing was approximately 50 percent greater than that of the 30 degree wing.

Table 7: Reference Wing: CL_{max}

	α	$C_{L\,max}$
30° Reference Wing	16°	0.77
60° Reference Wing	32°	1.21

Table 8 presents the minimum drag coefficients for the 30 and 60 degree wings. The 60 degree wing exhibited somewhat lower drag than the 30 degree wing. Both wings were at minimum drag at an incidence angle of 2 degrees. For a given lift coefficient, however, the 60 degree wing produced greater drag due to the increased incidence angle required to achieve the specific lift coefficient.

Table 8: Reference Wing: CD_{min}

	α	C_L	$C_{D\,min}$
30° Reference Wing	2°	0.097	0.019
60° Reference Wing	2°	0.065	0.018

As a result of its lower drag and greater lift at low incidence angles, the 30 degree wing exhibited better aerodynamic efficiency than the 60 degree wing. In terms of maximum aerodynamic efficiency (Table 9), the two wings differed by almost 28 percent. Both wings reached their respective maximum values at identical incidence

angles but differing lift coefficients. These lift coefficient values are relatively low and are indicative of the need for improving the general aerodynamic performance of the reference wing designs.

Table 9: Reference Wing: Aerodynamic Efficiency

	α	C_L	L/D_{max}
30° Reference Wing	6°	0.32	10.72
60° Reference Wing	6°	0.24	8.40

Both wings exhibited significant moment variation with change in angle of attack when the geometric quarter-chord was used as the moment center. However, for low to moderate incidence angles, the respective moments varied linearly with angle of attack, indicating a roughly constant moment about the true aerodynamic center of the wing. As shown in Table 10, the true aerodynamic center of the 30 degree wing was found to be forward of its quarter chord whereas the opposite was true of the 60 degree wing. For incidence angles up to 14 degrees, the 60 degree wing showed an average moment coefficient of -0.0031. The 30 degree wing was approximately linear up to 9 degrees angle of attack with an average moment coefficient of -0.0068. Outside of these linear ranges, both wings experienced a significant increase in moment magnitude, although the change in moment of the 30 degree wing was significantly more extreme. These changes in moment at high angles of attack were a result of wing losing vortex lift, causing the aerodynamic center to move rearward behind the center of mass. The fact that the average moment coefficients are negative (nose down) is typical of wings that are not

stabilized by a tail surface. To satisfy static stability requirements, the moment about a complete aircrafts aerodynamic center must be positive. For this reason, both reference wings were unstable in the absence of additional control surface input.

Table 10: Reference Wing: Aerodynamic Efficiency

	α	X_{ac}	$C_{M,ac}$ *(avrg.)*
30° Reference Wing	0° - 9°	16.8 % MAC	-0.0068
60° Reference Wing	0° - 14°	30.7 % MAC	-0.0031

The primary purpose for comparing the 30 degree and 60 degree reference wings was to gain insight into the flow behavior governing the difference in aerodynamic performance between the two wings. This knowledge then helped to provide a better understanding of the improved aerodynamic behavior achieved by the addition of LEVF devices.

In summary, the 30 degree wing possessed the greatest overall aerodynamic efficiency but was significantly more limited in terms of maximum lift coefficient than the 60 degree wing. This trend was inherently linked to the formation and stability of the leading edge vortex. Both wings possessed a negative moment about their respective aerodynamic centers that was relatively constant at low angles of attack. However, the moment coefficient of the 60 degree wing was constant up to higher angles of attack and changed less abruptly with the onset of stall.

4.4 Flap Comparison

Based on the 2D analysis alone, the attached flap clearly outperformed the slotted flap. Further analysis, however, showed that 3D effects significantly modified and improved the performance of the slotted flap in comparison to the 2D analysis. For that reason, a comparison was made of the relative improvements each flap achieved when applied to the reference wings.

4.4.1 Vortex Behavior

An important characteristic of the attached flap design was the fact that its curvature connected smoothly to the wings upper surface at the 30 degree deflection angle used for analysis. This was beneficial in maintaining vortex stability at angles of attack close to stall. Adding a slot to the flap geometry also aided in delaying vortex breakdown, although by means of a different mechanism. The slot allowed a secondary flow to mix with the primary flow at the flap hinge line, adding energy. Figures 61 and 62 depict the vortices that exist on the upper surface of the 60 degree wing in each flap case. The attached flap appears to produce a uniform primary vortex with a single, secondary vortex inside while the slotted flap produces multiple secondary vortices and is more chaotic. The depicted flow visualizations represent both flaps at an angle of attack corresponding to their respective maximum lift.

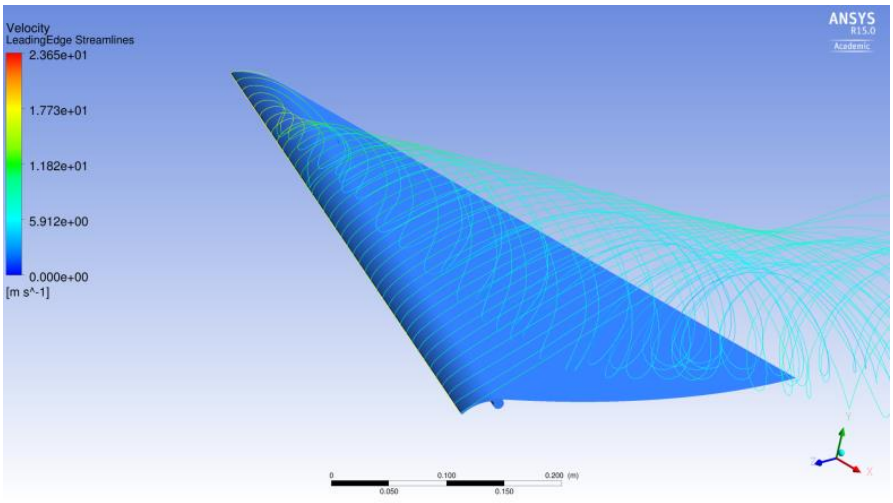

Figure 61: Sixty Degree Wing at α = 30 – Attached Flap

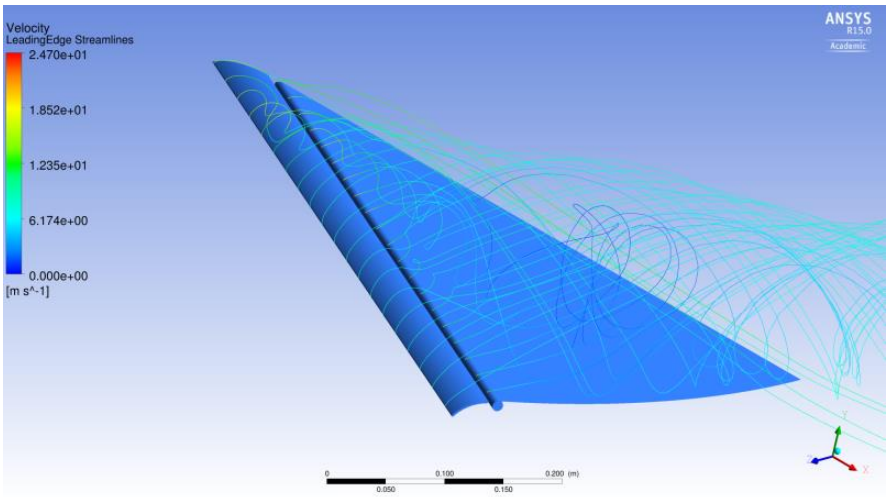

Figure 62: Sixty Degree Wing at α = 32 – Slotted Flap

4.4.2 Aerodynamic Forces

An interesting result was that the attached flap produced the highest maximum lift coefficient for the 60 degree wing but at a slightly lower angle of attack than was

achieved by the slotted flap. As shown in Table 11, both flap designs reached maximum lift at the same incidence angle for the 30 degree wing, although the slotted flap outperformed the attached flap by 7 percent.

Table 11: Flap Comparison – Maximum Lift Coefficient

	Attached Flap		*Slotted Flap*	
	α	$C_{L\ max}$	α	$C_{L\ max}$
30° Wing	18°	0.97	18°	1.037
60° Wing	30°	1.42	32°	1.38

At lift coefficients ranging from 0 to 0.8 for the 30 degree wing and 0 to 0.55 for the 60 degree wing, the attached flap clearly produced less drag than the slotted flap. This resulted from the slotted flap losing part of the thrust gained by repositioning the vortex over the leading edge flap. Minimum drag was attained by both flap geometries at almost identical angles of attack for both wings. For the 60 degree wing, the attached flap produced a noticeably lower minimum drag coefficient when compared to the slotted flap. Table 12 lists the respective minimum drag data.

Table 12: Flap Comparison – Minimum Drag

	Attached Flap			*Slotted Flap*		
	α	C_L	$C_{D\,min}$	α	C_L	$C_{D\,min}$
30° Wing	3°	0.13	0.027	3°	0.14	0.027
60° Wing	3°	0.099	0.023	2°	0.050	0.026

As has been discussed above, the attached flap generally exhibited the best lift and drag characteristics with the exception of the 30 degree wing at high angles of attack. Consequently, it achieved better maximum aerodynamic efficiency in both wing cases when compared to the slotted flap. Based on the values given in Table 13, the attached flaps maximum aerodynamic efficiency was on average 11 percent greater than that of the slotted flap.

Table 13: Flap Comparison –Aerodynamic Efficiency

	Attached Flap			*Slotted Flap*		
	α	C_L	$L/D_{\,max}$	α	C_L	$L/D_{\,max}$
30° Wing	9°	0.51	10.82	9°	0.50	9.61
60° Wing	9°	0.39	9.278	9°	0.39	8.50

The key to this advantage lies in the inherently lower drag produced by having the flap completely attached to the wing leading edge. This is illustrated by the following two figures showing both flap designs applied to the 60 degree wing at their common incidence angle for maximum aerodynamic efficiency. On the upper wing surface,

vectors indicate both the magnitude and direction of the force being exerted by the fluid on the wing. In Figure 63, a significant number of force vectors are tilted slightly forward in a direction normal to the leading edge flap surface. The forward tilt of these vectors is responsible for the small component of thrust that helps to cancel drag, thereby making LEVF devises successful at improving delta wing aerodynamic efficiency.

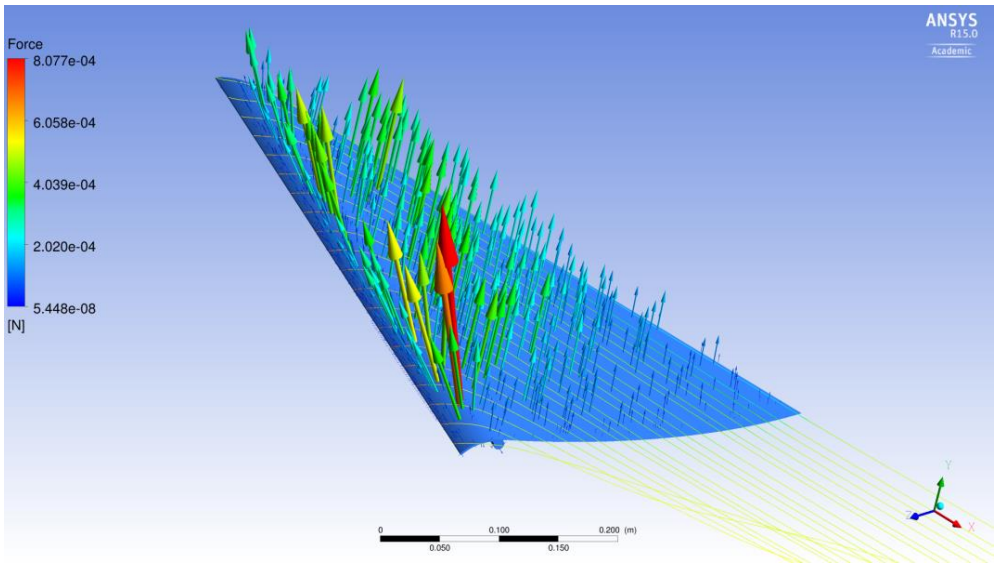

Figure 63: Attached Flap Force Vectors – alpha = 9

Figure 64 shows the slotted flap in the same scenario. The force vectors are clearly not providing the added component of thrust. This is likely a result of the secondary flow moving the primary vortex back onto the main wing upper surface where the normal vector is tilted slightly downstream.

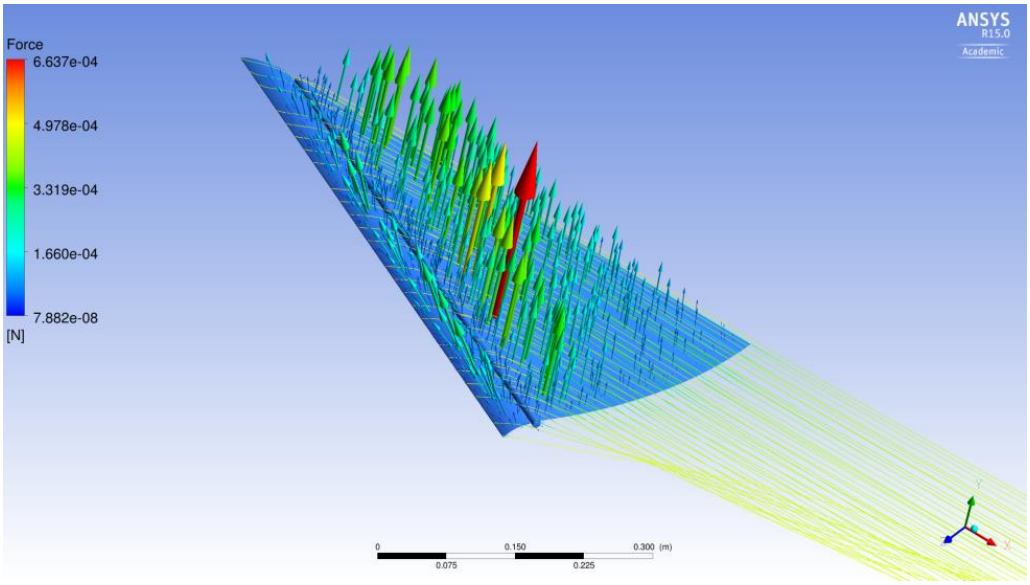

Figure 64: Slotted Flap Force Vectors – alpha = 9

Both flap designs produced similar effects on the moment behavior about each wings aerodynamic center. As would be expected, addition of a flap resulted in the true aerodynamic center shifting forward relative to its location without the flap. Since the reference wing mean aerodynamic chord (MAC) was kept as the reference length, the new aerodynamic center locations were both forward of the quarter chord point. Table 14 shows that aerodynamic center of the 30 degree wing was significantly forward of the quarter chord location in contrast to the 60 degree wing, which was very close to the 25 MAC percent location. It was interesting to note that the slotted flap extended the constant moment behavior of each wing to higher angles of attack.

Table 14: Flap Comparison – Moment about the Aerodynamic Center

	Attached Flap			*Slotted Flap*		
	α	X_{ac}	$C_{M\,ac}$ *(avrg.)*	α	X_{ac}	$C_{M\,ac}$ *(avrg.)*
30° Wing	0° - 14°	11.1 % MAC	-0.022	0° - 16°	11.6 % MAC	-0.023
60° Wing	0° - 18°	23.0 % MAC	-0.019	0° - 24°	24.5 % MAC	-0.014

In terms of key metrics such as lift, drag, and aerodynamic efficiency, both flap designs produced significant improvements in aerodynamic performance over the baseline reference wings data. When compared to each other, some differences in performance become evident.

The attached flap performed best overall, especially when applied to the 60 degree wing. It achieved the highest maximum aerodynamic efficiency for both wing cases and also exhibited the most consistent moment behavior. While the slotted flap did achieve the highest maximum lift for the 30 degree wing case, the attached flap reached a maximum value of similar magnitude and also exhibited more gradual stall behavior. Based on this brief comparative analysis, the attached flap was selected as the final flap design due primarily to its advantage in terms of improved aerodynamic efficiency over the widest range of lift coefficients.

4.5 Control Effectiveness

As was shown earlier in this study, a stable moment about the aerodynamic center of a delta wing – flap combination can exist over a reasonable range of wing incidence angles and flap deflections angles. It has also been shown that CFD analysis predicts a linear relationship between moment magnitude and flap deflection for delta wings of both 30 and 60 degree sweeps. Figure 15 provides a plot of average moment coefficient values versus flap deflection angle. The moment coefficients were averaged over the linear region of the respective moment curves; generally incidence angles of 0 to 10 degrees. The slopes of the curves in Figure 65 are an important relationship that has implications in terms of stability and control. Defined as the change in moment with respect to flap deflection ($\partial C_M / \partial VF$), the negative values of these stability derivatives are indicative of positive longitudinal stability. Based on these results it is reasonable to conclude that a delta wing equipped with only a leading edge flap could be successfully trimmed to steady, level flight.

Table 15: Derivative of $C_{M\,ac}$ with respect to vortex flap deflection angle

	$\partial C_{M\,ac} / \partial VF$
30° Wing	-0.0007747
60° Wing	-0.00058297

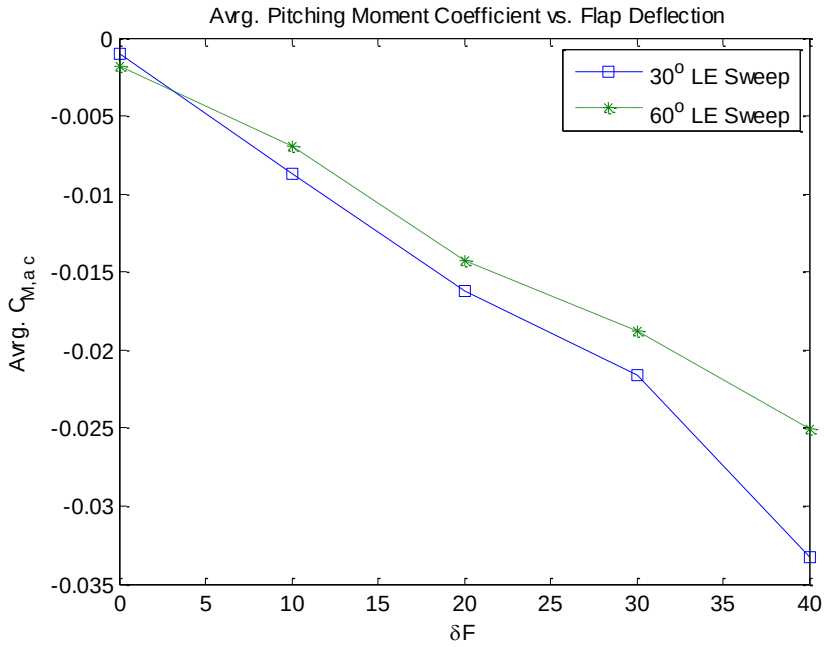

Figure 65: Plot of Average $C_{M\,ac}$ With Respect to Flap Deflection Angle

CHAPTER 5: CONCLUSION AND FUTURE WORK

5.1 Results Review

Portability is an important requirement for many current and emerging UAV missions. A foldable delta wing made of a flexible material would provide excellent portability and versatility if a solution can be found for improving the inherently poor performance of delta wings at low speeds and Reynolds numbers. Leading edge vortex flaps have been successfully used to improve the performance of delta wings at high speeds and show potential to do the same at low speeds. With this goal in mind, CFD analysis was conducted on a series of 2 and 3 dimensional delta wing models in order to design a leading edge flap optimized with respect to four key performance parameters: aerodynamic efficiency, maximum lift coefficient, stall behavior, and moment characteristics about the reference quarter chord. The geometric optimization variables included flap length, curvature, gap, and deflection angle. Wings with leading edge sweeps of both 30 degrees and 60 degrees were included in the study. Upon completion of the analysis, it was determined that leading edge vortex flaps can provide meaningful improvement in the performance of delta wings and possibly be used as a means of vehicle control.

5.2 Final Flap Design

As a result of the preceding 2D and 3D analysis, the attached flap configuration with constant curvature was chosen as the final design based on its potential for improving aerodynamic efficiency, high maximum lift coefficient, moderate stall behavior, and constant moment about the wings aerodynamic center. The flap dimensions are provided in Table 16 as percentages of the reference wings MAC. The optimum deflection angle was determined to be 20 degrees in the positive direction (down). In this configuration, the flap contributed the best average performance increase to both the 30 and 60 degree wings.

Table 16: Final Flap Dimensions Referenced to Wing MAC

Chord Length	8 %
Radius of Curvature	10 %
Thickness	0.5 %
Optimum Deflection Angle	20°

In fulfillment of a primary goal of this research, the final flap design was shown to provide meaningful improvement to the maximum aerodynamic efficiency of both the 30 degree and 60 degree reference wing models. The increments in maximum lift and aerodynamic efficiency achieved by the flap are listed in Table 17 as a percentage increases over each reference wings performance. As can be seen, the flap was most successful when applied to the 60 degree wing

Table 17: Final LEVF Design Performance Increment Relative to Reference Wing

	$C_{L\ max}$	$L/D_{\ max}$
30° Wing	10.26	3.92
60° Wing	21.84	9.24

For the sake of completeness, Table 18 provides a list of the actual performance numbers achieved by each flap / wing combination.

Table 18: Final LEVF Aerodynamic Performance Numbers

	$C_{L\ max}$	$C_{D\ min}$	$L/D_{\ max}$	$C_{M\ ac}$
30° Wing	0.8693	0.02312	11.14	-0.01626
60° Wing	1.473	0.02149	9.172	-0.01425

In terms of stability, the flap was found to produce a constant moment about each wings aerodynamic center that varied linearly with flap deflection angle. CFD results indicated that a sufficiently negative flap deflection angle (deflected upward) could produce the required positive moment about the aerodynamic center necessary to establish positive static longitudinal stability for a flying wing.

5.3 Application

Potential applications for the LEVF system developed from this research are many, and varied. In the context of delta wings, the addition of a flap system that can

both improve aerodynamic performance as well as provide vehicle control would greatly facilitate numerous alternative design concepts such as the flexible, Rogallo type delta wings mentioned in Chapter 1. By implementing a leading edge flap system as the primary means of vehicle control, need for conventional tail surfaces and / or canards is avoided and considerable weight savings could be realized. Additionally, the relocation of all control connections and mechanisms to the wing main spar region would reduce the complexity of the wing, possible further reducing weight. Reduction in weight would strongly benefit the portability of small UAVs and expand their options in terms of deployment.

5.4 Future Work

While endeavoring to be as thorough as possible, the scope of the current research was intended to be narrowly focused on a few key variables and applications in order to gain clearer insight into the complex problem of delta wing aerodynamic performance. Time and available resources placed additional constraints on the research that necessitated a progressively deductive approach to refining the project goals.

During the research process, results were occasionally encountered that produced unanswered question. For example, when the 2D flap cross sections were being compared based on various amounts of curvature, the resultant relationship between curvature and maximum lift was non-linear and considerably different from the expected behavior. Further, more detailed CFD analysis would be beneficial in understanding the reason for the observed behavior. In general, additional CFD analysis on a wider range of geometric

variables would likely produce a more refined flap design that is better optimized to achieve maximum aerodynamic efficiency. At the outset of the research project, it was planned to break the flap into multiple elements in order to study the change in moments observed when an individual element was set at varying deflection angles with the rest held constant. Ultimately, only deflection of the flap as a whole was analyzed. A multi-element study would, however, be necessary in order to definitely assess the flaps suitability as a means of primary vehicle control.

Future work would begin by using wind tunnel tests to verify the results obtained through CFD. Additional CFD analysis as well as wind tunnel testing of other wing sweep angles and flow Reynolds numbers would be useful in better defining the range of conditions for which LEVF devices could be used to improve delta wing performance. Once sufficient confidence in the flap design is established, a prototype could be built and test on a small RC aircraft. Focus could be given to designing a hinge mechanism that is simple and light, yet maintains a smooth surface over the hinge line.

REFERENCES

[1] Anderson Jr., J. D. (2010). *Fundamentals of Aerodynamics* (5 ed.). Boston: McGraw-Hill.

[2] Anderson Jr., J. D. (2012). *Introduction to Flight* (7 ed.). New York: McGraw-Hill.

[3] Anderson, Jr., J. D. (1995). *Computational Fluid Dynamics: The Basics With Applications.* New-York: McGraw-Hill.

[4] ANSYS, Inc. (Release 15, November 2013). *ANSYS Fluent Theory Guide.* Canonsburg, PA: ANSYS, Inc.

[5] ANSYS, Inc. (Release 15, November 2013). *ANSYS Fluent User's Guide.* Canonsburg, PA: ANSYS, Inc.

[6] Brandon, J. M., Hallissy, J. B., Brown, P. W., & Lamar, J. E. (2003). *In-Flight Flow Visualization Results of the F-106B with a Vortex Flap.* Langley Research Center. Hampton, VA: NASA .

[7] Department of Defense, United States of America. (2005). *Unmanned Aircraft Systems Roadmap 2005 - 2030.*

[8] Kuethe, A. M., & Chow, C.-Y. (1998). *Foundations of Aerodynamic Design.* New York: John Wiley & Sons, Inc.

[9] Noll, T. E., Brown, J. M., Perez-Davis, M. E., Ishmael, S. D., Tiffany, G. C., & Gaier, M. (2004). *Investigation of the Helios Prototype Aircraft Mishap, Volume I, Mishap Report.* Langley Research Center. Hampton, VA: NASA.

[10] Polhamus, E. C. (1966). *A Concept of the Vortex Lift of Sharp-Edged Delta Wings Based on a Leading-Edge Suction Analogy.* Washington, D.C.: NASA Technical Notes, TN-D3767.

[11] Schmidt, D. K. (2012). *Modern Flight Dynamics.* New York: McGraw-Hill.

[12] Stollery, J. L., & Hu, B. K. (1990). *The Performance of 60 degree Delta Wings: The Effects of Leading Edge Radius on Vortex Flaps and the Wing.* Cranfield Institute of Technology, College of Aeronautics. Bedford, England: Cranfield.

[13] Warchol, M. L. (2009). *An Investigation of Flexible Rogallo Type Wing Aerodynamics and the Applications to UAVs.* Columbus, OH: The Ohio State University.

[14] Whitfield, C. A., & Warchol, M. (March 2011). Flight Performance Characteristics of Highly Flexible Wing Rogallo-type Aerodynamics with Applications to UAVs. *AIAA Dayton-Cincinnati Aerospace Sciences Symposium.*

APPENDIX A

Table A1: Two-Dimensional Straight & Slotted Flap Cross Section Data

C_d						
α	length = 4%	length = 8%	length = 12%	Slot = 1.2%	Slot = 2.3%	Slot = 3.5%
0	0.0335	0.0498	0.0677	0.0548	0.0701	0.0623
1	0.0280	0.0405	0.0546	0.0445	0.0589	0.0519
2	0.0237	0.0344	0.0452	0.0378	0.0498	0.0434
3	0.0226	0.0304	0.0391	0.0366	0.0436	0.0378
4	0.0235	0.0283	0.0353	0.0391	0.0444	0.0410
5	0.0255	0.0274	0.0334	0.0431	0.0499	0.0480
6	0.0289	0.0278	0.0329	0.0541	0.0559	0.0541
7	0.0350	0.0305	0.0331	0.0758	0.0707	0.0725
8	0.0456	0.0359	0.0365	0.0958	0.0927	0.0919
9	0.0652	0.0469	0.0455	0.1088	0.1121	0.1107
10	0.0964	0.0845	0.0923	0.1188	0.1277	0.1218
11	0.1163	0.1120	0.1131	0.1279	0.1414	0.1323
12	0.1290	0.1242	0.1249	0.1369	0.1540	0.1432
13	0.1403	0.1345	0.1348	0.1466	0.1662	0.1540
14	0.1518	0.1448	0.1444	0.1572	0.1782	0.1654
15	0.1643	0.1557	0.1546	0.1685	0.1905	0.1774
16	0.1783	0.1675	0.1655	0.1802	0.2033	0.1900
C_l						
α	length = 4%	length = 8%	length = 12%	Slot = 1.2%	Slot = 2.3%	Slot = 3.5%
0	-0.0592	-0.1899	-0.3371	-0.2045	-0.2035	-0.2145
1	0.0631	-0.0270	-0.1522	-0.0498	-0.0701	-0.0771
2	0.1798	0.1138	0.0223	0.0931	0.0631	0.0571
3	0.2888	0.2433	0.1779	0.2261	0.1931	0.1891
4	0.3942	0.3660	0.3180	0.3505	0.3209	0.3167
5	0.4978	0.4844	0.4487	0.4757	0.4392	0.4394
6	0.5995	0.5989	0.5733	0.5820	0.5571	0.5584

7	0.6974	0.7054	0.6957	0.6986	0.6542	0.6732
8	0.7886	0.8063	0.8051	0.7500	0.7322	0.7299
9	0.8709	0.8979	0.9027	0.7349	0.7660	0.7498
10	0.9133	0.9606	0.9499	0.7103	0.7722	0.7282
11	0.8797	0.9097	0.9009	0.6932	0.7704	0.6920
12	0.8455	0.8631	0.8643	0.6867	0.7686	0.6671
13	0.8265	0.8414	0.8469	0.6909	0.7703	0.6639
14	0.8188	0.8380	0.8455	0.7038	0.7754	0.6720
15	0.8175	0.8470	0.8565	0.7206	0.7855	0.6871
16	0.8181	0.8652	0.8757	0.7397	0.7996	0.7061
$C_{m\ c/4}$						
α	length = 4%	length = 8%	length = 12%	Slot = 1.2%	Slot = 2.3%	Slot = 3.5%
0	-0.0211	-0.0250	-0.0037	-0.0211	-0.0194	-0.0153
1	-0.0171	-0.0327	-0.0298	-0.0326	-0.0298	-0.0273
2	-0.0115	-0.0305	-0.0397	-0.0359	-0.0345	-0.0337
3	-0.0069	-0.0238	-0.0379	-0.0322	-0.0365	-0.0347
4	-0.0033	-0.0153	-0.0298	-0.0259	-0.0340	-0.0353
5	0.0001	-0.0061	-0.0188	-0.0208	-0.0309	-0.0324
6	0.0031	0.0029	-0.0067	-0.0209	-0.0261	-0.0277
7	0.0053	0.0096	0.0066	-0.0438	-0.0308	-0.0411
8	0.0053	0.0150	0.0163	-0.0773	-0.0517	-0.0584
9	-0.0039	0.0175	0.0224	-0.0920	-0.0734	-0.0758
10	-0.0442	-0.0186	-0.0344	-0.0964	-0.0869	-0.0896
11	-0.0710	-0.0643	-0.0667	-0.0961	-0.0946	-0.0984
12	-0.0792	-0.0732	-0.0739	-0.0938	-0.0985	-0.1021
13	-0.0815	-0.0747	-0.0741	-0.0910	-0.1002	-0.1005
14	-0.0818	-0.0737	-0.0716	-0.0885	-0.1001	-0.0984
15	-0.0818	-0.0718	-0.0683	-0.0864	-0.0992	-0.0965
16	-0.0823	-0.0698	-0.0648	-0.0847	-0.0977	-0.0949

Table A2: Two-Dimensional Reference & Curved Geometry Flap Cross Section Data

C_d						
α	Ref. C.S.	radius = 22.1%	radius = 9.8%	radius = 8.6%	radius = 7.1%	radius= 5.2%
0	0.0296	0.0546	0.0561	0.0519	0.0548	0.0505
1	0.0271	0.0451	0.0467	0.0423	0.0453	0.0411
2	0.0264	0.0388	0.0399	0.0357	0.0385	0.0349
3	0.0272	0.0347	0.0351	0.0312	0.0337	0.0310
4	0.0298	0.0323	0.0320	0.0285	0.0307	0.0287
5	0.0343	0.0316	0.0304	0.0273	0.0290	0.0276
6	0.0411	0.0322	0.0301	0.0271	0.0289	0.0276
7	0.0515	0.0342	0.0318	0.0285	0.0305	0.0297
8	0.0777	0.0393	0.0350	0.0315	0.0334	0.0332
9	0.1044	0.0486	0.0393	0.0357	0.0377	0.0388
10	0.1234	0.0966	0.0452	0.0416	0.0440	0.0479
11	0.1389	0.1197	0.0532	0.0506	0.0528	0.0654
12	0.1529	0.1326	0.0641	0.0671	0.0649	0.1123
13	0.1666	0.1439	0.0795	0.1238	0.0819	0.1283
14	0.1801	0.1552	0.1046	0.1395	0.1078	0.1398
15	0.1939	0.1673	0.1504	0.1519	0.1430	0.1506
16	0.2081	0.1802	0.1729	0.1642	0.1660	0.1621
C_l						
α	Ref. C.S.	radius = 22.1%	radius = 9.8%	radius = 8.6%	radius = 7.1%	radius= 5.2%
0	-0.0278	-0.2034	-0.1620	-0.1943	-0.1612	-0.1919
1	0.0789	-0.0398	-0.0177	-0.0324	-0.0164	-0.0296
2	0.1836	0.1046	0.1161	0.1092	0.1177	0.1112
3	0.2866	0.2373	0.2438	0.2396	0.2449	0.2410
4	0.3876	0.3621	0.3661	0.3631	0.3670	0.3633
5	0.4859	0.4816	0.4846	0.4821	0.4852	0.4809
6	0.5803	0.5972	0.5998	0.5980	0.5995	0.5955
7	0.6689	0.7091	0.7093	0.7087	0.7088	0.7034
8	0.7492	0.8127	0.8150	0.8142	0.8146	0.8076
9	0.8013	0.9082	0.9175	0.9164	0.9172	0.9064
10	0.8121	0.9511	1.0151	1.0133	1.0131	0.9969
11	0.8056	0.8925	1.1050	1.1009	1.1005	1.0695
12	0.7964	0.8460	1.1840	1.1685	1.1757	1.0006
13	0.7896	0.8201	1.2448	1.0082	1.2306	0.9336
14	0.7847	0.8097	1.2639	0.9358	1.2420	0.9022
15	0.7830	0.8093	1.1222	0.9014	1.1565	0.8898

16	0.7833	0.8152	1.0514	0.8868	1.0899	0.8906
$C_{m\ c/4}$						
α	Ref. C.S.	radius = 22.1%	radius = 9.8%	radius = 8.6%	radius = 7.1%	radius= 5.2%
0	-0.0096	-0.0110	-0.0221	-0.0185	-0.0242	-0.0227
1	-0.0085	-0.0214	-0.0259	-0.0272	-0.0279	-0.0309
2	-0.0072	-0.0214	-0.0235	-0.0260	-0.0252	-0.0290
3	-0.0061	-0.0160	-0.0175	-0.0200	-0.0190	-0.0225
4	-0.0052	-0.0082	-0.0098	-0.0120	-0.0111	-0.0142
5	-0.0048	0.0005	-0.0014	-0.0030	-0.0027	-0.0056
6	-0.0051	0.0093	0.0070	0.0059	0.0055	0.0029
7	-0.0068	0.0176	0.0147	0.0138	0.0130	0.0104
8	-0.0207	0.0241	0.0216	0.0207	0.0199	0.0170
9	-0.0510	0.0282	0.0281	0.0271	0.0263	0.0222
10	-0.0722	-0.0249	0.0339	0.0326	0.0315	0.0252
11	-0.0847	-0.0613	0.0384	0.0359	0.0354	0.0203
12	-0.0922	-0.0711	0.0406	0.0321	0.0367	-0.0477
13	-0.0971	-0.0737	0.0384	-0.0499	0.0327	-0.0639
14	-0.1004	-0.0737	0.0225	-0.0626	0.0146	-0.0672
15	-0.1024	-0.0730	-0.0361	-0.0655	-0.0269	-0.0670
16	-0.1041	-0.0726	-0.0553	-0.0660	-0.0476	-0.0661

Table A3: Three-Dimensional Wing Data – $\Lambda = 30°$

C_D				
α	Flat Plate	Reference	Curved LEVF	Slotted LEVF
0	0.0133	0.0206	0.0374	0.0385
2	0.0160	0.0193	0.0288	0.0377
3	0.0193	0.0203	0.0266	0.0270
5	0.0314	0.0257	0.0282	0.0333
6	0.0405	0.0302	0.0314	0.0371
9	0.0780	0.0563	0.0467	0.0520
12	0.1269	0.1098	0.0708	0.0753
14	0.1570	0.1514	0.0938	0.0970
16	0.1815	0.1940	0.1330	0.1241

18	0.2057	0.2155	0.1941	0.1588
20	0.2278	0.2403	0.2393	0.2256
22	0.2493	0.2683	0.2740	0.2573
24	0.2712	0.2964	0.3152	0.2930
C_L				
α	Flat Plate	Reference	Curved LEVF	Slotted LEVF
0	-0.0008	-0.0161	-0.0573	-0.0628
2	0.1053	0.0967	0.0651	0.0725
3	0.1586	0.1531	0.1312	0.1350
5	0.2665	0.2672	0.2583	0.2580
6	0.3193	0.3238	0.3195	0.3172
9	0.4661	0.4949	0.5052	0.4995
12	0.5829	0.6484	0.6913	0.6846
14	0.6185	0.7249	0.8121	0.8064
16	0.6222	0.7667	0.9240	0.9255
18	0.6235	0.7400	0.9658	1.0375
20	0.6176	0.7329	0.9337	1.0132
22	0.6104	0.7359	0.9036	0.9511
24	0.6043	0.7368	0.8862	0.9173
$C_{M\ c/4}$				
α	Flat Plate	Reference	Curved LEVF	Slotted LEVF
0	0.0006	-0.0083	-0.0306	-0.0309
2	0.0087	0.0005	-0.0152	-0.0153
3	0.0130	0.0047	-0.0056	-0.0080
5	0.0220	0.0129	0.0124	0.0040
6	0.0257	0.0169	0.0208	0.0112
9	0.0306	0.0271	0.0453	0.0364
12	0.0044	0.0238	0.0673	0.0608
14	-0.0220	0.0067	0.0794	0.0748
16	-0.0346	-0.0315	0.0841	0.0864
18	-0.0407	-0.0503	0.0393	0.0933
20	-0.0426	-0.0571	-0.0058	0.0230
22	-0.0430	-0.0629	-0.0247	-0.0175
24	-0.0440	-0.0637	-0.0385	-0.0393

Table A4: Three-Dimensional Wing Data – $\Lambda = 60°$

C_D				
α	Flat Plate	Reference	Curved LEVF	Slotted LEVF
0	0.0147	0.0188	0.0310	0.0338
2	0.0165	0.0178	0.0238	0.0255
3	0.0189	0.0187	0.0232	0.0257
5	0.0306	0.0236	0.0256	0.0295
6	0.0391	0.0285	0.0284	0.0324
9	0.0754	0.0560	0.0423	0.0460
12	0.1283	0.1001	0.0690	0.0687
14	0.1658	0.1379	0.1051	0.0915
16	0.2203	0.1770	0.1577	0.1323
18	0.2807	0.2316	0.2143	0.1892
20	0.3454	0.2928	0.2845	0.2546
22	0.4181	0.3575	0.3617	0.3241
24	0.4918	0.4280	0.4476	0.3858
26	0.5650	0.5041	0.5381	0.4560
28	0.6132	0.5666	0.6234	0.5338
30	0.5486	0.6271	0.7004	0.6108
32	0.5646	0.6869	0.7306	0.7025
34	0.5978	0.6490	0.7337	0.7193
C_L				
α	Flat Plate	Reference	Curved LEVF	Slotted LEVF
0	0.0006	-0.0206	-0.0599	-0.0583
2	0.0791	0.0645	0.0471	0.0496
3	0.1215	0.1074	0.0988	0.1008
5	0.2132	0.1941	0.1988	0.1972
6	0.2610	0.2394	0.2479	0.2459
9	0.4122	0.3854	0.3923	0.3904
12	0.5654	0.5378	0.5413	0.5341
14	0.6342	0.6368	0.6624	0.6316
16	0.7473	0.7094	0.7927	0.7466
18	0.8516	0.8132	0.8951	0.8751
20	0.9410	0.9153	1.0206	0.9992
22	1.0328	1.0029	1.1382	1.1055
24	1.1034	1.0803	1.2461	1.1562
26	1.1588	1.1550	1.3394	1.2111
28	1.1523	1.1836	1.3971	1.2724

30	0.9433	1.2007	1.4176	1.3160
32	0.8986	1.2092	1.3337	1.3801
34	0.8827	1.0494	1.2195	1.2903
$C_{M\ c/4}$				
α	Flat Plate	Reference	Curved LEVF	Slotted LEVF
0	0.0001	-0.0044	-0.0190	-0.0181
2	-0.0065	-0.0088	-0.0157	-0.0177
3	-0.0099	-0.0111	-0.0143	-0.0178
5	-0.0166	-0.0159	-0.0117	-0.0162
6	-0.0200	-0.0186	-0.0107	-0.0153
9	-0.0320	-0.0281	-0.0083	-0.0123
12	-0.0449	-0.0396	-0.0079	-0.0107
14	-0.0449	-0.0471	-0.0126	-0.0107
16	-0.0695	-0.0486	-0.0155	-0.0163
18	-0.0846	-0.0717	-0.0170	-0.0239
20	-0.1038	-0.0874	-0.0275	-0.0307
22	-0.1270	-0.1021	-0.0361	-0.0332
24	-0.1511	-0.1263	-0.0540	-0.0326
26	-0.1776	-0.1522	-0.0731	-0.0490
28	-0.1994	-0.1744	-0.0950	-0.0705
30	-0.2062	-0.2001	-0.1252	-0.0966
32	-0.2545	-0.2338	-0.1722	-0.1263
34	-0.2795	-0.2551	-0.2174	-0.1487

Table A5: Flap Deflection Data – $\Lambda = 30°$

C_D					
α	*δF = 0*	*δF = 10*	*δF = 20*	*δF = 30*	*δF = 40*
-2	0.0294	0.0277	0.0422	0.0374	0.0646
0	0.0264	0.0227	0.0282	0.0288	0.0511
2	0.0265	0.0225	0.0231	0.0266	0.0423
4	0.0298	0.0259	0.0247	0.0282	0.0373
6	0.0392	0.0328	0.0307	0.0314	0.0380
8	0.0666	0.0443	0.0406	0.0467	0.0434
10	0.1073	0.0631	0.0548	0.0708	0.0539
12	0.1511	0.1065	0.0754	0.0938	0.0697

16	0.2206	0.2039	0.1767	0.1330	0.1165
18	0.2500	0.2384	0.2190	0.1941	0.1621
20	0.2772	0.2674	0.2570	0.2393	0.2123
22	0.3045	0.3015	0.2937	0.2740	0.2574
24	0.3308	0.3231	0.3249	0.3152	0.2863
C_L					
α	*δF = 0*	*δF = 10*	*δF = 20*	*δF = 30*	*δF = 40*
-2	-0.1221	-0.1430	-0.1643	-0.0573	-0.1941
0	-0.0032	-0.0227	-0.0389	0.0651	-0.0820
2	0.1161	0.0995	0.0867	0.1312	0.0347
4	0.2363	0.2208	0.2088	0.2583	0.1603
6	0.3589	0.3430	0.3303	0.3195	0.2896
8	0.4827	0.4650	0.4527	0.5052	0.4187
10	0.5932	0.5872	0.5747	0.6913	0.5467
12	0.6863	0.7022	0.6967	0.8121	0.6708
16	0.7442	0.7984	0.8693	0.9240	0.9128
18	0.7466	0.7990	0.8639	0.9658	1.0198
20	0.7410	0.7861	0.8544	0.9337	1.0015
22	0.7376	0.7922	0.8506	0.9036	1.0156
24	0.7281	0.7644	0.8333	0.8862	0.9750
$C_{M\ ac}$					
α	*δF = 0*	*δF = 10*	*δF = 20*	*δF = 30*	*δF = 40*
-2	-0.0009	-0.0102	-0.0172	-0.0233	-0.0157
0	-0.0005	-0.0093	-0.0185	-0.0234	-0.0264
2	-0.0005	-0.0083	-0.0168	-0.0223	-0.0318
4	-0.0010	-0.0075	-0.0156	-0.0204	-0.0338
6	-0.0020	-0.0074	-0.0147	-0.0198	-0.0337
8	-0.0078	-0.0080	-0.0144	-0.0190	-0.0329
10	-0.0241	-0.0103	-0.0152	-0.0206	-0.0321
12	-0.0537	-0.0266	-0.0177	-0.0239	-0.0321
16	-0.1322	-0.1185	-0.0880	-0.0334	-0.0366
18	-0.1447	-0.1409	-0.1272	-0.0836	-0.0543
20	-0.1532	-0.1525	-0.1522	-0.1246	-0.1005
22	-0.1572	-0.1630	-0.1658	-0.1396	-0.1474
24	-0.1651	-0.1653	-0.1739	-0.1513	-0.1690

Table A6: Flap Deflection Data – Λ = 60°

C_D					
α	*δF = 0*	*δF = 10*	*δF = 20*	*δF = 30*	*δF = 40*
-2	0.0261	0.0263	0.0363	0.0310	0.0649
0	0.0234	0.0217	0.0246	0.0238	0.0465
2	0.0234	0.0215	0.0215	0.0232	0.0354
4	0.0276	0.0244	0.0233	0.0256	0.0305
6	0.0398	0.0311	0.0288	0.0284	0.0315
8	0.0691	0.0439	0.0378	0.0423	0.0376
10	0.1077	0.0748	0.0525	0.0690	0.0478
12	0.1537	0.1188	0.0824	0.1051	0.0626
16	0.2676	0.2253	0.1814	0.1577	0.1132
18	0.3378	0.2946	0.2467	0.2143	0.1624
20	0.4168	0.3702	0.3199	0.2845	0.2179
22	0.4998	0.4532	0.4012	0.3617	0.2877
24	0.5842	0.5384	0.4887	0.4476	0.3673
26	0.6746	0.6316	0.5793	0.5381	0.4529
28	0.7370	0.7046	0.6727	0.6234	0.5433
30	0.7999	0.7659	0.7568	0.7004	0.6340
32	0.7138	0.7433	0.8257	0.7306	0.7054
34	0.7324	0.8022	0.8380	0.7337	0.7478
C_L					
α	*δF = 0*	*δF = 10*	*δF = 20*	*δF = 30*	*δF = 40*
-2	-0.1084	-0.1224	-0.1524	-0.0599	-0.2032
0	-0.0106	-0.0211	-0.0402	0.0471	-0.0923
2	0.0871	0.0750	0.0596	0.0988	0.0138
4	0.1865	0.1719	0.1555	0.1988	0.1188
6	0.2933	0.2692	0.2514	0.2479	0.2221
8	0.4226	0.3702	0.3466	0.3923	0.3223
10	0.5531	0.4965	0.4454	0.5413	0.4212
12	0.6780	0.6311	0.5641	0.6624	0.5164
16	0.9089	0.8619	0.8062	0.7927	0.7174
18	1.0232	0.9902	0.9341	0.8951	0.8435
20	1.1350	1.1041	1.0600	1.0206	0.9329
22	1.2339	1.2129	1.1775	1.1382	1.0372
24	1.3094	1.2979	1.2791	1.2461	1.1501
26	1.3825	1.3833	1.3657	1.3394	1.2535
28	1.3852	1.4079	1.4375	1.3971	1.3375

30	1.3851	1.4018	1.4730	1.4176	1.3978
32	1.1404	1.2442	1.4696	1.3337	1.3951
34	1.0853	1.2398	1.3599	1.2195	1.3344
$C_{M\ ac}$					
α	*δF = 0*	*δF = 10*	*δF = 20*	*δF = 30*	*δF = 40*
-2	-0.0011	-0.0074	-0.0144	-0.0179	-0.0260
0	-0.0005	-0.0063	-0.0132	-0.0166	-0.0257
2	-0.0004	-0.0057	-0.0119	-0.0161	-0.0249
4	-0.0009	-0.0056	-0.0117	-0.0153	-0.0239
6	-0.0022	-0.0060	-0.0118	-0.0153	-0.0233
8	-0.0034	-0.0070	-0.0125	-0.0154	-0.0232
10	-0.0037	-0.0110	-0.0137	-0.0178	-0.0233
12	-0.0027	-0.0129	-0.0190	-0.0247	-0.0241
16	-0.0147	-0.0188	-0.0201	-0.0299	-0.0312
18	-0.0221	-0.0267	-0.0338	-0.0334	-0.0431
20	-0.0384	-0.0399	-0.0433	-0.0461	-0.0423
22	-0.0523	-0.0540	-0.0574	-0.0568	-0.0590
24	-0.0739	-0.0723	-0.0766	-0.0768	-0.0792
26	-0.0993	-0.0960	-0.0969	-0.0975	-0.1002
28	-0.1267	-0.1208	-0.1231	-0.1205	-0.1277
30	-0.1655	-0.1531	-0.1525	-0.1511	-0.1580
32	-0.2305	-0.2095	-0.1874	-0.1965	-0.1926
34	-0.2536	-0.2638	-0.2442	-0.2397	-0.2280